


3-11-2016

# An Optical Design Configuration for Wireless Data Transmission

Seyed Mohammad Amin Motahari Bidgoli  
*Florida International University, smota002@fiu.edu*

**DOI:** 10.25148/etd.FIDC000284

Follow this and additional works at: <https://digitalcommons.fiu.edu/etd>

 Part of the [Electrical and Electronics Commons](#), [Signal Processing Commons](#), and the [Systems and Communications Commons](#)

---

## Recommended Citation

Motahari Bidgoli, Seyed Mohammad Amin, "An Optical Design Configuration for Wireless Data Transmission" (2016). *FIU Electronic Theses and Dissertations*. 2439.

<https://digitalcommons.fiu.edu/etd/2439>

This work is brought to you for free and open access by the University Graduate School at FIU Digital Commons. It has been accepted for inclusion in FIU Electronic Theses and Dissertations by an authorized administrator of FIU Digital Commons. For more information, please contact [dcc@fiu.edu](mailto:dcc@fiu.edu).

FLORIDA INTERNATIONAL UNIVERSITY  
Miami, Florida

AN OPTICAL DESIGN CONFIGURATION FOR WIRELESS DATA  
TRANSMISSION

A dissertation submitted in partial fulfillment of the  
requirements for the degree of  
DOCTOR OF PHILOSOPHY  
in  
ELECTRICAL ENGINEERING  
by  
Seyed Mohammad Amin Motahari Bidgoli

2016

To: Interim Dean Ranu Jung  
College of Engineering and Computing

This dissertation, written by Seyed Mohammad Amin Motahari Bidgoli, and entitled An Optical Design Configuration for Wireless Data Transmission, having been approved in respect to style and intellectual content, is referred to you for judgment.

We have read this dissertation and recommend that it be approved.

---

Armando Barreto

---

Mercedes Cabrerizo

---

Sakhrat Khizroev

---

Naphtali Rishe

---

Malek Adjouadi, Major Professor

Date of Defense: March 11, 2016

The dissertation of Seyed Mohammad Amin Motahari Bidgoli is approved.

---

Interim Dean Ranu Jung  
College of Engineering and Computing

---

Dean Andrés G. Gil  
Vice President for Research and Economic Development  
and Dean of the University Graduate School

Florida International University, 2016

© Copyright 2016 by Seyed Mohammad Amin Motahari Bidgoli  
All rights reserved.

DEDICATION

To my beloved parents

## ACKNOWLEDGMENTS

I would like to express my gratitude and appreciation to Dr. Malek Adjouadi, my advisor and mentor from whom I learned more than one could imagine. He always believed in me and his contributions may not be appreciated enough. I want to thank my dissertation committee members Dr. Armando Barreto, Dr. Mercedes Cabrerizo, Dr. Sakhrat Khizroev and Dr. Naphtali Rishe for their support, dedication and advice. This work was supported by the National Science Foundation under grants CNS 1532061, CNS-0959985, HRD-0833093, CNS-1042341 and IIP-1338922. The support of the Ware Foundation is also greatly appreciated. I want to acknowledge the dissertation year fellowship from the FIU graduate school during summer and fall 2015.

ABSTRACT OF THE DISSERTATION  
AN OPTICAL DESIGN CONFIGURATION FOR WIRELESS DATA  
TRANSMISSION

by

Seyed Mohammad Amin Motahari Bidgoli

Florida International University, 2016

Miami, Florida

Professor Malek Adjouadi, Major Professor

The concept of 2D barcodes is of great relevance for use in wireless data transmission between handheld electronic devices. In a typical setup, any file on a cell phone for example can be transferred to a second cell phone through a series of images on the LCD which are then captured and decoded through the camera of the second cell phone. In this research, a new approach for data modulation in 2D barcodes is introduced, and its performance is evaluated in comparison to other standard methods of barcode modulation. In the proposed method, Orthogonal Frequency Division Multiplexing (OFDM) modulation is used together with Differential Phase Shift Keying (DPSK) over adjacent frequency domain elements to modulate intensity of individual pixels. It is shown that the bit error rate performance of the proposed system is superior to the current state of the art in various scenarios. A specific aim of this study is to establish a system that is proven tolerant to camera motion, picture blur and light leakage within neighboring pixels of an LCD. Furthermore, intensity modulation requires the input signal used to modulate a light source to be positive, which requires the addition of a dc bias. In the meantime, the high crest factor of OFDM requires a lower modulation index to limit clipping distortion. These two factors result in poor power efficiency in radio over fiber applications in which signal bandwidth is generally much less than the carrier frequency. In this

study, it is shown that clipping a bipolar radio frequency signal at zero level, when it has a carrier frequency sufficiently higher than its bandwidth, results in negligible distortion in the pass band and most of the distortion power is concentrated in the baseband. Consequently, with less power provided to the optical carrier, higher power efficiencies and better receiver sensitivity will result. Finally, a more efficient optical integrated system is introduced to implement the proposed intensity modulation method which is optimized for radio over fiber applications.



## TABLE OF CONTENTS

CHAPTER	PAGE
1. INTRODUCTION . . . . .	1
1.1 Motivation . . . . .	1
1.2 General Statement of Problem Area . . . . .	1
1.2.1 Barcode Modulation . . . . .	2
1.2.2 Unipolar OFDM . . . . .	3
1.2.3 High frequency optical modulation apparatus . . . . .	4
1.3 Significance of study . . . . .	4
1.4 Display-Camera communications channel . . . . .	6
1.4.1 Display . . . . .	6
1.4.2 Camera . . . . .	7
1.4.3 Data Transmission . . . . .	7
1.4.4 Distortion . . . . .	8
1.4.5 Information Theoretic Limits . . . . .	8
1.4.6 Perspective Correction . . . . .	9
1.4.7 Location Aware Modulation . . . . .	9
1.5 Unipolar OFDM for Intensity Modulation . . . . .	9
1.6 Research Purpose . . . . .	11
1.7 Research Questions and Hypotheses . . . . .	11
1.8 Methods . . . . .	13
1.9 Dissertation Structure . . . . .	13
2. BARCODE MODULATION METHOD FOR DATA TRANSMISSION IN MOBILE DEVICES . . . . .	16
2.1 Data Transfer Capacity . . . . .	19
2.1.1 Camera Limitations . . . . .	20
2.1.2 Power Limitations . . . . .	21
2.1.3 Inter-Symbol Interference (ISI) . . . . .	22
2.1.4 Interference, Distortion and Noise . . . . .	25
2.2 DPSK-OFDM . . . . .	26
2.2.1 Similarities of barcode and wireless RF channel . . . . .	27
2.2.2 Transmitter . . . . .	28
2.2.3 Receiver . . . . .	34
2.2.4 Error Correction . . . . .	36
2.2.5 Computational Complexity . . . . .	37
2.3 Simulation . . . . .	37
2.3.1 Noise and Clip Ratio . . . . .	39
2.3.2 Low Pass Filtering . . . . .	41
2.3.3 Camera movement . . . . .	42
2.4 Conclusion . . . . .	47

3. RF CLIPPED OPTICAL OFDM . . . . .	50
3.1 RFCO-OFDM . . . . .	54
3.1.1 Zero clipping an RF signal . . . . .	54
3.1.2 Resulting distortion . . . . .	56
3.2 Limits on distortion . . . . .	57
3.3 Parameters Affecting performance . . . . .	60
3.3.1 OFDM Modulator . . . . .	61
3.3.2 Biasing and Clipping . . . . .	61
3.3.3 Optical Amplifier . . . . .	63
3.3.4 Noise . . . . .	63
3.4 Simulation . . . . .	64
3.4.1 Without optical amplifier . . . . .	64
3.4.2 With optical amplifier . . . . .	67
3.5 Conclusion . . . . .	70
4. INTEGRATED DUAL BEAM OPTICAL MODULATOR . . . . .	73
4.1 Generating RoF signals . . . . .	73
4.1.1 Electrical Generation . . . . .	74
4.1.2 Optical Generation . . . . .	74
4.2 RFCO-OFDM . . . . .	75
4.3 Double beam optical modulator . . . . .	76
4.3.1 Mode Locked Laser . . . . .	78
4.3.2 Electro-absorption Modulator . . . . .	80
4.4 Frequency Stabilization . . . . .	81
4.5 Simulation . . . . .	81
4.5.1 OFDM Modulator . . . . .	82
4.5.2 Electrical Field for Pulses . . . . .	82
4.5.3 Modulation Index . . . . .	84
4.5.4 Mode Locking Frequency . . . . .	86
4.6 Results . . . . .	88
5. CONCLUSIONS AND RETROSPECTIVE . . . . .	90
BIBLIOGRAPHY . . . . .	94
VITA . . . . .	103

## LIST OF FIGURES

FIGURE	PAGE
2.1	An illustration of transmission of data between two handheld camera-phones using a sequence of 2D barcodes. . . . . 17
2.2	A diagram of the algorithm used for data transfer. Data stream is supposed to include source coding and error correction coding . . . . 19
2.3	Various truncations of number $\pi$ encoded into QR codes to test the read rate in docked and handheld camera situations. . . . . 24
2.4	Hermitian symmetric matrix used for DPSK-OFDM modulation. The IFFT of this matrix would have real-valued output on display. Bended lines show location of complex conjugate pairs. . . . . 29
2.5	The probability that the OFDM modulated 2D signal has a PAPR greater than a certain value for different image sizes. . . . . 32
2.6	Final image shown on the LCD after applying the DPSK-OFDM modulation algorithm . . . . . 34
2.7	Bit error rate vs. clip ratio and noise power. As noise level increases clip ratio should be increased in order to maintain optimum bit error rate. 40
2.8	Effect of low pass filtering on BER performance. When cutoff frequency is higher than 20%, OFDM based methods are superior to the PAM method. . . . . 42
2.9	20% Butterworth filter applied to DPSK modulated signal . . . . . 43
2.10	Location of erroneous bits. White areas are detected correctly . . . . . 44
2.11	(a) Sample image. (b) $H(u, v)$ applied. (c) $H_c(u, v)$ applied. . . . . 45
2.12	BER for various $r$ and $\theta$ in PAM modulation . . . . . 46
2.13	BER for various $r$ and $\theta$ in QPSK-OFDM modulation . . . . . 47
2.14	BER for various $r$ and $\theta$ in DPSK-OFDM modulation . . . . . 48
2.15	BER for various $r$ averaged uniformly over angle range for three modulation methods studied. . . . . 49
3.1	In a typical RoF application, mm-Wave signal passes from the central station to the base station through fiber optics, and transmitted to mobile stations by wireless RF transceiver and vice versa. . . . . 51
3.2	Proposed system structure, an optical filter along with optical amplifier may be used after intensity modulator for carrier suppression. . . . . 55

3.3	Approximation of $ x $ using Chebyshev polynomials and $\alpha = 2$ . Only $T_2(x)$ and $T_4(x)$ are used in this approximation. . . . .	58
3.4	Error in different approximations of $ x $ . Error amplitude is inversely proportional to the number of Chebyshev polynomials used in the approximation. . . . .	59
3.5	Power difference between BACO-OFDM and RFCO-OFDM calculated using $10\log(P_{BACO}/P_{RFCO})$ . . . . .	66
3.6	Q-factor comparison for two different number of subcarriers corresponding to 5GHz and 3GHz signal bandwidth. It is measured at the output of the modulator where noise power is negligible. . . . .	67
3.7	Q-factor comparison for two different number of subcarriers corresponding to 5GHz and 3GHz signal bandwidth. Measurements are done at the receiver input considering a 20dB OSNR for BACO-OFDM. . . . .	68
3.8	Effect of carrier suppression and modulation index on Q-factor for BACO-OFDM. . . . .	70
3.9	BACO-OFDM with 23dB carrier suppression compared to RFCO-OFDM for various modulation indexes. . . . .	71
3.10	Q-factor achievable on different OSNR values at the receiver. . . . .	72
4.1	Schematic of the proposed modulator . . . . .	77
4.2	Comparison of cw vs mode locked output intensity. . . . .	79
4.3	Two pulse trains at the outputs of electroabsorption modulators. . . . .	83
4.4	Spectrum of a single pulse train for the simulated mode locked laser. . . . .	84
4.5	Comparison of spectrum for the modulated signals. . . . .	85
4.6	Optical power difference between single modulator and the proposed dual modulator. At lower modulation indexes dual modulator achieves the same signal power at the receiver with much less optical power. . . . .	86
4.7	Changes in Q-factor due to Modulation index. . . . .	87
4.8	Changes in Q-factor due to carrier frequency. . . . .	88

# CHAPTER 1

## INTRODUCTION

### 1.1 Motivation

From fire signaling methods of ancient times to the sophisticated semaphore-line system proposed in the 17th century [Bur04] to the recent NASAs Lunar Laser Communications Demonstration (LLCD) [BSM<sup>+</sup>09] project, light has always been used as a reliable communications method throughout history. Unlike radio communications, optical medium is intrinsically more secure as the transmitter can send the signal on a narrow light beam. Moreover, signal interference which requires strict regulations to ensure reliable performance is much less an issue in optical communications as high isolations can easily be achieved. After all, extremely high transmission bandwidth available for optical communications is also another important motivation for research on this topic.

### 1.2 General Statement of Problem Area

Barcodes, as traditional means of optical communications, continue to play a great role in facilitating numerous identification processes since their invention in 1952 [WS52]. In fact the notion of barcodes is a simple cost-effective method for storing machine readable digital data on paper or product packages. As pressing needs to transfer even more data faster and with higher reliability have emerged, there have been many improvements that were made on the original barcode design. The invention of two dimensional (2D) or matrix barcodes opened new fronts in their application to more complex data transfer scenarios like storing contact information and URLs among other things, in which Quick Response (QR) codes [Int06] have

become increasingly popular. A typical 2D barcode performance in camera phone applications can be found in [KT07a].

Barcodes dynamically shown on the LCD of a handheld device can be used to transfer a stream of data to a receiving device as implemented in [LDL08], achieving bit rates of under 10 kbps for state-of-the-art mobile devices. Later, the idea was further developed in [PAK10] for which a computer monitor and a digital camera are used for transmission and reception with bit rates of more than 12Mbps achieved in docked transmitter and receiver conditions. The superior performance of the later implementation is achieved using a more effective modulation and coding scheme for mitigation of image blur and pixel to pixel light leakage [RMA12].

### **1.2.1 Barcode Modulation**

The general idea for providing a viable solution to barcode modulation is to use the inverse Fourier transform (IFT) of data, like in the OFDM method, to modulate the light sources, i.e. the LCD pixels. While image blur and light leakage greatly reduce the performance of QR decoders, they still have a limited effect on OFDM modulation. Furthermore performance degradation in OFDM is confined to known portions of the decoded data. This prior knowledge on non-uniform error probability may be used for adaptive error correction coding based on data region as in [PAK10]. There is an increasing interest in design and implementation of LCD-camera based communication systems as indicated in [MSWS13], [PZZ13] and [KWH13]. Nevertheless, this would require additional investigations in determining optimal modulation and demodulation schemes for this type of innovative communications medium.

### 1.2.2 Unipolar OFDM

Dynamic barcode transmission like many Visible Light Communications (VLC) modulations utilizes intensity modulation. However, non negativity of light intensity by it's definition, imposes that the modulating signal be unipolar, requiring special techniques. The most obvious one would be adding a dc offset to the signal called DCO-OFDM [Arm09], which requires a high average power. A more power efficient method is modulation of odd carrier frequencies in an OFDM signal and then clipping the negative part which is called ACO-OFDM [AL06]. It can be shown that all the distortions related to clipping would occur on even frequency components while odd frequency components would only be attenuated by 3dBs. In [LRBK09] a method similar to ACO-OFDM is introduced using only imaginary components of OFDM for modulation. There is also SFO-OFDM [AFH11] which is marginally better than ACO-OFDM but far more computationally complex.

The research for finding the best intensity modulation method in terms of power and bandwidth usage remains a worthwhile endeavor for its many potential applications. In Radio-over-Fiber (RoF) systems, intensity modulation is used to transmit a high frequency signal often in the range of 60GHz over a fiber optic channel. In this case, the power and cost efficiency of the system are far more important than the bandwidth efficiency on optical channel. Moreover, as the data transmitted optically is supposed to be sent on a wireless radio channel after detection, the choice of the modulation method is limited by the radio channel requirements and standards. Optical carrier suppression along with double side band modulation is thus used in many systems.

### **1.2.3 High frequency optical modulation apparatus**

The communications distance in RoF systems is rather short compared to long-haul optical communications networks which span over longer distances. On the other hand, the number of nodes is much higher. As a result, power efficiency, complexity and channel dispersion requirements are totally different from other fiber optic applications. In many cases, due to short communications distance, even the use of an optical amplifier would no longer be necessary if an efficient modulation is used. In this study, an innovative method is also introduced that can efficiently modulate an optical signal for RoF applications.

### **1.3 Significance of study**

Why is it helpful to transmit more data reliably using dynamic barcodes? Apart from the general advantages of VLC for transmission of data, virtually any electronic device with LCD display would be able to transmit data to a cell phone without any hardware modifications, requiring instead only a software update. This applies to printers, scanners, digital cameras, cell phones, among other devices. Furthermore, the security and privacy issues are going to be reinforced in this kind of communications. An eavesdropper would be required to have a camera in front of the LCD of a transmitting device at the time of data transmission which is not trivial as the legitimate receiver could be blocking the line of sight.

To be more ambitious, NASAs Lunar Laser Communications Demonstration (LLCD) [BSM<sup>+</sup>09] revealed that Visible Light Communication (VLC) can be the future for space communications. Such a VLC system is comprised of a diode laser transmitter and four superconducting nanowire single photon detectors playing the role of a receiver. When an array of transmitting lasers are coupled with an array



of photo detectors to accommodate demanding bandwidth requirements of the the future, it might well seem like a laser generated barcode with Giga frames per second rate. To maximize data transmission rate, one should consider extracting maximum data from a single image shown on an LCD and then increase the rate at which consecutive frames will be decoded. In relation to this issue, any method that is introduced should efficiently utilize the available bandwidth while taking into consideration any potential motion distortions.

Coherent optical communications still dominates long-haul applications where ideal performance efficiencies are required to utilize maximum capacity available from expensive intercontinental fiber lines. However a lot of shorter range fiber applications can benefit from research on intensity modulation / direct detection of optical signals.

One of the challenges for the next generation of wireless networks is in managing the distribution of a signal from a central station to other base stations. High bandwidth requirements along with scarcity of low frequency bands have pushed for the adoption of mm-Wave bands around 60GHz to be the next choice for implementing wireless data networks. Higher attenuation of RF signals in mm-Wave band results in utilization of smaller cells which in turn requires more base stations. Copper is not a viable choice for distribution of signal from central station to base stations due to its high attenuation of the mm-Wave RF signals. As a result fiber optics cables have been used for this propose. These fiber optic cables are cheap and attenuate much less the embedded optical signal than a copper cable would attenuate an RF signal.

With an increase in the number of base stations to provide seamless coverage, the cost per base station is of utmost importance in the adoption of such technologies. In an ideal case, the base station is merely a repeater which receives the RF signal

modulated on optical carrier and transmits the mm-Wave RF signal after amplification. On the uplink side, the base station receives a mm-Wave signal from a mobile station and modulates it on an optical carrier before transmitting it back to the central station through fiber optic cable. Ideally, no RF power amplification would be required and the optical signal would have enough power to create a sufficiently powered mm-Wave RF signal at the base station. Thus a cost-effective intensity modulation method for RoF applications can greatly impact their adaptation as a reliable distribution method of RF signals.

Modulation of baseband electrical signal onto optical carrier can be done in various ways each with certain benefits and drawbacks balancing performance vs complexity and cost. Handling RF electrical signals to modulate the optical carrier is one of the cost increasing factors in these systems. If the baseband electrical signal can be used to modulate the optical carrier in a way that optically generates the RF mm-Wave signal, the system will be much simpler in its design construct.

## **1.4 Display-Camera communications channel**

### **1.4.1 Display**

In a typical LCD or liquid crystal display, a polarized back-light is passed through a mesh of polarized filters creating pixels. Polarization in each pixel can be modified by applying an electrical field. When polarizations for back-light and the pixel align the back-light passes with a minimal loss resulting in a bright pixel. On the other hand, when the polarizations are normal between back-light and pixel, only a small amount of back-light passes resulting in a dark pixel. When the back-light is generated by LED (Light Emitting Diode) the display is said to be an LED

backlighted LCD, which can be marketed as LED display. Eventually each pixel can also be an independent LED creating an LED display.

To create a color display, pixels have also some chromatic filters according to a predefined subpixel geometry which depends on the technology and manufacturer. This geometry defines the pattern by which red, green and blue pixels are arranged. In order to create the perception of whole color range, the intensity of each colored pixel can be adjusted independently. Regardless of the implementation technology, these displays can be considered as an array of intensity modulators. Thus digital data like files on a cell phone can be transmitted by this array of pixels by a proper modulation scheme.

### **1.4.2 Camera**

An image sensor is an array of arranged photo detectors generally implemented by CCD (Charge-coupled device) or CMOS (Complementary metal-oxide semiconductor) technology [Nak05]. These sensors also have a mesh of chromatic filters to pass selective light spectra. Combined with an optical lens the image sensor will be a digital camera.

### **1.4.3 Data Transmission**

When the camera is focused on an LCD display, each pixel of the display will be mapped to multiple image sensor pixels. As a result, the image sensor can digitally sample the LCD display. If the Nyquist sampling criteria is satisfied, a replica of the signal shown on the display can be generated with proper filtering and perspective correction. If the camera and LCD are carefully fixed to eliminate movement, the

transfer function from LCD to image sensor can be extracted by showing known patterns on the LCD and comparing it to the received signal at the image sensor.

#### **1.4.4 Distortion**

If one or both of the camera or LCD move during the capture process. The resulting image would suffer from random motion blur distortion. Upon careful examination of the motion blur, it can be seen that the relative movements during image capture causes the photons accumulated on a single pixel of the image sensor to be coming from multiple adjacent pixels of the display. A somewhat similar phenomenon happens in multi-path radio channels. Thus it is expected that the modulation methods capable of mitigating multi-path like OFDM will be well suited to resolve this relevant issue.

#### **1.4.5 Information Theoretic Limits**

While the performance of OFDM modulation in various radio channels has been studied extensively, it remains an open question for studying the theoretical limits of dynamic barcode modulation under relative movement conditions between transmitter and receiver. Although the work done on intensity modulation for VLC applications may be extended to 2D barcode modulation with adequate effort, it should be noted that current formulated VLC capacity limits are based on average power constraints, while in a dynamic barcode modulation using LCD as transmitter, maximum power would be the constraint not the average.

### **1.4.6 Perspective Correction**

Each static barcode standard has its own guide patterns to help the receiver find the location of data. Design of these patterns requires trade-off between size of the pattern, accuracy, required processing and power for detection, among others. While detection of static patterns is based on capture of multiple frames from the same barcode, in an asynchronous dynamic barcode each frame is only captured 2 times in order to have at least one acceptable frame. Furthermore, time required to detect the guidance pattern is ought to be minimized, otherwise the system may not work in real time.

### **1.4.7 Location Aware Modulation**

In dynamic barcode modulation using OFDM, signal attenuation at the receiver depends on the location of frequency element as discussed in [PAK10]. While a preliminary study is done there, a present problem remains to find the best modulation and bit loading method for such circumstances.

## **1.5 Unipolar OFDM for Intensity Modulation**

Intensity modulation and direct detection (IM/DD) has always been a cost-effective method for utilizing optical communications. Moreover, OFDM modulation as a well-suited method for mitigating channel dispersion requires transmission of bipolar signals. Adapting OFDM to intensity modulation, calls for extra measures which require careful consideration of the application requirements. In the special case of RoF communications, the signal transmitted on the fiber should be relayed to a wireless RF transmitter without much processing after detection. Consequently,

many innovative solutions which require special modification of the transmitted OFDM signal are rendered useless as they cannot be forwarded directly to the RF transmitter.

In the meantime, the high crest factor of OFDM requires lower modulation index to limit the clipping distortion. As a result, single or double side band optical modulation along with carrier suppression is used in RoF applications. However, In RoF systems, signal bandwidth is much less than the carrier frequency and the rest of the spectrum is unused and is available only for utilization in a way to increase power efficiency. In this research, it is shown that clipping a bipolar radio frequency (RF) signal at zero level, when it has a carrier frequency sufficiently higher than its bandwidth, imposes negligible distortion in the pass band, and most of the distortion power is concentrated in the baseband. Consequently, with less power provided to the optical carrier, higher power efficiencies and better receiver sensitivity will result.

The proposed unipolar OFDM method is based on an electrically upconverted signal which adds cost and complexity considering high frequencies involved in mm-wave RoF applications. There will be a significant improvement if it can be paired with optical upconversion in a way that yields the same results. Moreover, it is also favorable if the system can be integrated in a single optical chip. Having a lower cost due to integration and lack of high speed electronics, the integrated system can modulate baseband OFDM signal.

These requirements can be met by appropriately using of two electro-absorption modulators coupled to opposite ends of a mode locked laser cavity and combining their outputs. If the mode locked laser is tuned to have a mode spacing equal to the intended mm-Wave carrier, it can be shown that the combined output will be an efficient intensity modulated optical signal around the carrier frequency.

## 1.6 Research Purpose

The main purpose of this research endeavor is to develop efficient modulation algorithms for data transmission in LCD-camera communications systems that can tolerate relative movements without dropping any data frames. Developing novel unipolar OFDM techniques capable of achieving better power efficiencies in intensity modulation scenarios would complement this research. Performance of these algorithms are evaluated against current state of the art methods to validate their superiority.

## 1.7 Research Questions and Hypotheses

**Question 1:** Current methods of 2D barcode modulation like QR-codes are just fine. In these systems, the major challenge of camera distortion is not the Inter-Symbol Interference (ISI), but the blurring. This leads to the question as to why a new modulation method is needed?

**Hypothesis 1:** The current challenge in the detection of 2D barcodes would be pixel blur either due to camera defocus or in the leakage of light from bright pixels into dark ones. However, this is true for the case of detecting a single non-variant barcode image, where several frames captured with a camera in preview mode are analyzed to select the least distorted picture before decoding the barcode. Thus, due to the low frequency oscillating nature of hand movements, there would be little motion at the peaks of the movement and capture of some frames with little ISI distortion is guaranteed. In fact, when a handheld reader is hovering over a barcode, it will not decode the barcode if the platforms (reader and barcode) are not stable to some extent. On the other hand, for the case of dynamic barcode transmission, considering that the data shown as a barcode is different for every

captured frame (or every two frames in case of asynchronous image capture) then there would be only one image for each shown barcode with a high probability that this image has a considerable ISI due to movement of sending or receiving platforms at the particular shutter opening time of that frame. This hypothesis is evaluated by measuring decoding probability for QR-codes under platform movement.

**Question 2:** How does differential modulation yield better performance in dynamic barcode transmission versus other modulation methods?

**Hypothesis 2:** While compensation of LCD-camera relative motion may be possible using pilot tones when there is only a simple linear motion, it is expected to be extremely difficult when there are complex motions between frames. However, in differential modulation, although the phase at a particular frequency bin may have completely changed at the receiver, the difference between adjacent bins only changes only slightly. Therefore application of differential modulation may be the ultimate answer even with doubling of error rate due to contribution of each phase value to two symbols in differential modulation.

**Question 3:** What happens when only the positive parts of a bipolar real OFDM signal is used to modulate the light intensity?

**Hypothesis 3:** It is known that if only the odd subcarriers of the OFDM signal are modulated with data then the distortion resulting from clipping it at zero level and sending only the positive part of the signal only affects even subcarriers. However this distortion gradually decreases with frequency, it is expected that if the original OFDM signal is modulated on a carrier with a high frequency compared to OFDM bandwidth, then zero clipping distortions will be diminished before reaching the original OFDM signal around the carrier frequency.

**Question 4:** Is there a better way to generate the intensity modulated signal for RoF applications rather than using mm-Wave up-conversion circuitry?



**Hypothesis 4:** Further examinations reveal that if subsequent pulses in an optical pulse train can be modulated independently with positive and negative parts of the OFDM signal the result will be similar to the high frequency OFDM signal clipped at zero. The hypothesis is that if the intensity of a pulsed light source can be modulated separately for even and odd pulses, then an effective modulation method can be implemented for various modulation schemes including the one proposed in this dissertation.

## 1.8 Methods

Generally for performance evaluation, each system is implemented in MATLAB where the input data is fed to the algorithm and the received data after modulation or transmission is retrieved. The simulations include the distortions induced in LCD-camera transmission in a controlled way such that the same distortion may be applied to different algorithms. By selecting random data for transmission and sufficient number of trials, Monte Carlo [JBS00] bit error rate calculations are used for assessing the performance of various modulation/demodulation algorithms in this context. The same method is also used for the evaluation of the Q-factor in the proposed intensity modulation algorithms.

## 1.9 Dissertation Structure

A novel 2D barcode modulation method is introduced in chapter 2 which is shown to be well suited for the transmission of data between an LCD and a handheld device. After a discussion on potential data transmission capacity of the system, an experiment is made to study the effect of motion of the receiving device on the per-

centage of the frames that can be decoded flawlessly in normal QR-Codes. Then the similarities between LCD-camera communications medium and multi-path wireless radio channel are discussed, establishing the basis of using an OFDM signal as the barcode in order to mitigate the effects of relative movement between transmitter and receiver.

Due to unknown camera movements relative to LCD it is not trivial to cancel motion effects on the captured image. As a result, this can greatly distort the phase of the received signals extracted from the Fourier transform of the image. However, it is expected that the distortion would be limited between adjacent frequency components. As a result, an algorithm is introduced to create a 2D barcode from input bits using DPSK-OFDM and its bit error rate is compared to simple Quadrature Phase Shift Keying (QPSK) OFDM and Pulse Amplitude Modulation (PAM) as used in regular 2D barcodes. Defining comparison metrics, various simulations are made showing that the performance of the proposed Differential Phase Shift Keying (DPSK) is superior to simple QPSK OFDM and PAM when used as a barcode modulation method and in fact it can be reliably used along with current error correction technologies to implement motion tolerant LCD-Camera data transmission systems.

In chapter 3, a unipolar OFDM method suitable for intensity modulation in RoF systems is introduced. This led to the design of power efficient intensity modulation methods for the algorithm created in chapter 2. Starting with a review of current systems, a mathematical analysis of the proposed method is provided essentially for proving that clipping an RF signal at zero level to create a unipolar OFDM signal has a better performance under appropriate assumptions. There are also some simulations performed to compare the proposed system to current intensity modulation techniques used in RoF systems, which confirm the validation of the results obtained.

Chapter 4 introduces a novel integrated configuration for intensity modulation well suited for implementation of the method discussed in chapter 3. It starts with a mathematical analysis on the generation of RF Clipped Optical-OFDM (RFCO-OFDM) signals that results in an alternative method of generating them instead of using high frequency electrical up-conversion circuits. The study is augmented by providing a schematic for the proposed system and discussing some details on key elements within it. To assess the effect of carrier frequency and modulation index, simulations are performed for the proposed system and the single modulator counterpart.

Conclusions on findings and design perspectives of this dissertation together with a retrospective on final thoughts related to pertinent issues are provided in 5.

## CHAPTER 2

### BARCODE MODULATION METHOD FOR DATA TRANSMISSION IN MOBILE DEVICES

Barcodes have played a great role in facilitating numerous identification processes since their invention in 1952 [WS52]. In fact barcode is a simple and cost-effective method of storing machine readable digital data on paper or product packages. As pressing needs to transfer even more data faster and with high reliability have emerged, there have been many improvements that were made on the original barcode design. Invention of two dimensional (2D) or matrix barcodes opened a new front for these cost-effective codes and their application in more complex data transfer scenarios like storing contact information, URLs among other things, in which QR codes [Int06] have become increasingly popular. A comparison of 2D barcode performance in camera phone applications can be found in [KT07a].

Much of the efforts in matrix barcode development have been dedicated to barcodes displayed on a piece of paper as that is the way they are normally used. With the replacement of books with tablets and e-Book readers one could contemplate that replacement of the paper with LCD may open another promising front for broader applications of 2D barcodes as a mean of data transfer. Moreover unlike the static paper, the LCD may display time-varying barcodes for the eventual transfer of streams of data to the receiving electronic device(s) as depicted in Fig. 2.1.

This idea has been implemented in [LDL08] where transmission of data between two cell phones through a series of 2D QR codes is studied, achieving bit rates of under 10 kbps for state of the art mobile devices. Later the idea was further developed in [PAK10] in which a computer monitor and a digital camera are used for transmission and reception with bit rates of more than 14Mbps achieved in docked transmitter and receiver conditions over distances of up to 4 meters. However, this

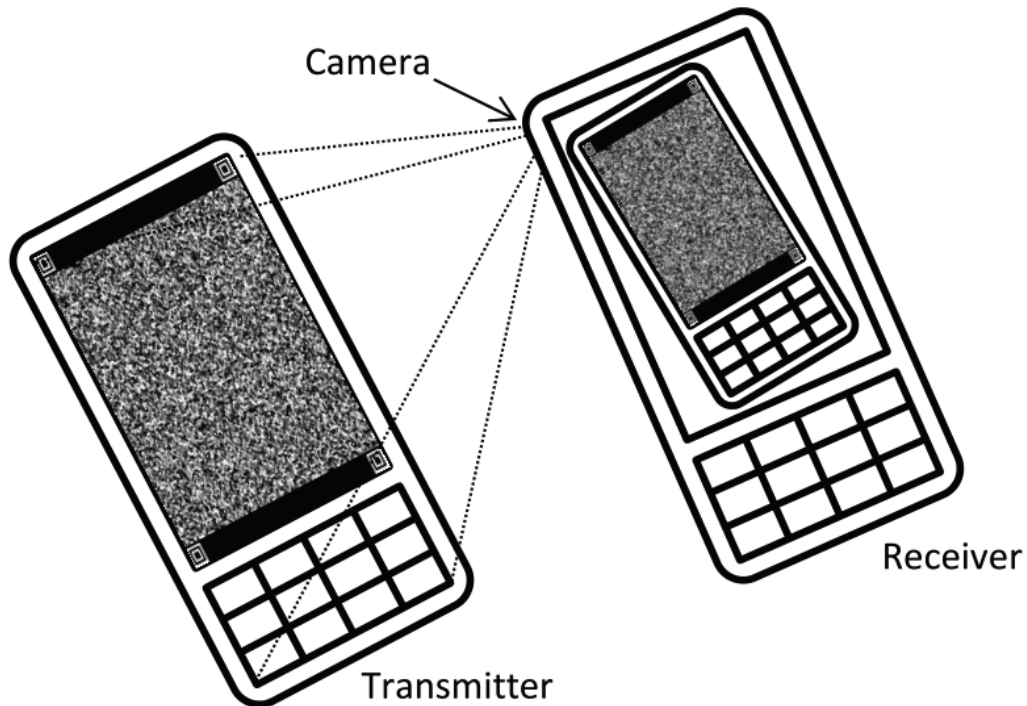


Figure 2.1: An illustration of transmission of data between two handheld camera-phones using a sequence of 2D barcodes.

rate drops to just over 2Mbps when the distance is increased to 14 meters. The superior performance of the later implementation is achieved using a more effective modulation and coding scheme for mitigation of image blur and pixel to pixel light leakage. The general idea is to use the inverse Fourier transform (IFT) of data like OFDM to modulate LCD pixels. While image blur and light leakage greatly reduce the performance of QR decoders they have a limited effect on OFDM modulation. Furthermore their performance degradation is confined to known portions of the decoded data. This prior knowledge on non-uniform error probability may be used for adaptive error correction coding based on data region as in [PAK10]. There is an increasing interest in design and implementation of LCD-Camera based communication systems as indicated in [MSWS13], [PZZ13] and [KWH13]. This would

require additional investigations in determining optimal modulation and demodulation schemes for this type of innovative communications medium.

The OFDM modulation uses orthogonal frequency subcarriers to transfer data and can confine image blur, which is essentially a low pass filter, to high frequency components such that low frequency data bits are transmitted intact. This method requires high phase coherency to detect the data bits correctly. The current study extends this idea through additional modifications on the modulation scheme in a way to mitigate LCD-camera relative movements during the capture of a single frame, which results in motion blur distortion on the captured images. This kind of distortion as would be detailed later severely degrades the performance of Quadrature Phase Shift Keying (QPSK) modulated OFDM signals.

The required movement tolerance is achieved by putting data in phase differences of adjacent frequency components leading to a DPSK-OFDM scheme which would be called simply the DPSK method throughout this dissertation. Observing that any phase distortion due to motion blur would affect neighboring frequency components negligibly, data may be transmitted reliably even in the vicinity of high LCD, camera relative motion. A diagram of the system envisioned is shown in Fig.2.2. This method also eliminates the channel estimation requirements resulting in lower processing power.

To maximize data transmission rate, one should consider extracting maximum data from a single image shown on an LCD and then increase the rate at which consecutive frames will be decoded. In consideration of this issue, any method that is introduced should efficiently utilize the available bandwidth considering motion distortions.

Previous studies have demonstrated the feasibility of such systems and have addressed the effects of single distortions like linear misalignment [MA12], defocus blur

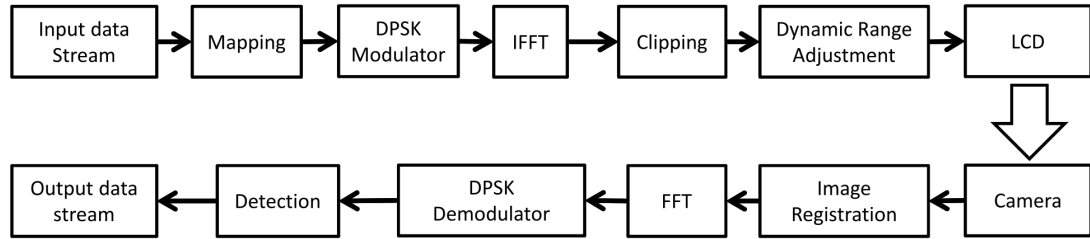


Figure 2.2: A diagram of the algorithm used for data transfer. Data stream is supposed to include source coding and error correction coding

[RMA12] and vignetting [MA14] on the modulation methods under consideration, but they have not provided a comparative assessment of these systems in a controlled environment. Moreover, no comparisons were made in case of LCD camera motions which greatly affect the performance of the system in applications that involve handheld camera-phone receivers. As a consequence, this chapter introduces DPSK-OFDM as a means of mitigating LCD camera motion distortions and sets a series of simulations based on mathematical modeling for blur and motion on the received images in a way that the distortion would be the same for PAM (Pulse Amplitude Modulation), QPSK-OFDM and DPSK-OFDM modulations. As a result, a reliable comparison can be made between these major modulation methods regardless of other parameters affecting the performance of such practical systems.

## 2.1 Data Transfer Capacity

There are many factors affecting the amount of data that can be extracted from a particular LCD, some of them depend on the LCD design itself and others on the camera working as the receiver. Moreover, there are some limitations due to the system's processing capability and power consumption. Although in practice, it might be challenging to obtain a fair assessment of the system's performance, it is

important to know what affects the transfer rate and what can be done about each limiting factor in this data transmission medium. The data capacity of an LCD may be calculated by considering for instance the maximum number of bits in a raw image as shown on the LCD. A display having the  $M_D$  rows and  $N_D$  columns, showing a color image in  $L_D$  channels (typically  $L_D = 3$  for red, green and blue) and color bit depth of  $B_D$  bits per channel, would have the maximum information of:

$$C_I = M_D \times N_D \times L_D \times B_D \text{ bits per image} \quad (2.1)$$

This is the maximum information that can be shown on the LCD on a single image due to the discrete nature of the data shown. A refresh rate of  $R$  for the LCD leads to a data rate of  $C_V = R \times C_i$ . For a state of the art cell phone with a high resolution display having 16M colors, the parameters would be  $M_D = 1136$ ,  $N_D = 640$ ,  $P_D = 3$ ,  $B_D = 8$  and  $R_D = 60\text{Hz}$  resulting in  $C_I \approx 17$  Mbits and  $C_V \approx 1\text{Gbps}$ , which is an extremely high data rate even when compared to current radio frequency wireless technologies. Unfortunately, this rate cannot be achieved due to the limitations as described in the next sections:

### 2.1.1 Camera Limitations

A digital camera could be considered as a device which digitally samples a 2D signal. For correct sampling of consecutive frames in time, camera capture rate should be 2 times the display refresh rate ( $R_D$ ) unless there is a synchronization system in place to activate the camera shutter when the image is stabilized on the display (exactly between frame changes). As it is not normally the case, if the camera capture rate is for example  $R_C = 8\text{Hz}$  then the display refresh rate could not exceed 4Hz.



To satisfy the Nyquist criteria for image resolution, each pixel of the image shown on the LCD should be sampled by 2 or more pixels in the camera [GW07]. The image sensor uses limited number of bits per channel for conversion of each color pixel, resulting into quantization noise. To limit the effect of this noise on the overall detection performance it should be maintained  $6 - 10dB$  below system noise level [SS77], which on the other hand must be maintained well below signal power level, depending on the modulation method used, in order to have acceptable bit error rates (BER) [PS07].

### 2.1.2 Power Limitations

The capacity of every communication channel depends on the power of the signal sent through that medium as predicted by Shannon theorem [CT06], and in this case the power would be limited by the intensity of light an LCD can generate. Increasing this intensity would improve signal to interference and noise ratio (SINR) in the receiver. Like RF power transmitters, LCD displays are limited in terms of the maximum power leading to the Peak to Average Power Ratio (PAPR) limitation, which is a common challenge for OFDM signals. When maximum available intensity is fixed, higher PAPR yields lower average intensity and thus lower SINR. Therefore transmission of OFDM signals over an LCD requires a trade-off between the average power transmitted and the resulting distortion due to clipping of the peaks, another issue that is addressed in this study. Although various PAPR reduction methods are available, they would affect QPSK-OFDM and DPSK-OFDM methods in a same manner, and DPSK modulation would still be superior when the same method of PAPR reduction is used. Further discussions on clipping OFDM signals can be found in [OI02a] and [DSH12a].

### 2.1.3 Inter-Symbol Interference (ISI)

When a barcode is printed on paper, a white pixel does not affect its neighboring black pixels provided that the print quality is good and the resolution is high enough. On the other hand, when data is shown on an LCD, light that is passing through white pixels may leak into neighboring black pixels making them look gray. The straightforward solution to this problem is to increase the size of the pixels so that they have minimal effects on each other. This is called barcode granularity in QR coding [Int06]. On a lower level this is exactly the way a printed barcode is generated, where each printed dot is not corresponding to a data symbol but rather many printer dots contribute to a single black symbol. In the case of LCD, each  $k \times k$  pixel set is assigned the same color to generate just one symbol, isolating the center pixel from bordering pixels that may be affected by neighbors. Unfortunately this method greatly decreases the transfer rate because the  $M \times N$  independent data symbols reduce to  $\frac{M}{k} \times \frac{N}{k}$  which leads to a  $k^2$  to 1 rate decrease. The inter-symbol interference could happen in the receiver camera as well becoming a major obstacle for increasing the pixel density of barcodes.

Moreover, any movements between camera and LCD during the capture of an image for barcode processing results in motion blur which is translated into ISI as neighboring pixels affect each other in the captured image. At first this effect might not be evident based on common experiments with 2D barcodes like QR codes. These codes are decoded successfully without major efforts in terms of stability of code or camera. While performance of some QR code detection algorithms are studied in [LYL08] and first read rate performances of some 2D barcodes have been studied in [KT07b], the research is rather focused on user experience as an important factor, which is to determine if the user is able to decode the barcode at first try. In fact, performance of 2D barcode decoders are measured by the frames

processed per second, thus when a barcode scanner tries to decode a stationary 2D barcode, multiple frames are processed within a second and a successful decode will be reported if only one frame is captured in good conditions.

To investigate if a relative barcode camera motion affects the performance of the decoder, the following experiment was conducted. Alphanumeric strings of various lengths of number  $\pi$  were encoded into QR Codes of increasing dimensions, in a way to fill the barcode capacity as shown in Fig. 2.3. Error correction level is set to medium (M) which is capable of correcting roughly 15% error rate. Consecutive frames were captured using a hand-held camera phone, first by fixing the camera and then by holding it in one hand by a non-experienced user. Camera focus was locked the same way in both cases and normal office lighting and a distance of 12cm were maintained. Moreover, the width of rectangular QR code pixels was .312mm regardless of the code capacity. As a result the largest QR code which had  $121 \times 121$  pixels was 37.7mm in width which is double the density of ordinary QR barcode. Encoding and decoding of the QR codes were accomplished using ZXing open-source libraries [IEE14].

In order to limit the effect of perspective distortion, camera and barcode are held parallel in the docked case, and although this angle cannot be guaranteed in the handheld scenario, the performance drop would be negligible as reported in [AJG<sup>+</sup>14]. The captured images taken at 10 frames per second were processed to detect the QR code, and the percentage of decodable images are shown in Table 2.1. As can be seen from these results, for smaller QR codes it does not make any difference if the camera is held by hand or fixed as all the frames would be detected successfully. However, as the size of the QR code increases, more and more frames are dropped in the moving case compared to the fixed camera setup. In any setup studied, user experience would not be a problem as there was at least one detectable

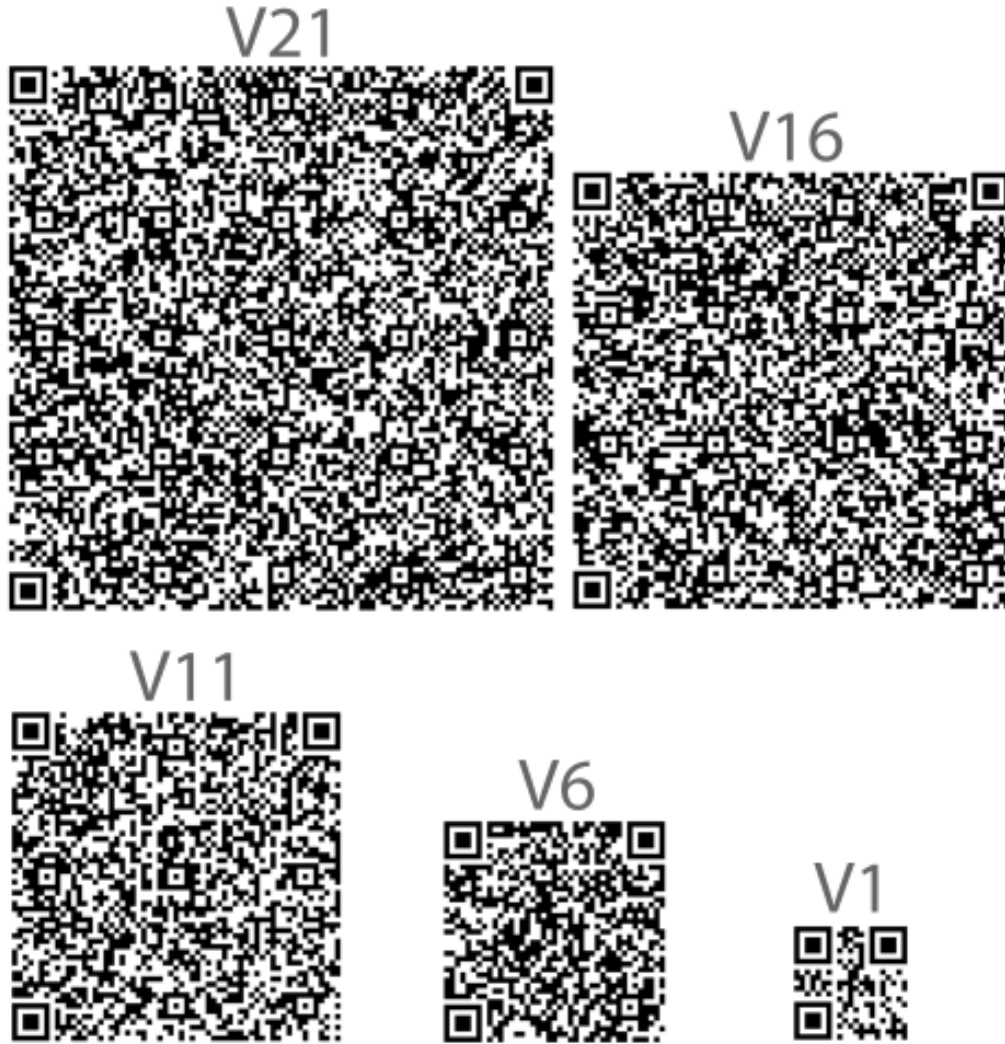


Figure 2.3: Various truncations of number  $\pi$  encoded into QR codes to test the read rate in docked and handheld camera situations.

frame within one second of recording onset.

Table 2.1: Read rate of QR codes in docked and handheld conditions

QR Version	V1	V6	V11	V16	V21
QR Size	21×21	41×41	61×61	81×81	101×101
Docked	100%	100%	97%	99%	10%
Handheld	100%	100%	84%	71%	6%

After all, the current challenge in detection of 2D barcodes is be pixel blur either due to camera defocus or in the leakage of light from bright pixels into dark ones. However, this is true for the case of detecting a single non-variant barcode image, where several frames captured with a camera in preview mode are analyzed to select the least distorted picture before decoding the barcode.

Thus, due to the low frequency oscillating nature of hand movements, there would be little movement at the peaks of the motion and capture of some frames with little ISI distortion is guaranteed. In fact when a handheld reader is hovered over a barcode, it will not decode the barcode if the platforms (reader and barcode) are not stable to some extent.

On the other hand, for the case of dynamic barcode transmission, considering that the data shown as a barcode is different for every captured frame (or every two captured frames in case of asynchronous image capture) then there would be only one image for each shown barcode and there is a high probability that this image has a considerable ISI due to movement of sending or receiving platforms at the particular shutter opening time of that frame.

Moreover, although there is a considerable body of literature about motion deblurring, its application to traditional stationary barcode detection is limited because of the availability of tens of images from a single barcode within a reasonable time to select a clear shot in current static barcode decoding scenarios.

#### **2.1.4 Interference, Distortion and Noise**

When a camera is used to take a picture of a 2D barcode, certain image artifacts could impact the result of data extraction method. These artifacts are mainly due to the following:

- Distance and angle between Camera and LCD (Perspective distortion)
- Camera and subject relative motion
- Out of focus lens
- Compression Distortions
- Unwanted ambient light sources
- Dirt and permanent marks on the LCD
- Noise (primarily additive Gaussian noise)

Moreover, nonlinear distortions exist in a typical optical wireless data transmission setup due to transmitter and receiver physical limitations that are discussed in [TSH13]. These undesirable effects should be addressed to ensure the feasibility of the algorithm under realistic scenarios, while preserving the ability for attaining high data transfer rates.

## **2.2 DPSK-OFDM**

While LCD technology is improving on pixel to pixel isolation, some of the image capture distortions still remain, causing neighboring pixels of the barcode mix up in the image and resulting in some kind of Inter Symbol Interference. The main idea in resolving this problem is to interpret the barcode image as a wireless radio signal for which ISI reduction techniques have already been proven successful. One of the best and most feasible modulation methods capable of coping with severe conditions in band limited communication channels is the so-called Orthogonal Frequency Division Multiplexing or OFDM [NP00]. The general idea is that when dealing with band-limited, power-constrained, multipath channels, it is more efficient to transfer a bunch of narrow-band signals in parallel instead of a single high bandwidth signal.

### 2.2.1 Similarities of barcode and wireless RF channel

For simplicity each 2D image is reformulated into a 1D row vector containing all pixels in the 2D image. Each row can be considered as a time domain signal which has Pulse Amplitude Modulation (zeros are black and ones are white pixels). Consider taking a picture of this single row, in a band limited channel which has a combination of camera focus problems, resolution limitations, light leakage from white to black pixels, among other things. Moreover in a multipath channel in which the camera moves during image capture and mixes up the image of several neighboring pixels, the resulting image will suffer from high ISI. To solve these problems in a time domain radio signal, OFDM method is used to essentially divide the channel into multiple orthogonal low bandwidth channels and the low rate data is sent into these channels in parallel. So in case of the 1D data the inverse Fourier transform is used for displaying the data instead of using the PAM modulated process, where Hermitian symmetry conditions should be met to have real-valued outputs. As a result, most artifacts only affect the high frequency components leaving low frequency components intact for data transmission.

This idea may be generalized to 2D signals to meet the requirement for transferring the entire image at once. Instead of 1D inverse Fourier transform, the 2D version is used such that the effect of artifacts acting on two axes would be confined to high frequency components. The exact modulation scheme will be discussed later in this chapter.

In general each sub-carrier in an OFDM signal is modulated using M-quadrature amplitude modulation (M-QAM). Thus proper phase shift of each element should be estimated and compensated for before demodulation. This generally requires specific conditions on the channel characteristics like fast fading where pilot tones are used for channel estimation or slow fading where most methods would require

multiple symbols in seeking similar channel responses (i.e. similar transfer functions) [CEPB02] and [MM01].

When using OFDM for transmission of data as images, all the channel equalization computations should be based on a single OFDM frame due to the independent channel response between subsequent frames, unless the frame rate is very high. In fact each frame is distorted by LCD-Camera relative motion during its own capture time. To mitigate this problem the phase difference between adjacent elements is used to convey data. Using DPSK modulation prior to applying the inverse Fourier transform in OFDM modulation, data would not have to be stored in the absolute phase of the received elements but rather in its phase difference to the neighboring element, which eliminates the requirement for channel estimation and equalization if the channel response does not vary abruptly between adjacent subcarriers.

### 2.2.2 Transmitter

One of the advantages of using OFDM is its effective computation method which uses the Inverse Fast Fourier Transform (IFFT) to modulate input data into orthogonal frequencies. The modulated signal should be real-valued in order to be shown on an LCD, so the input to the IFFT algorithm should have Hermitian symmetry. This requirement is shown in the following equation:

$$\mathbf{T}(M - m, N - n) = \mathbf{T}(m, n)^* \quad (2.2)$$

where  $0 \leq m < M$  and  $0 \leq n < N$ , and  $*$  denotes the complex conjugate operator. Figure 2.4 shows the elements relationship in order to have a real-valued IFFT for  $\mathbf{T}$  matrix. In this configuration, only regions 1 and 2 are used for data transmission independently, and regions 3 and 4 are calculated accordingly to have



a real-valued IFFT. Moreover, the symmetry requirements for elements that have been deliberately set to zero would be automatically satisfied.

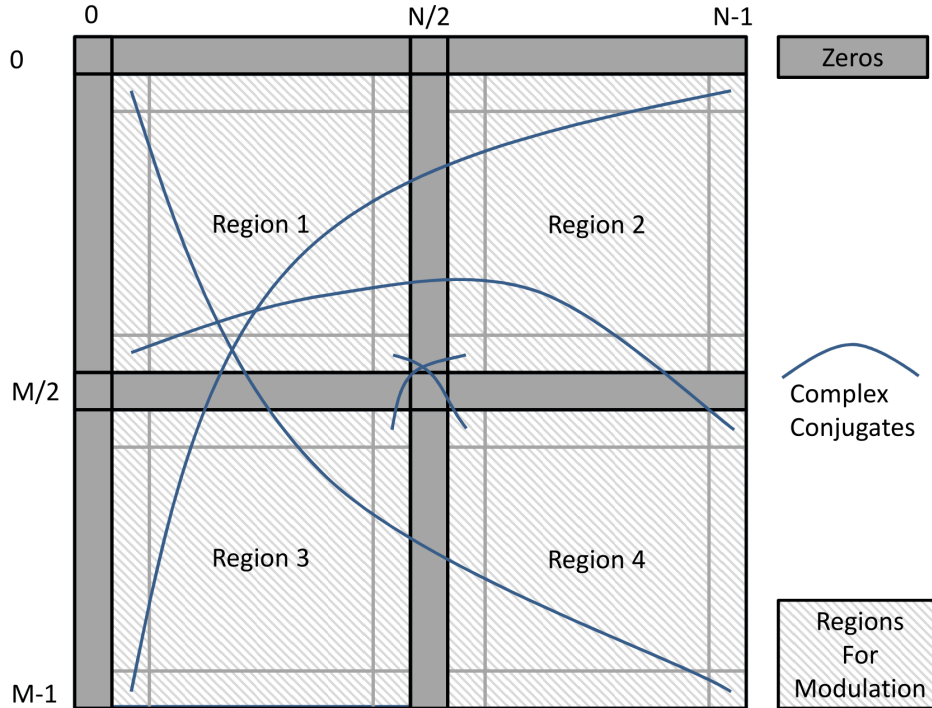


Figure 2.4: Hermitian symmetric matrix used for DPSK-OFDM modulation. The IFFT of this matrix would have real-valued output on display. Bended lines show location of complex conjugate pairs.

### Constellation Mapping

The input data is decomposed into 2-bit symbols. Each symbol is converted to a complex phase by the following rules:

$$11 \rightarrow e^{j\frac{1\pi}{4}}, 10 \rightarrow e^{j\frac{7\pi}{4}}, 01 \rightarrow e^{j\frac{3\pi}{4}}, 00 \rightarrow e^{j\frac{5\pi}{4}}$$

Therefore the first bit modulates the real component and the second bit modulates the imaginary component of the phase for each data symbol. These symbols

are placed in a  $\frac{M-2}{2} \times \frac{N-2}{1}$  matrix  $\mathbf{S}$  which contains the absolute phase elements that are going to be modulated using DPSK.

### Differential PSK

Matrix  $\mathbf{S}$  is transferred into a differential matrix  $\mathbf{D}$  using the following method:

- $\mathbf{D}(0, 0) = \mathbf{S}(0, 0)$
- $\mathbf{D}(0, n) = \mathbf{D}(0, n - 1) \times \mathbf{S}(0, n)$   
 $1 \leq n < N - 2$
- $\mathbf{D}(m, n) = \mathbf{D}(m - 1, n) \times \mathbf{S}(m, n)$   
 $1 \leq m < \frac{M}{2} - 1, 0 \leq n < N - 2$

Subsequently, the DPSK modulated  $\mathbf{D}$  matrix is divided into two matrices:

- $\mathbf{D}^1(m, n) = \mathbf{D}(m, n)$
- $\mathbf{D}^2(m, n) = \mathbf{D}(m, n + \frac{N-2}{2})$

where  $0 \leq m < \frac{M}{2} - 1, 0 \leq n < \frac{N}{2} - 1$ . These two matrices are used to fill regions 1 and 2 of the matrix  $\mathbf{T}$ . Regions 3 and 4 of  $\mathbf{T}$  are generated based on the Hermitian symmetry requirement, and all the remaining strips on  $\mathbf{T}$  are set to zero. These small regions, especially around region 1 (left top corner), may be used for special data transmission such as frame rate or type of error correction coding used.

### Inverse FFT

Considering  $\mathbf{T}$  is the frequency domain representation of the signal, the IFFT is applied on it to have the time domain signal referred to as  $\mathbf{D}_i$ . This signal would have zero mean because  $\mathbf{T}(0, 0) = 0$ , so it should be adjusted in order to use the full dynamic range of pixels.

## PAPR adjustment

$\mathbf{D}_i$  is a real-valued 2D signal with high peak to average ratios. In fact, the probability of having a high PAPR increases as the number of frequency components increases as can be seen in Fig. 2.5. There are several methods to limit the PAPR of OFDM signals which might be applied here with slight modifications for 2D signals. One of the most practical methods would be soft clipping of the signal in which a threshold level of  $A_{max}$  based on signal average power level is set such that:

$$ClippRatio = \frac{A_{max}}{\sqrt{P_{avg}}} \quad (2.3)$$

where  $P_{avg}$  is average power per element in the OFDM signal before clipping. Any components with higher amplitude than  $A_{max}$  are consequently clipped to  $A_{max}$  resulting in a 2D matrix  $\mathbf{D}_c$ .

## Amplitude adjustment

The pixel levels in the PAPR adjusted image need to be transformed into LCD dynamic range levels for efficient utilization of transmission power. Normally the intensity levels on the LCD goes from 0 to  $I_{max}$ . So  $\mathbf{D}_c$  values are transformed linearly to this range using the following equation:

$$\mathbf{D}_a(i, j) = \frac{\mathbf{D}_c(i, j) - \text{Min}(\mathbf{D}_c)}{\text{Max}(\mathbf{D}_c) - \text{Min}(\mathbf{D}_c)} I_{max} \quad (2.4)$$

Thus the average power of  $\mathbf{D}_a$  is maximized for LCD projection.

## Finder patterns

Proper demodulation of data requires precise extraction of the modulated data from captured image and compensating for any perspective distortions. While finder patterns to seek specific points in a barcode are generally expandable to dynamic

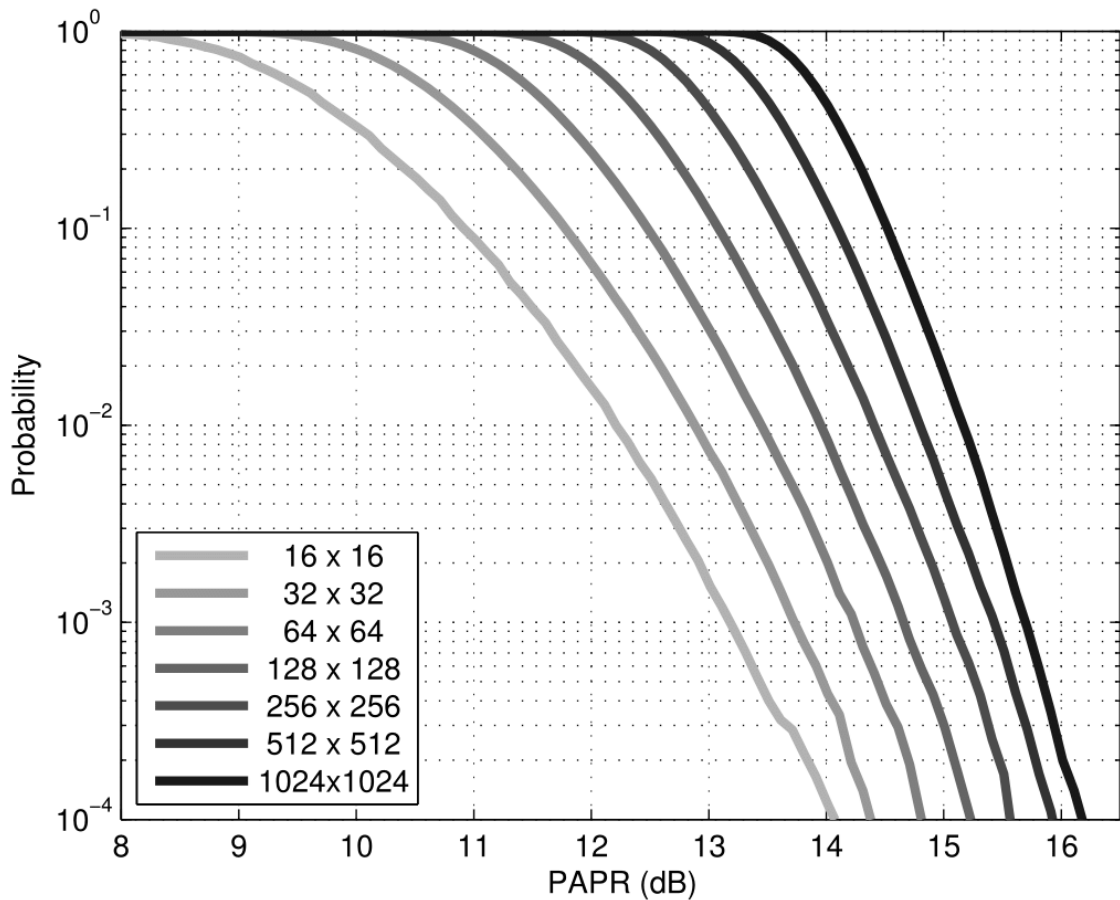


Figure 2.5: The probability that the OFDM modulated 2D signal has a PAPR greater than a certain value for different image sizes.

barcode case, two challenging issues should be met for any pattern to be applicable. Firstly, the pattern should not alter the integrity of data bearing image because OFDM symbol should be maintained intact. Secondly, knowing the approximate location of the finder pattern should reduce the complexity of finding it because the location is minimally changed in a frame by frame basis. Thus patterns like QR code finder become favorable. General finder patterns used with 2D barcodes may be used here like the 1,1,3,1,1 pattern used in QR-codes, for which fast and efficient detection algorithms have already been developed in [BH13] and [LF13].

## Image Size

If the display has more pixels than OFDM symbol which is usually the case, multiple OFDM symbols may be used next to each other considering the guard band involved. This method was successfully used in the PixNet system [PAK10], and hence can be applied here too. Although larger images were tested in our simulations and had good results, they were not provided here on the account that perspective correction requirements would not be met in a practical system using larger single symbol images. Moreover, the largest size defined for a QR-code is  $177 \times 177$  and many decoders have problem dealing with larger barcode sizes. A sample  $128 \times 128$  image generated by the preceding transmitter is shown in Fig. 2.6 as it would be seen on the LCD of the transmitting device.

## Cyclic Extension

OFDM systems require cyclic extension to prevent inter carrier interference (ICI) [MCW01]. To be sufficient, the length of the added cyclic extension must be more than the time spread of the channel. In case of the 2D barcode, periodic extension of the image generated by 2D-IFFT is required to prevent ICI. The length of this extension is determined by the impulse response of the channel, which in turn depends on the image blur and the amount of movement anticipated between LCD and camera. However, since in this research the channel response is modeled in the frequency domain, frequency domain filtering [GW07] is applied on the barcode, and effective cyclic extension is achieved by frequency domain multiplication which results in time domain cyclic convolution. Hence in all the following simulations the length of the cyclic extension is the same for DPSK-OFDM and QPSK-OFDM ensuring ICI elimination in the longest channel responses simulated.

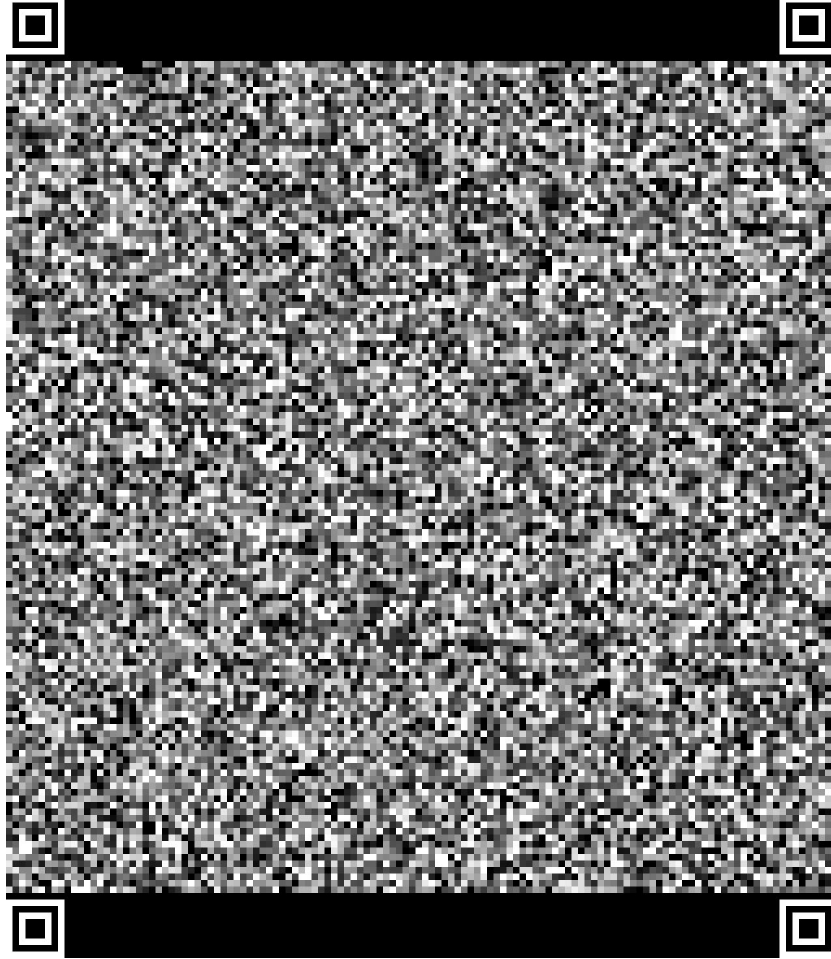


Figure 2.6: Final image shown on the LCD after applying the DPSK-OFDM modulation algorithm

### 2.2.3 Receiver

After displaying the generated image of Fig. 2.6, the receiver uses its camera for sampling and registering the acquired image so that a fairly acceptable copy of  $\mathbf{D}_a$  is created at the receiver end. The effects of interference, noise and distortions encountered in this step are addressed in the simulation section. To obtain the transmitted data successfully, the following steps should be taken into consideration at the receiver end:

## **Image Capture**

Digital camera and display systems have a limited refresh rate which tends to be more than 23 Hz for different standards. In a synchronous system the camera can capture each displayed frame at the exact moment when it is fully stable. However if the receiver does not know when a new frame is ready on the display, the sampling rate should be at least twice the display rate to ensure capture of at least one acceptable frame. Moreover the relative distance and angle between camera and display is bounded by the Nyquist criteria where each pixel on the display frame should map into a minimum of  $2 \times 2$  block in the camera.

## **Image Registration**

The first step in processing the captured image is to extract the displayed image from background which depends on predefined finder patterns put into the image. For example, data matrix guidance lines are used in [PAK10]. Because measurement errors in finder pattern location and perspective correction errors are not part of this study, the simulated images and their distorted received signals are ideally registered isolating the effects of blur and camera movement on error rate of different schemes.

## **FFT**

Applying Fast Fourier Transform on the registered image results in frequency domain data which is comprised of the differential phase modulated elements stored in  $\mathbf{R}_f$  matrix.

## **DPSK Demodulation**

The original constellation mapped data can be extracted using phase differences between respective elements, but first data corresponding to regions 1 and 2 should

be concatenated together to form matrix  $\mathbf{R}$  corresponding to the transmitted matrix  $\mathbf{T}$ .

- $\mathbf{R}_d(0, 0) = \mathbf{R}(0, 0)$
- $\mathbf{R}_d(0, n) = \mathbf{R}(0, n) \times \mathbf{R}^*(0, n - 1)$   
 $0 < n < N - 2$
- $\mathbf{R}_d(m, n) = \mathbf{R}(m, n) \times \mathbf{R}^*(m - 1, n)$   
 $0 < n < N - 2, 0 < m < \frac{M}{2} - 1$

The resulting  $\mathbf{R}_d$  would be a distorted copy of  $\mathbf{S}$  in transmitter path.

## Detection

Now that the phase differences have been extracted, each input bit may be calculated using the constellation map of the transmitter. Each element is evaluated using its real and imaginary components. The sign of the real component determines the first bit and the sign of the imaginary component determines the second bit.

### 2.2.4 Error Correction

Error correction coding is often used in communication systems to correct for the different number of bits lost in the transmission process. For example, Reed-Solomon (RS) coding is used in QR codes, where depending on the level of error correction used, error rates of 7% up to 30% can be corrected at the receiver end [Int06]. While the selection of error correction coding has a great influence on the overall performance of the communication system, they are generally used on top of the modulation-demodulation scheme and after source coding. Therefore, based on the achievable error rates without error correction coding, one can select an appropriate coding scheme to create a reliable communication channel. As a result,



when considering the BER performance plots provided in the simulation section, it should be noted that error rates in excess of 30% are not correctable even with the most redundant RS codes defined in [Int06] and would consequently be considered a non-reliable channel for this kind of transmission.

### 2.2.5 Computational Complexity

An important issue regarding the applicability of such a system would be the computational power required to implement the system. Although a thorough investigation of such requirements and any optimization process can be subject to further study, it should be noted that the proposed DQPSK-OFDM system has a limited processing overhead compared to the equivalent QPSK-OFDM system which is already implemented and tested. More specifically, on the transmitter side, although the differential modulation is described by complex multiplications, it can be easily implemented using a small look-up table taking current phase and data to be modulated as inputs. However, in the receiver side about  $M \times N$  multiplications are required to extract phase differences before detection which is not prohibitive compared to the complexity of the 2D FFT preceding it which is in the order of  $M \times N \times \log (M \times N)$ .

## 2.3 Simulation

Current 2D barcodes use PAM as the preferred modulation method [Int06]. To compare them with the proposed modulator and demodulator, both systems are implemented in MATLAB. A Simple PAM modulator which translates bits into light and dark pixels of an image is compared to the proposed DPSK-OFDM method which uses the described algorithm for modulation and demodulation. Furthermore,

the performance of QPSK-OFDM [ST01], which is essentially the same as 4-QAM (Quadrature Amplitude Modulation) OFDM used in PixNet [PAK10], is compared to the proposed DPSK-OFDM system. The main parameters that are considered include:

- Noise and Clip Ratio
- Low pass filtering
- Camera Movement

To study the effect of each of these parameters, first a random data stream is modulated to the displayed image using the algorithm under test. Then a controlled distortion is applied to the image before passing it to the receiver. The bit stream at the output of the decoder is compared to the input random stream to count for erroneous bits. This process is repeated several times using various random data streams and the same amount of distortion. The average result would be the bit error rate corresponding to that particular situation and assumed distortion. The process is then repeated for another distortion amount resulting in a plot for bit error rate against distortion.

It should be noted that, the parameters used are based on the models assumed for the distortions involved. For instance, here a linear motion during a camera shutter open and close interval is assumed and motions magnitude and angle are considered as parameters of the movement. Another study might consider a more complex motion and selects the parameters accordingly. The fact is that the differential nature in DPSK modulation will help it outperform the other methods when reasonable motion is involved. Of course if motion is so harsh that phase difference applied by the motion to adjacent subcarriers is substantially different, the DPSK-

OFDM method would fail. However, the other two methods would have failed long before that.

### 2.3.1 Noise and Clip Ratio

In a barcode setup where PAM is used to modulate data onto image pixels, the average power is maximized. Consider the maximum amplitude driving a fully "on" pixel is  $A_p$  leading to a transmitted energy of  $P_p$ . In QR coding which uses binary-PAM, amplitude of each pixel may be either 0 or  $A_p$ . Considering that the dc offset is removed, each element would then have an amplitude of  $\pm \frac{A_p}{2}$ , yielding the following average power per pixel:

$$P_{ave} = \frac{P_p}{A_p^2} \frac{1}{M \times N} \sum_{m=1}^M \sum_{n=1}^N A_{mn}^2 \quad (2.5)$$

where  $A_{mn}$  is the amplitude of element  $(m, n)$ . Thus  $P_{ave} = \frac{P_p}{4}$ . Moreover peak power in a PAM scheme would be  $\frac{P_p}{4}$  too. The fact that peak to average power ratio in binary-PAM signal is always 1 no matter what the data is, makes it suitable for situations where there is a limit on peak available power like LCD transmission. On the other hand, OFDM modulation has the intrinsic problem of PAPR which increases with increasing number of elements. In Fig. 2.5 PAPR for different image sizes is calculated. The figure shows the probability of PAPR being greater than a certain value.

High PAPR and limited peak power enforces a reduction in average power for the signal if it is going to be transmitted as is. Low average power means higher error rate in the presence of noise. To mitigate this problem, PAPR should be decreased as the maximum power is limited by physical constraints of LCD. Here soft clipping method is used as described before and the output after clipping is mapped linearly

to the [0 255] interval for a grey scale image. In Fig. 2.7 the effect of various clipping levels is shown along with additive white Gaussian noise. As the clipping increases, the average power also increases due to fixed maximum power and lower PAPR. However this increased average power is at the expense of a more distorted signal which translates into more BER. In this figure BER approaches 18% as clipping ratio decreases. Moreover, increasing noise level forces the BER approach 50%. It can also be observed that increased noise level requires a lower clipping threshold to obtain optimal error rate, but the induced distortion causes the benefit of increased average power to be limited and at some point BER actually starts to increase while average power is also increasing.

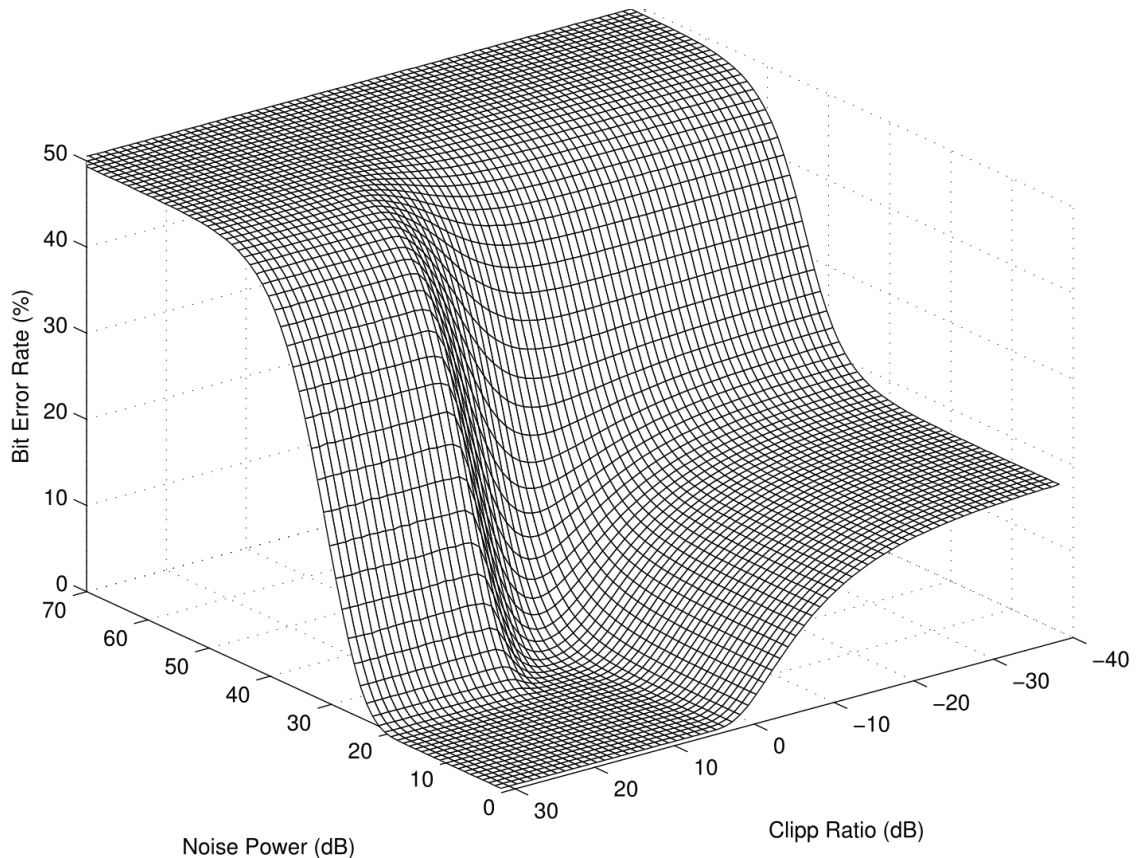


Figure 2.7: Bit error rate vs. clip ratio and noise power. As noise level increases clip ratio should be increased in order to maintain optimum bit error rate.

### 2.3.2 Low Pass Filtering

Inter symbol interference and out of focus lens may be modeled by applying low pass filtering on the captured image. To simulate this out of focus effect, the Butterworth low pass filter in the frequency domain is used with various cutoff frequencies and the resulting BER is measured. Equation 2.6 defines the applied filter.

$$L(u, v) = \frac{1}{1 + (u^2 + v^2)^n / d_0^{2n}} \quad (2.6)$$

The resulting BER-based performance plots using different modulation methods are shown in Fig. 2.8. It can be observed in these plots that the BER increases with lower cutoff frequencies. Here  $D_0 = d_0/N$  defines the cutoff frequency as a percentage of image width ( $N$ ). It can be seen that unless the cutoff frequency is less than 20%, frequency domain modulations have better error performance than the PAM method.

Figure 2.9 shows the effect of 20% filtering on the  $128 \times 128$  DPSK modulated image of Fig. 2.6. Consider the raw data which was mapped to matrix  $\mathbf{S}$  described in 2.2.2. After decoding the signal at the receiver and comparing it to  $\mathbf{S}$ , matrix  $\mathbf{E}$  may be generated to show the location of each detected bit that differs from its corresponding bit in  $\mathbf{S}$ . To show the errors both in real and imaginary parts of  $\mathbf{S}$ , the lower half of  $\mathbf{E}$  provides errors in the imaginary part of  $\mathbf{S}$  while the upper part indicates errors in the real part of  $\mathbf{S}$ . The generated  $\mathbf{E}$  is shown in Fig. 2.10, An interesting point that can be seen here is that unlike PAM modulation, the location of error bits are not distributed randomly. In fact error bits are more concentrated in the high frequency areas of the OFDM based modulation methods.

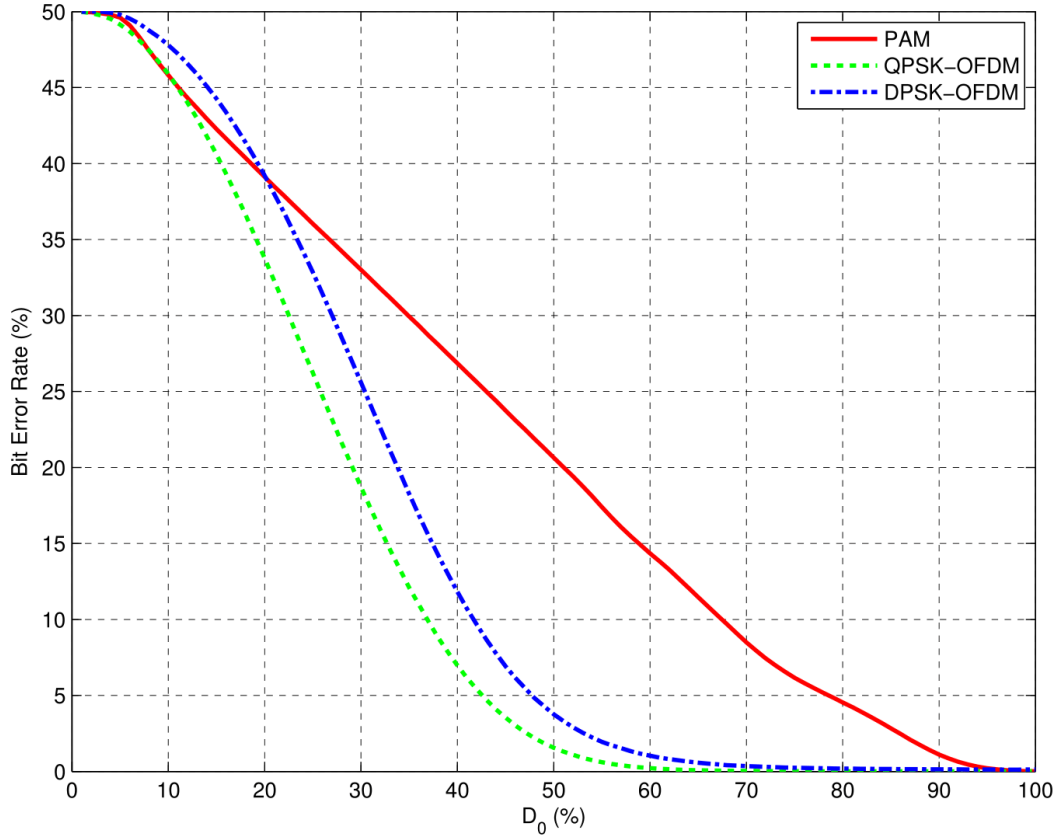


Figure 2.8: Effect of low pass filtering on BER performance. When cutoff frequency is higher than 20%, OFDM based methods are superior to the PAM method.

### 2.3.3 Camera movement

Assuming linear image motion in  $x$  and  $y$  directions and instantaneous shutter opening and closing, the motion may be modeled by the following transfer function as described in [GW07]:

$$H(u, v) = \frac{T}{\pi(ua + vb)} \sin[\pi(ua + vb)] e^{-j\pi(ua+vb)} \quad (2.7)$$

where  $T$  is the exposure time, the  $a$  and  $b$  elements are the assumed image movements in the  $x$  and  $y$  direction respectively during the exposure time. As can be observed, this transfer function consists of a sinc function which is in fact blurring the image due to motion and a translation function which shifts the image. To asses only the

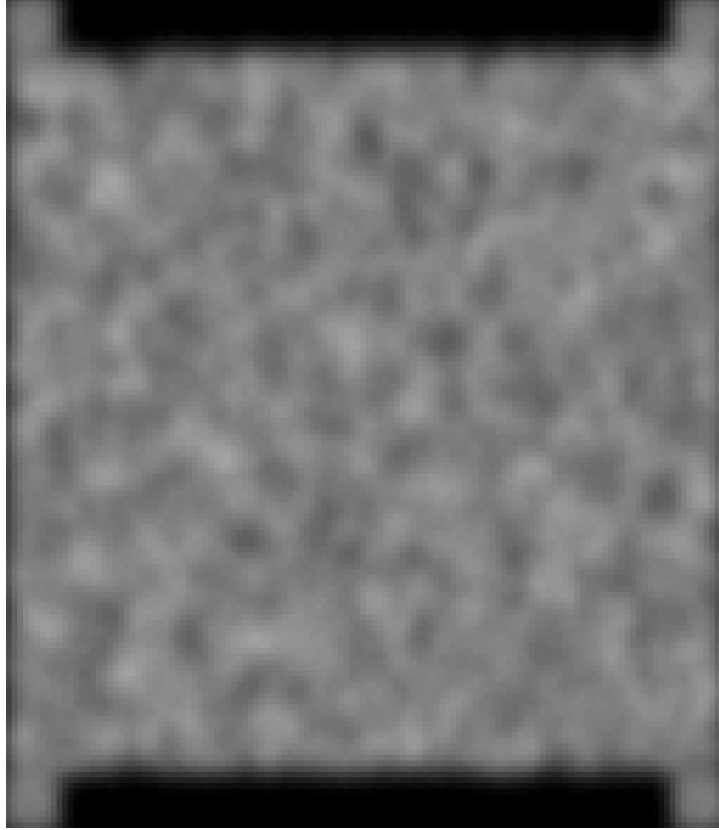


Figure 2.9: 20% Butterworth filter applied to DPSK modulated signal

effect of camera motion it is supposed that the received image is ideally located and registered at the receiver end. So by shifting the image half the induced camera motion, the processed image would be at the exact same location of the transmitted image but is blurred due to motion. Figure 2.11 shows the effect of linear motion with and without the translation portion. Thus the following centralized transfer function is used to simulate the camera motion effect:

$$H_c(u, v) = \frac{T}{\pi(ua + vb)} \sin[\pi(ua + vb)] \quad (2.8)$$

It was already shown that OFDM based modulations have a great advantage over PAM modulation in dealing with image blur. The QPSK-OFDM had a slight advantage over DPSK-OFDM in that case. However, when the camera motion



Figure 2.10: Location of erroneous bits. White areas are detected correctly

effect is considered, DPSK-OFDM shows its superiority. When  $H_c$  is applied to the received image in the frequency domain it may attenuate some elements resulting in SINR decrease or it may reverse the phase of the original elements resulting in constellation rotation and hence in error bits. Frequency attenuation in sub channels is something that affects both OFDM methods. On the other hand, constellation rotation does not affect DPSK-OFDM decisively because the sign of  $H_c$  would be the same for adjacent sub channels unless  $H_c$  is near zero where attenuation would dominate the capability of the system in detecting the modulated data.

The linear motion described by Eq. 2.7 can be considered as a motion of magnitude  $r = \sqrt{a^2 + b^2}$  and angle  $\theta = \arctan(\frac{a}{b})$ . The  $H_c$  transfer function for each magnitude and angle is calculated using Eq. 2.8. Two dimensional plots of BER for



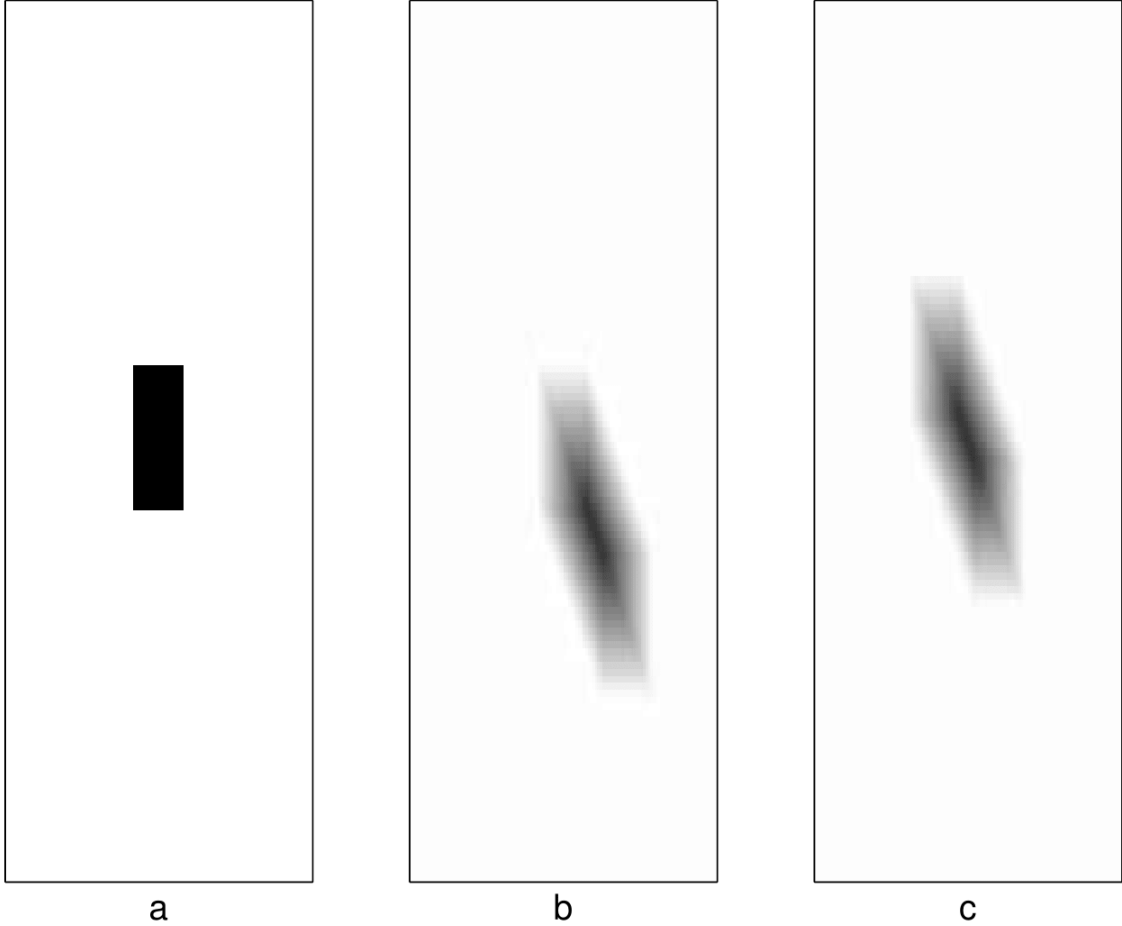


Figure 2.11: (a) Sample image. (b)  $H(u, v)$  applied. (c)  $H_c(u, v)$  applied.

different  $r$  and  $\theta$  are shown in Figs. 2.12, 2.13 and 2.14.

BER for OFDM and PAM modulations introduces oscillations as a function of motion's magnitude and angle due to the sampling point residing between transmitted pixels. In order to eliminate these oscillations, sub-pixel registration measures are required as described in [BOO98].

In the proposed DPSK-OFDM method BER is maximized as  $\theta$  reaches about  $\pi/2$ . This is the case where the motion is perpendicular to the differential phase modulation path. Because vertical phase difference of the elements is what transfers data, if the movement is in the vertical direction, then errors may emerge. On

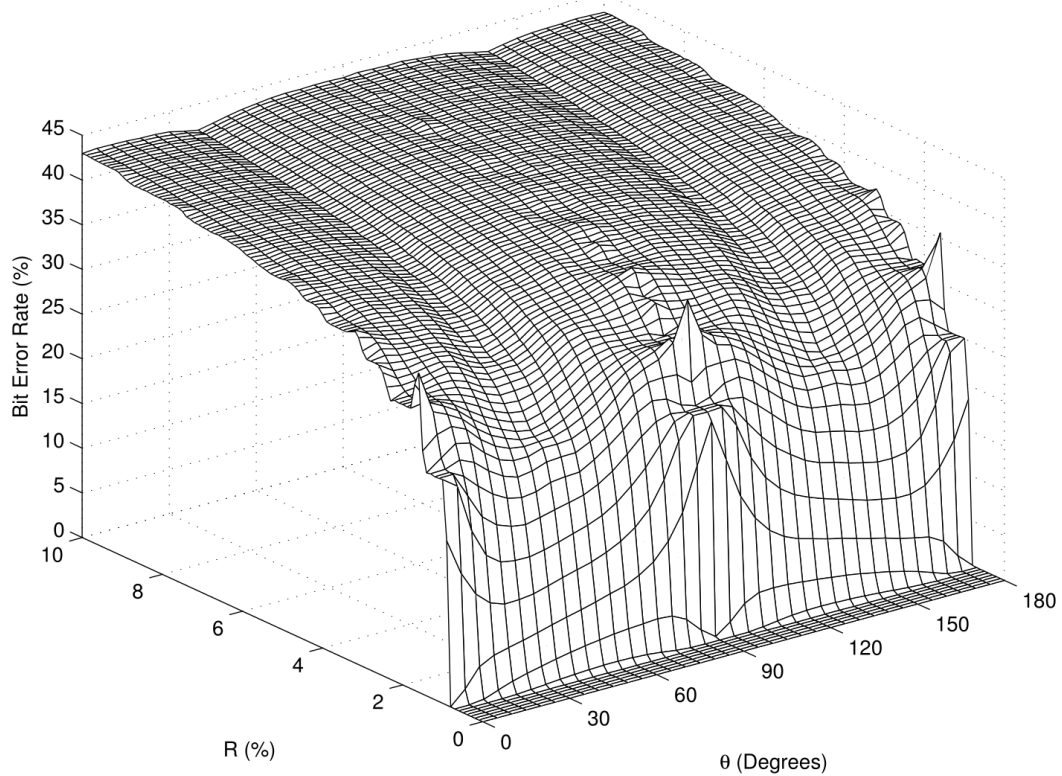


Figure 2.12: BER for various  $r$  and  $\theta$  in PAM modulation

the other hand, if the movement is horizontal it is not going to change the phase differences of elements in two consecutive rows, thus no error is generated (The errors, if any, in that case will be due to amplitude attenuation). Exact vertical movement has slightly less error rate in Fig. 2.14 due to the fact that the first row is modulated horizontally and vertical movement has minimal effect on it.

Because in practical data transmission scenarios frame to frame relative movement of camera and LCD may be considered uniformly distributed over different angles, it is safe to average the BER over  $\theta$  where  $0 \leq \theta < \pi$ . This result is shown in Fig. 2.15 for  $128 \times 128$  image.

This is where DPSK modulated OFDM shows its promising capabilities in mitigating aggressive relative movements between transmitter and receiver. Moreover it should be noted that in Fig. 2.15, PAM modulation is using about 5dB more

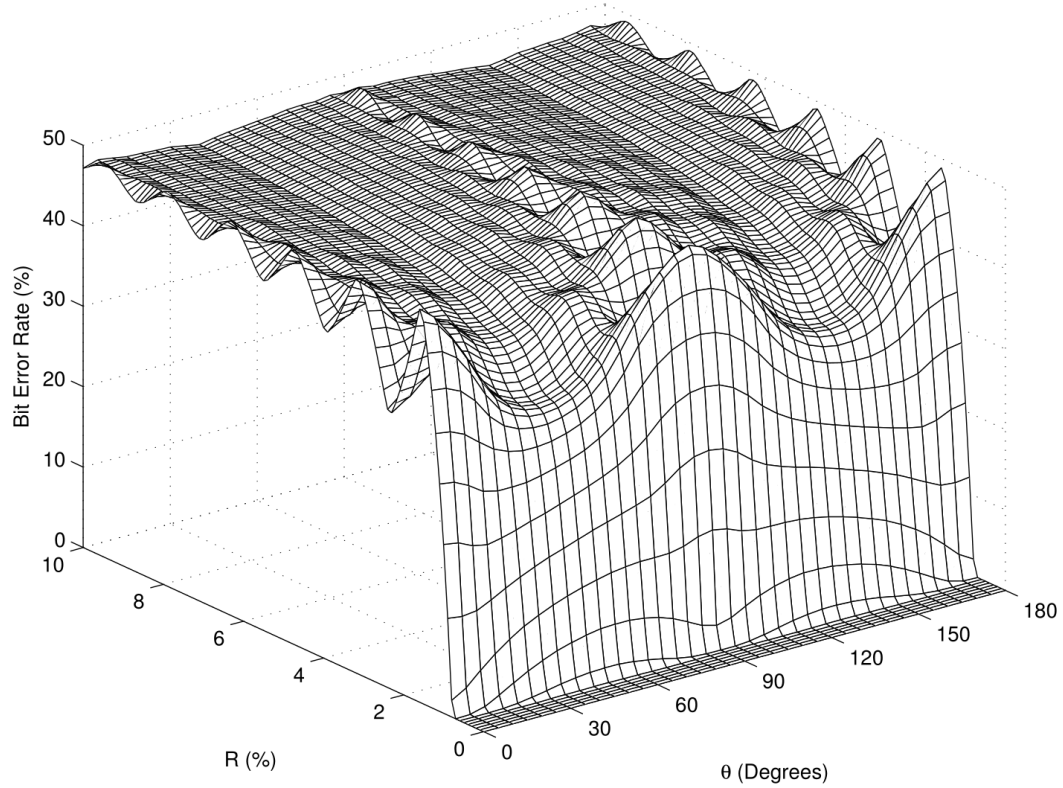


Figure 2.13: BER for various  $r$  and  $\theta$  in QPSK-OFDM modulation

average power than OFDM and DPSK methods. This is due to the fact that the peak and average power of PAM are the same, and the full intensity range of LCD is utilized. As any practical system would use full power of the LCD, this type of comparison between the three methods is meaningful. Should the SNR for all three methods be the same, BER performance for PAM would be worse than what is shown in Fig. 2.15.

## 2.4 Conclusion

In this chapter, Differential Phase Shift Keying was combined with Orthogonal Frequency Division Multiplexing in order to modulate data stream into visual two dimensional barcodes. It was shown that QPSK-OFDM modulation has serious

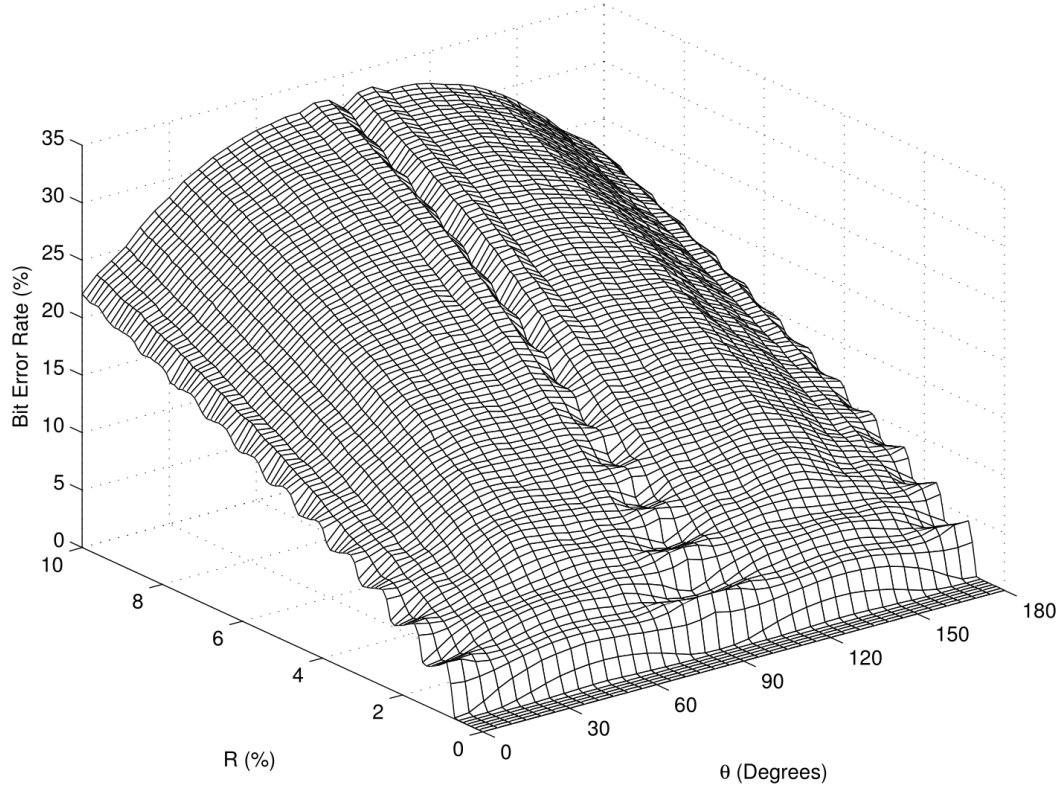


Figure 2.14: BER for various  $r$  and  $\theta$  in DPSK-OFDM modulation

shortcomings in the mitigation of camera LCD movements where the phase of each element changes continuously. On the other hand, addition of a differential phase modulator before OFDM to modulate the data stream into phase differences of adjacent elements (DPSK-OFDM) causes the motion effect to increasingly weaken because of its gradual change from element to element, contributing to a small deviation from the ideal phase in the received signal.

It was observed that under relative LCD-camera motions that generate error rates in excess of 30% in PAM and QPSK-OFDM, the proposed system of DPSK-OFDM will maintain an error rate less than 8% which is practically correctable using error correction coding. Future inquiries in a resolution to this problem have to address the best choice of differential pattern to optimize performance for various motion scenarios. Moreover, extension of the current two-bit per symbol constella-

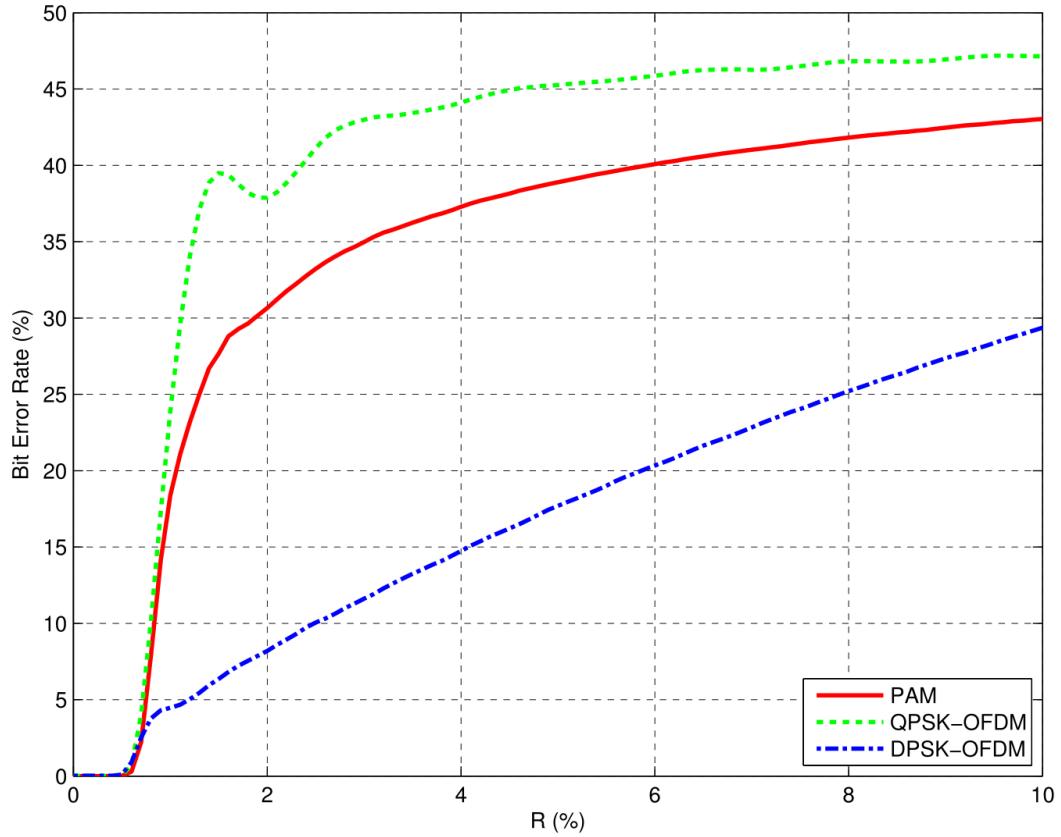


Figure 2.15: BER for various  $r$  averaged uniformly over angle range for three modulation methods studied.

tions increases data transfer capacity, and its BER performance evaluation would be required. Nevertheless, a study on the effect of perspective correction errors on the BER performance of this algorithm compared to the other ones could augment our understanding of its applicability to real world scenarios.

## CHAPTER 3

### RF CLIPPED OPTICAL OFDM

The requirement for fast and reliable wireless communications networks has grown rapidly during the past two decades. Cellular communications as a means of sharing valuable time-frequency resources is the main method of answering this demand. Moreover, with rapid growth of tablet and smart-phone adoption together with the requirements of high quality multimedia sources, it is always a challenge for wireless operators to keep up with this ever-expanding demand. As a result RoF technology has been proposed for distribution of radio signals from a central station (CS) to various base stations (BS) [WNG10]. RoF has the capability of dramatically reducing infrastructure costs as most of the expensive hardware would be kept at the central station and the radio signals can be transmitted over fiber optics medium to relatively long distances without requiring amplification [BCA<sup>+</sup>13]. In the mean time, congestion in current cellular communications bands and high cost of leasing these frequencies has been a great motivation to push the research in finding viable solutions for using higher frequencies in cellular communications.

Abundance of unlicensed low cost frequency bands between 57 to 64 GHz has made mm-wave wireless communication a good candidate for 5G cellular networks [RMA<sup>+</sup>13]. In a typical topology as shown in Fig. 3.1, a single central station connected to fiber backbone can drive numerous base stations covering a large area or different floors of a building. To minimize the cost of high-speed electronics, radio circuits and system maintenance in these networks, it is advisable to concentrate most of the components in the central stations to minimize the costs for the base stations. An ideal solution is for these base stations to serve as the RF front end. In this setup, a base station receives the RF radio signal from the central station and transmits it to the mobile station on the downlink path. For the uplink path,

the base station receives the RF signal from mobile stations and transfers it back to the central station. Ideally, the central station is to send the RoF signal in a way that its detection by a photo detector generates mm-wave radio signal at the base station. This method ensures that no expensive up/down conversion circuitry is required at the base stations.

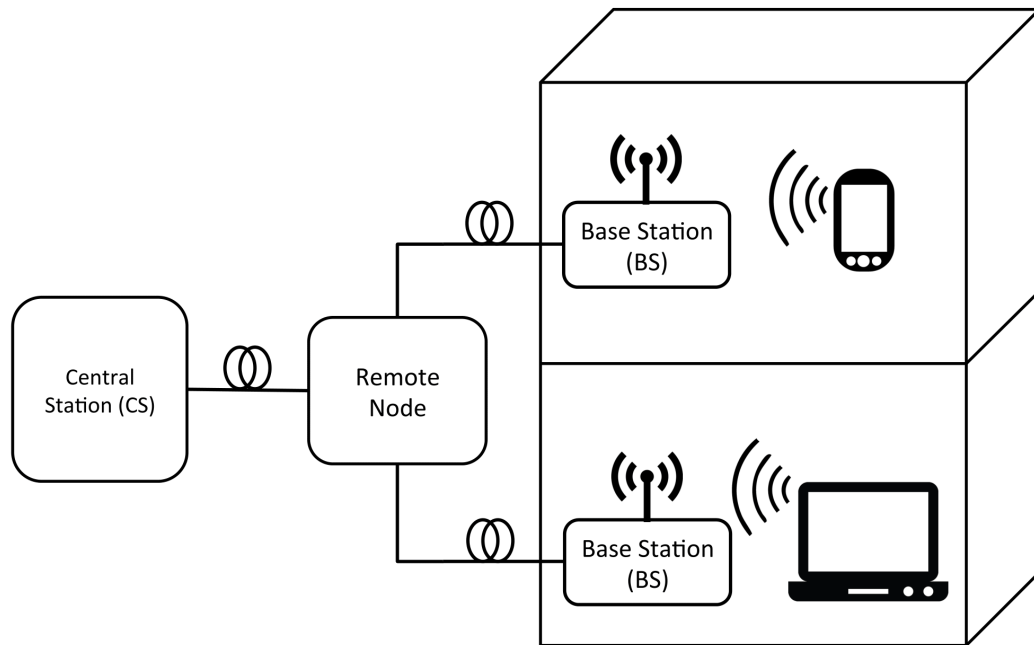


Figure 3.1: In a typical RoF application, mm-Wave signal passes from the central station to the base station through fiber optics, and transmitted to mobile stations by wireless RF transceiver and vice versa.

Thus, the most cost effective optical modulation scheme to use would be the Intensity Modulation/Direct Detection (IM/DD) where the electrical signal modulates the intensity of the laser rather than that of the optical field.

Direct modulation of the laser is a unique way of implementing IM/DD, requiring no additional components. This task requires applying the correctly biased electrical

signal to the input current of the laser. Although frequency chirp and laser nonlinearities greatly limit the performance of direct modulation, its lower cost and lesser complexity serve as great motivation to improve its bandwidth and power efficiency. To enhance direct modulation performance, optical injection may be employed as in [NFP<sup>+</sup>10].

Another method for generating RoF signals is through the use of an external modulator (EM) [LY03]. In this case, the laser itself works in a continuous way, resulting in higher stability. A Mach Zehnder modulator (MZM) or an electro-absorption modulator (EAM) will be able to modulate the laser intensity. The MZM modulator should be biased at quadrature point to achieve optimum performance in terms of linearity and dynamic range [HF05]. Intensity modulation by definition requires unipolar signals as there can be no negative intensity. In all of these methods, we add an appropriate dc bias to the signal to create a unipolar modulation signal. The added dc bias translates into an optical carrier component, which is necessary for direct detection of the signal received by the photo detector. Performing carrier suppression after modulating the signal using a large dc bias is essential in order to achieve better performance and receiver sensitivity.

Currently, orthogonal frequency division multiplexing (OFDM) remains the dominant modulation scheme for wireless and wireline communication systems. That includes current Wi-Fi and LTE (Long Term Evolution) wireless networks as well as DSL (Digital Subscriber Line) and DTV (Digital TV). It is also the default path for future expansion of cellular networks [ABC<sup>+</sup>14]. Consequently, in many RoF applications, we transmit an OFDM signal over the fiber to mitigate channel dispersion in the wireless medium after RF transmission in the base station, as the fiber is usually short enough to have negligible dispersion effects compared to the wireless portion of the signal path. As a result, IM/DD, which normally results



in optical double side band (ODSB) that is less tolerant to fiber dispersion, is still an effective option for RoF applications. However, OFDM signals intrinsically have high crest factor, which depends on the number of subcarriers used. Inevitably, we clip the signal in order to have good power efficiency. It can be shown that the signal power before clipping should be equal to carrier power in order to have optimum performance [SD09].

In this study, we propose an OFDM electrical signal modulated to an RF carrier frequency that is clipped at zero level to create a unipolar signal in which distortion power will be concentrated in the baseband. The clipping would have negligible effect on the RF signal. When peak signal level is limited either by laser power or by EM linearity requirements, the proposed RF clipped optical OFDM (RFCO-OFDM) method achieves higher sensitivity compared to a biased and clipped optical OFDM (BACO-OFDM) even when employing carrier suppression. This means that the proposed RFCO-OFDM method achieves the required Q-factor under lower optical signal to noise ratio (OSNR) conditions.

With this retrospective, the structure for the remainder of this chapter is as follows: Section II introduces the mathematical framework to prove that zero clipping of the OFDM RF signal creates a unipolar signal with much of the resulting distortions concentrated in baseband. Section III provides the derivations of the limits on the in-band distortion such that the effects of zero clipping are negligible. Section IV discusses the parameters affecting the simulated systems. Section V presents the simulation results that exemplify improvements achieved under various conditions. Section VI provides concluding remarks and suggestions for future work.

### 3.1 RFCO-OFDM

The previous section provided a retrospective on the various methods for implementing a RoF system; however, intensity modulation for its lower cost and lesser complexity is of interest here. In a typical IM/DD RoF scheme, the base band OFDM signal modulates the RF carrier. The resulting RF signal with the added dc bias is hence used to either modulate the input current of a laser diode directly or the laser light using an external modulator.

In the proposed RFCO-OFDM, instead of adding a dc bias to make the modulating signal unipolar, we clip the RF electrical signal at zero level before modulating the laser. Fig. 3.2 illustrates the block diagram of the proposed system. Clipping the RF signal thus creates a distorted signal which, based on Busgang's theorem, has two component as discussed in [OI02b] and [DSH12b]. The first component is a scaled version of the input signal, with an amplitude attenuated by a factor of two. The other is the distortion component, which is uncorrelated to the first component and hence uncorrelated to the input signal. This uncorrelated component, as proven through the derivations presented next, has most of its power in the baseband frequencies; and if the carrier frequency is high enough compared to the bandwidth of the OFDM signal, the distortion can be effectively filtered out.

#### 3.1.1 Zero clipping an RF signal

Suppose  $s(t)$  is the time domain representation of an arbitrary baseband signal with bandwidth  $B$ . As a result  $S(f)$  which is the frequency domain representation of  $s(t)$  is zero if  $|f| \geq B$  where  $2B$  is the passband bandwidth of the signal. As depicted in Fig. 3.2, this signal modulates an RF carrier at frequency  $f_c$ , with the resulting signal being:

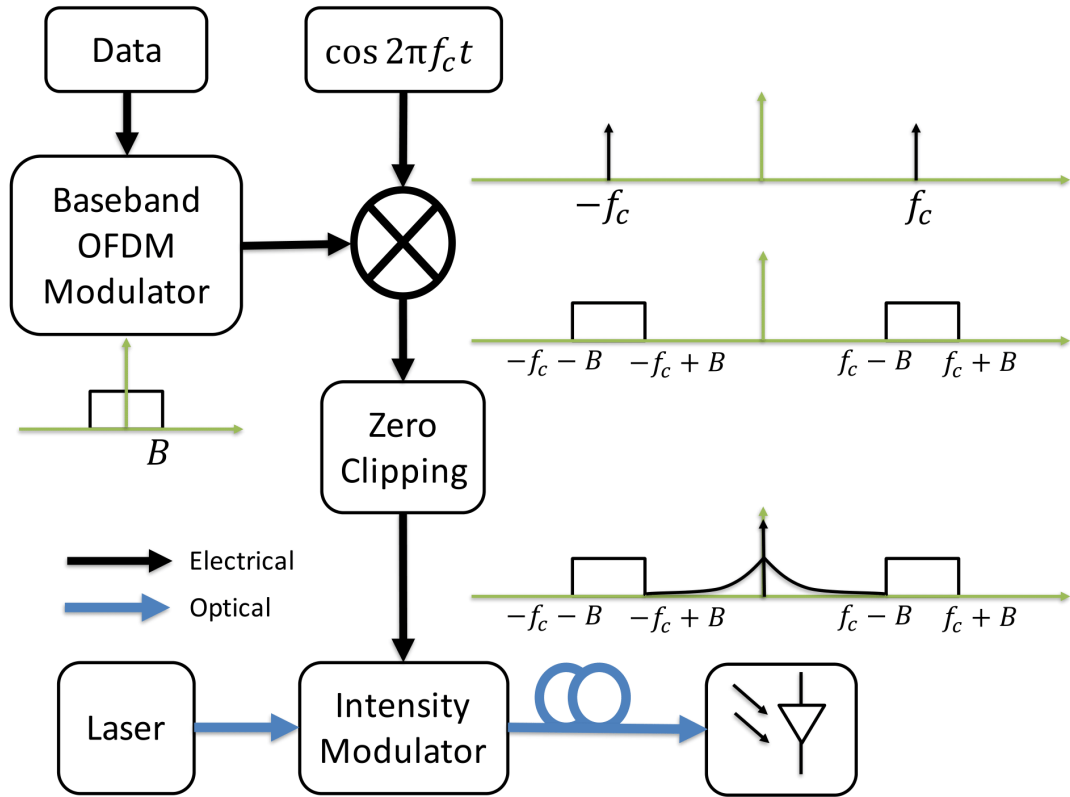


Figure 3.2: Proposed system structure, an optical filter along with optical amplifier may be used after intensity modulator for carrier suppression.

$$x(t) = s(t) \cos(2\pi f_c t) \quad (3.1)$$

By discarding the negative portion of  $x(t)$ , we express the  $x^+(t)$  signal as follows:

$$x^+(t) = \frac{x(t)}{2} + \frac{|x(t)|}{2} \quad (3.2)$$

The first term is a scaled copy of the signal  $x(t)$ , which carries the desired data and is detected by the receiver. The second term  $|x(t)|/2$  is the distortion caused by clipping. If the power of  $|x(t)|$  can be decreased arbitrarily at the desired modulated subcarriers in  $x(t)$ , then clipping is not going to affect the SNR of the received signal, except for the .5 amplitude attenuation, as suggested in (3.2).

### 3.1.2 Resulting distortion

The absolute value denoted by  $|\cdot|$ , is a nonlinear function that generates all even harmonics of the input signal at its output. However, for a bandpass  $x(t)$  in (4.1),  $|x(t)|$  is:

$$|x(t)| = |s(t)| |\cos(2\pi f_c t)| \quad (3.3)$$

This can be interpreted as sampling  $|s(t)|$  through the use of  $|\cos(2\pi f_c t)|$ . To determine the resulting distortions in the frequency domain, we know that the highest frequency component in  $s(t)$  is at  $B$ . Passing  $S(t)$  through the nonlinear absolute value function creates harmonics with higher frequencies. Without loss of generality, we assume that  $-1 < s(t) < 1$ . The absolute value function may be represented by the sum of its basis functions as detailed in [MH02] in the following way:

$$|x| = \frac{2}{\pi} - \frac{4}{\pi} \sum_{b=1}^{\infty} \frac{(-1)^b T_{2b}(x)}{-1 + 4b^2} \quad (3.4)$$

where  $T_n(x)$  is Chebyshev polynomial of the first kind of degree  $n$ . There are different explicit expressions for these polynomials [Pra04]. For  $T_n(x)$  we have:

$$T_n(x) = \frac{n}{2} \sum_{k=0}^{\lfloor \frac{n}{2} \rfloor} (-1)^k \frac{n}{n-k} \binom{n-k}{k} 2x^{n-2k}, \text{ for } n > 0 \quad (3.5)$$

Therefore, it is evident that if we assume a low-pass signal band limited to  $B$  into this nonlinear system polynomial, the output cannot have any components above  $nB$  frequency, which is the degree of the polynomial times the maximum frequency in the baseband signal. Considering that  $n$  goes to infinity in (3.4), for this method to work properly,  $T_n(x)$  should diminish considerably as  $n$  increases.

## 3.2 Limits on distortion

Next step is to find limits on the amount of high frequency harmonics after the application of the nonlinear absolute value function. Consider an arbitrary constant  $\alpha$  to be the largest integer such that the following holds:

$$2\alpha B < f_c - B \quad (3.6)$$

As a result harmonics generated by the first  $\alpha$  basis functions, accumulate up to frequency  $2\alpha B$  and are not going to affect data bearing frequency range from  $f_c - B$  to  $f_c + B$ . Subsequently,  $\hat{s}(t)$  defined as an estimate of  $|s(t)|$  using the first  $\alpha$  Chebyshev polynomial terms (up to  $T_{2\alpha}(x)$ ) can be evaluated as:

$$\hat{s}(t) = \frac{2}{\pi} - \frac{4}{\pi} \sum_{b=1}^{\alpha} \frac{(-1)^b T_{2b}(s(t))}{-1 + 4b^2} \quad (3.7)$$

Thus

$$|s(t)| = \hat{s}(t) + Er(t) \quad (3.8)$$

Where  $Er(t)$  is the error in estimating  $|s(t)|$ . Figure 3.3 shows Chebyshev polynomial approximation of  $|x|$  for  $\alpha = 2$ . As can be seen, the truncated Chebyshev series closely follows the  $|x|$  function with maximum error happening around 0.

The absolute value of error,  $|Er(t)|$ , is bounded by the Chebyshev truncation theorem [Boy00]:

$$|Er(t)| \leq \frac{4}{\pi} \sum_{b=\alpha+1}^{\infty} \left| \frac{(-1)^b}{-1 + 4b^2} \right| \quad (3.9)$$

Which is the sum of the absolute values of all the remaining Chebyshev polynomial coefficients not used in the approximation. Calculating the infinite sum results in the following relation:

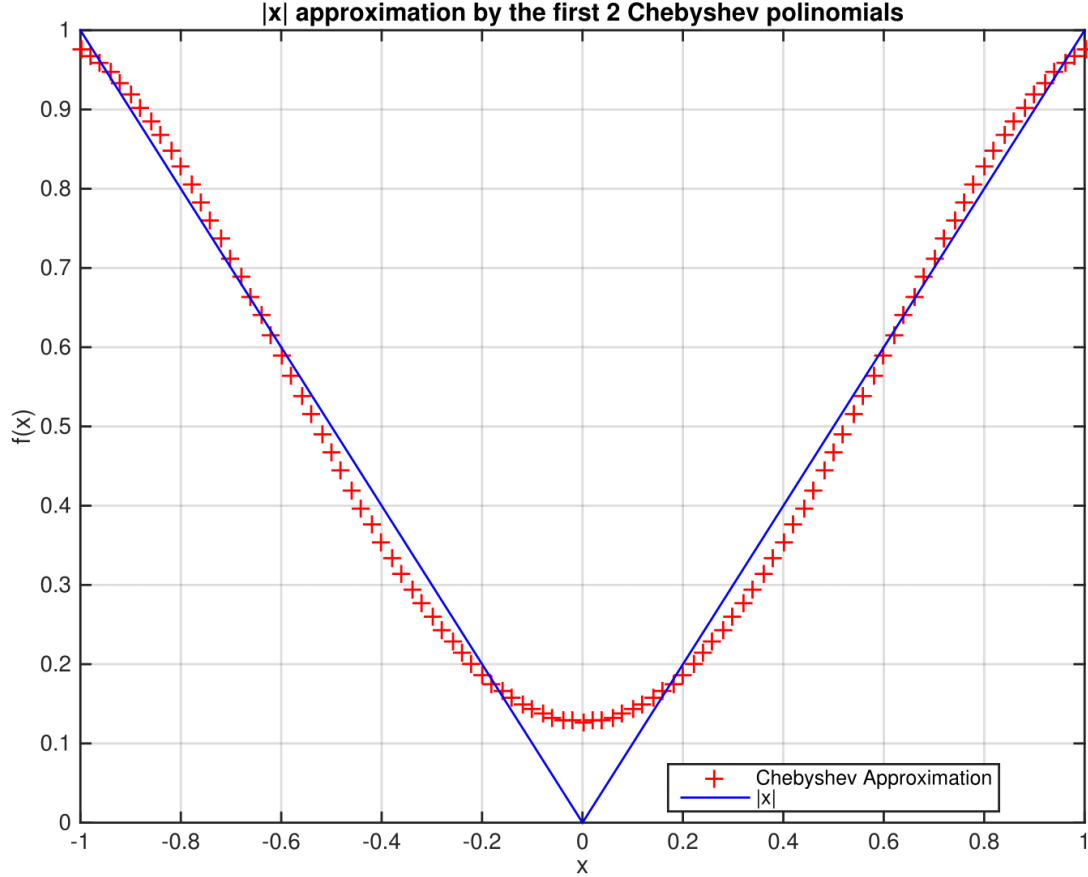


Figure 3.3: Approximation of  $|x|$  using Chebyshev polynomials and  $\alpha = 2$ . Only  $T_2(x)$  and  $T_4(x)$  are used in this approximation.

$$|Er(t)| \leq \frac{1}{\pi(\alpha + \frac{1}{2})} \quad (3.10)$$

The error for the whole  $[-1, 1]$  range is shown in Fig. 3.4 for  $\alpha = 2, 5, 10$ . The maximum of each plot, which is at the zero input level, exactly matches the predicted value from (3.10).

It can be shown that by selecting an appropriate value for  $\alpha$  the in-band distortions caused by clipping the RF signal would be limited to arbitrarily small values as predicted by (3.10). On the other hand, equation (3.6) can be rewritten as:

$$\frac{f_c}{B} > 2\alpha + 1 \quad (3.11)$$

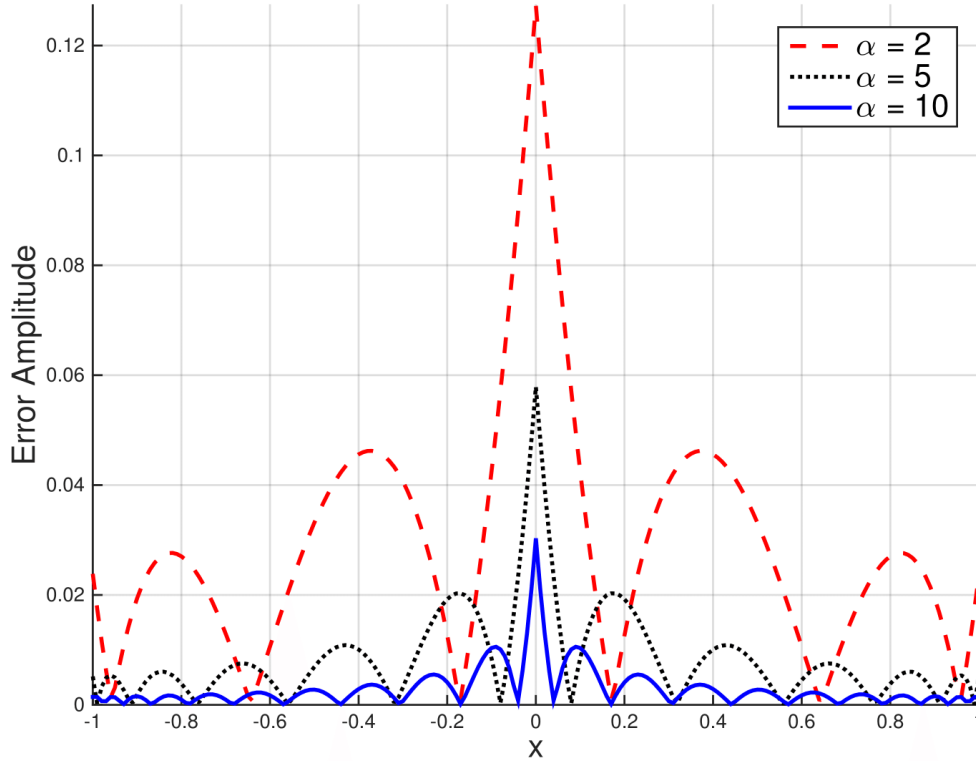


Figure 3.4: Error in different approximations of  $|x|$ . Error amplitude is inversely proportional to the number of Chebyshev polynomials used in the approximation.

The use of equations (3.10) and (3.11) will determine the required carrier to bandwidth ratio for the system to work in a way that its performance is limited by receiver noise level instead of by clipping distortion. In fact, considering that these systems generally use an analog to digital converter (ADC) with limited resolution in the receiver, maximum error in the time domain samples can be lowered to become comparable to the quantization level of the ADC.

For example, a 6-bit ADC used to digitize the  $[0 \ 1)$  range has a quantization level of  $1/64$ . This in turn is equivalent to  $\alpha \geq 20$  from (3.10). Hence, carrier to bandwidth ratio should be greater than 41. This means that a 1.46 GHz signal could modulate a 60 GHz carrier frequency and then clipped at zero with in-band distortions less than the quantization error of the ADC at the receiver.

This particular example serves as a rather conservative way for calculating the signals bandwidth. In the next section, we demonstrate that even with much lower carrier to bandwidth ratios, the resulting in-band distortions will be less significant in comparison to a clipped OFDM signal biased at the optimum dc level.

### 3.3 Parameters Affecting performance

Performance analysis of optical communication systems traditionally uses Q-factor instead of SNR. It is mainly because that for on-off keying (OOK) modulation used in fiber communications, shot noise would be different for on and off states. The Q-factor takes that into account this difference and gives a realistic sense of signal quality which can easily be translated into bit error ratio (BER). The Q-factor for an optical OFDM system can similarly be defined using the signal constellation points as in [LDA07]:  $q = \mu_x/\sigma_x = \mu_y/\sigma_y$  where  $\mu$  is the mean and  $\sigma$  is the standard deviation in each direction assuming the decision threshold levels are on  $x = 0$  and  $y = 0$ . This definition results in the BER being simply  $Q(q)$  where  $Q(\cdot)$  is the normal Q-function [PS08].

In this section it is considered that the external modulator is biased at quadrature point which is the best bias point in terms of available linear dynamic range [SBC<sup>+</sup>10]. Although modulator nonlinearities are not considered here for the sake of simplicity, they can be fairly compensated using pre-distortion techniques as described in [KWM<sup>+</sup>05]. System performance through simulations is affected by various parameters that are discussed next.



### 3.3.1 OFDM Modulator

Constellation size does not have a meaningful effect on the optimum bias and clipping levels of normal optical OFDM as discussed in [CKE12]. The assumption is that frequency difference between subcarriers  $\Delta f$  is constant and will depend on particular transmission channels parameters. For a RoF system,  $\Delta f$  generally should meet the requirements of the wireless radio channel between base and mobile station. As a result, increasing the number of subcarriers translates into higher bandwidth. Considering a fixed carrier frequency, the carrier to bandwidth ratio changes, which in turn affects the in-band distortion noise for RFCO-OFDM signals as predicted by (3.11) and (3.10).

Most of the experimental RoF systems use the whole 57 to 64 GHz bandwidth proposed for mm-wave radio applications. However the number of subcarriers utilized is different depending on the application; for example 37 subcarriers are used in [JLN<sup>+</sup>10] while 32 and 128 are both implemented in [SMAB15] and 480 subcarriers in [AAI<sup>+</sup>14]. It is generally accepted that more than 64 carriers are sufficient for the OFDM symbol to have Gaussian amplitude. In this study, 250 subcarriers are considered with a  $\Delta f$  of 10MHz, which corresponds to 5GHz of RF bandwidth. In an alternates case, 150 carriers are also used to study the effect of lower 3GHz RF bandwidth.

### 3.3.2 Biasing and Clipping

With different peak to average power ratio, the optimum bias and clipping level would be different for every OFDM frame. Some systems rely on adding sufficient bias to eliminate clipping and make it a statistically rare event, which is not power efficient. However, simultaneous biasing and clipping can result in optimum perfor-

mance in term of overall BER. Optimum levels can be found by exhaustive search for every symbol, and theoretical optimum bias levels are thoroughly studied in [CKE09]. A general rule is that half of the power should be devoted to the optical carrier [SD09].

Dc bias level and subsequent clipping have a great impact on power efficiency and distortion as revealed in [DSH12b, ZZ14]. OFDM clipping is often considered in the normalized form of clipping ratio:

$$\gamma = \frac{V_{clipp}}{\sigma} \quad (3.12)$$

Where  $V_{clipp}$  is the clipping threshold and  $\sigma$  is the standard deviation of the electrical OFDM signal. Considering the driving voltage to be in the 0 to 1 range, the external modulator is biased at .5, which corresponds to half its maximum intensity. Thus  $V_{clipp}$  is fixed at .5 and  $\sigma$  is adjusted by scaling the input OFDM signal to achieve the desired  $\gamma$  level. The resulting signal then mapped to the actual input range of the external modulator. We define modulation index to be the standard deviation of this electrical signal as a percentage of the input range for the intensity modulator. The input range is in fact the the range of electrical signals that drive the modulator from 0 to 100% intensity.

To have a fair comparison, we consider that the total transmitted optical power is the same for both systems where a power amplifier is involved. Because in IM the laser intensity is proportional to the input signal voltage, the average optical power is assumed proportional to  $E[x(t)]$  and not  $E[x^2(t)]$  [LRBK09]. As a result, the dc bias level determines the average optical power, and by setting it to half the maximum intensity, every simulation uses the same average optical power.

### 3.3.3 Optical Amplifier

For long haul communications, optical amplifiers are required to occasionally boost signal power along the fiber. However in short range applications it is possible to use the optical output of the external modulator paired with a sufficiently powered laser without amplification as suggested in [NS09]. As a result, we consider two cases here. The first, no optical amplifier is involved, which imposes no carrier suppression, and signal power is directly determined by laser power and modulation index. In this case the proposed method of RF clipping is expected to be a power efficient alternative for biased OFDM. The second case is when an optical amplifier is used after external modulation along with carrier suppression as proposed in [LDA07]. In this case, carrier suppression can enhance the power efficiency of the biased OFDM method by decreasing the power wasted on optical carrier. However, the proposed method of RFCO-OFDM still outperforms the suppressed carrier optical OFDM. Modulation indexes less than 10% are not practical, as they require very high gain amplifiers in order to create the required signal power. As a result 12% modulation index is selected along with a 23dB carrier attenuation as proposed by [LDA07].

### 3.3.4 Noise

In most practical direct detection systems, thermal noise is much larger than quantum shot noise and determines the performance of the receiver [RSS10]. However, in RoF systems, detection is not performed at the optical receiver, and the signal is relayed to the radio receiver over wireless RF channel rendering the base station node as a non-regenerative amplifier. As a result, the RoF system should have a high quality signal at the photo detector so that there are no significant distortions with the resulting RF signal before its transmission through the wireless channel.

Therefore, RoF systems can be considered similar to analog optical communications systems in which higher signal to noise ratio is required compared to digital systems [Ale97]. Consequently, in these systems intensity noise of the laser and the amplified spontaneous emission (ASE) of optical amplifier limit the performance of the system. For simplicity, we consider that as an effective additive Gaussian noise in electrical field [GM90] and its power is set by Optical SNR (OSNR).

### 3.4 Simulation

In measuring the Q-factor as the definitive performance factor, more than  $10^5$  random bits were modulated into both systems and an average Q-factor for each data point is measured. As discussed earlier, two different scenarios were simulated:

#### 3.4.1 Without optical amplifier

In RoF applications where no optical amplifier is used, there is no advantage in implementing carrier suppression, and we compute the output signal power using the modulation index along with input optical power. As a result, biased OFDM cannot benefit from high output power and low distortion simultaneously. If modulation index is set too high, clipping distortion will be high and if it is set too low, signal power will be low.

The output optical power of a BACO-OFDM modulator is set to half intensity when biased at quadrature point while the output optical power of the RFCO-OFDM depends on the modulation index. Figure 3.5, demonstrates the power dependence on the modulation index. The plots show how much the output optical power of BACO-OFDM is higher than RFCO-OFDM. The highest curve corresponding to

the case without carrier suppression shows BACO-OFDM has a much higher optical power in low modulation indexes.

Increasing modulation index increases the output optical power in RFCO-OFDM. This particular behavior is due to the fact that average output power in BACO-OFDM remains the same and does not depend on modulation index. On the other hand, for RFCO-OFDM the average output power increases by increasing modulation index because higher dc value in the zero clipped signal. However increasing the modulation index also increases the probability of signal highs being clipped. Considering that on average half of the output samples are zero and the other half at most have the full intensity, the average output optical power of RFCO-OFDM is limited to half the intensity which is equal to BACO-OFDM. Thus, as the modulation index increases, both systems tend to have the same output optical power.

In practice an OSNR of around 20dB is required to have a reliable link performance [RSS10]. On the other hand, Q-factor should also be higher than 7 to have a negligible bit error rate. Thus, the modulation index that cannot achieve a Q-factor of 7 is not desirable. Figure 3.6 shows the Q-factor in the absence of noise (due to clipping only) for various modulation indexes. As can be seen in Fig. 3.6, systems achieve almost the same Q-factor for higher modulation indexes.

However, when modulation index is low, clipping of the peaks in BACO-OFDM becomes a rare event resulting in high Q-factor values. On the other hand, in-band distortion due to zero clipping limits the RFCO-OFDM performance, which clearly depend on the bandwidth of the OFDM signal assuming a fixed carrier frequency.

This situation completely changes when measurements are done at the receiver end. High Q-factors for lower modulation indexes were achieved by dedication a high power optical carrier in BACO-OFDM. However having a fixed OSNR at the receiver results in low signal power for BACO-OFDM. This effect is shown in Fig.

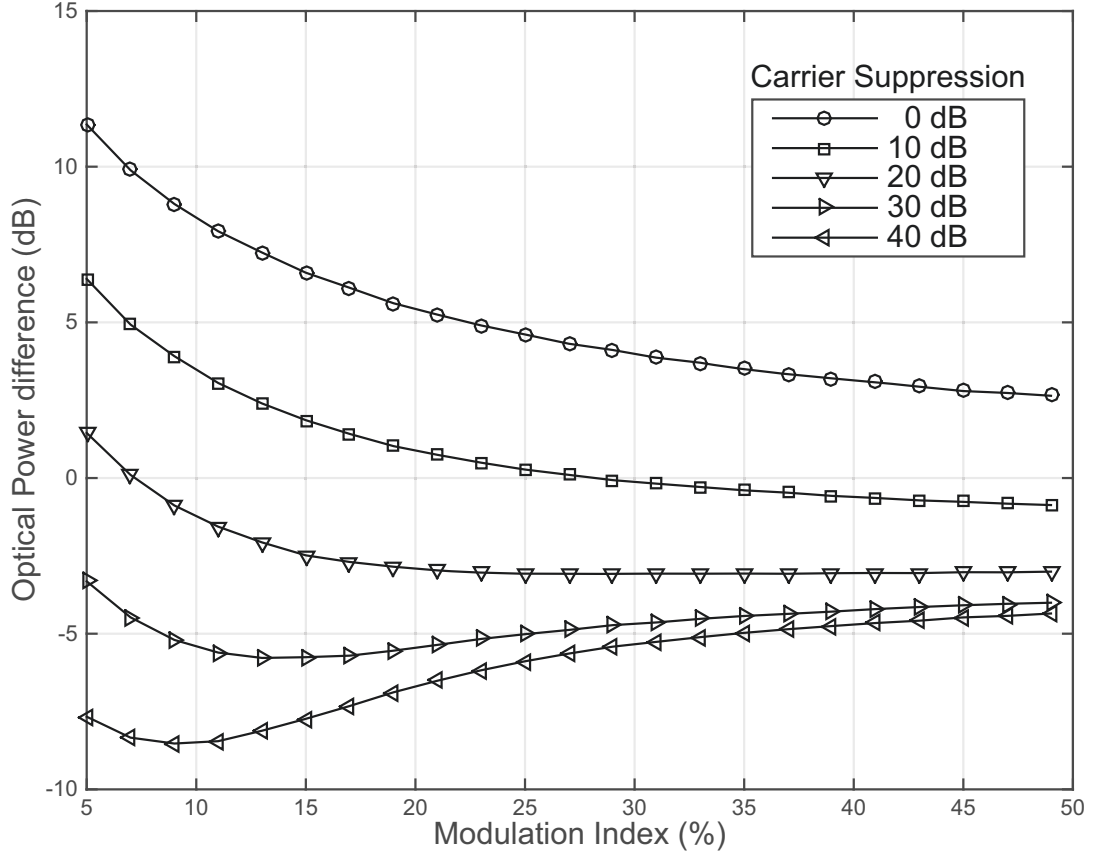


Figure 3.5: Power difference between BACO-OFDM and RFCO-OFDM calculated using  $10\log(P_{BACO}/P_{RFCO})$ .

3.7 where a 20dB OSNR is assumed at the receiver for BACO-OFDM. It should be noted that because of the difference in optical power between two schemes as shown in Fig. 3.5 then OSNR for BACO-OFDM is higher than RFCO-OFDM if the same noise level is present at the receiver.

This situation completely changes if we take the measurements at the receiver end. To achieve high Q-factors for lower modulation indexes, we need to provide high power to the optical carrier in BACO-OFDM. However, having a fixed OSNR at the receiver results in low signal power for BACO-OFDM. Figure 3.7 illustrates this effect with a 20dB OSNR at the receiver for BACO-OFDM. Because of the difference in optical power between two schemes as shown in Fig. 3.5, we observe

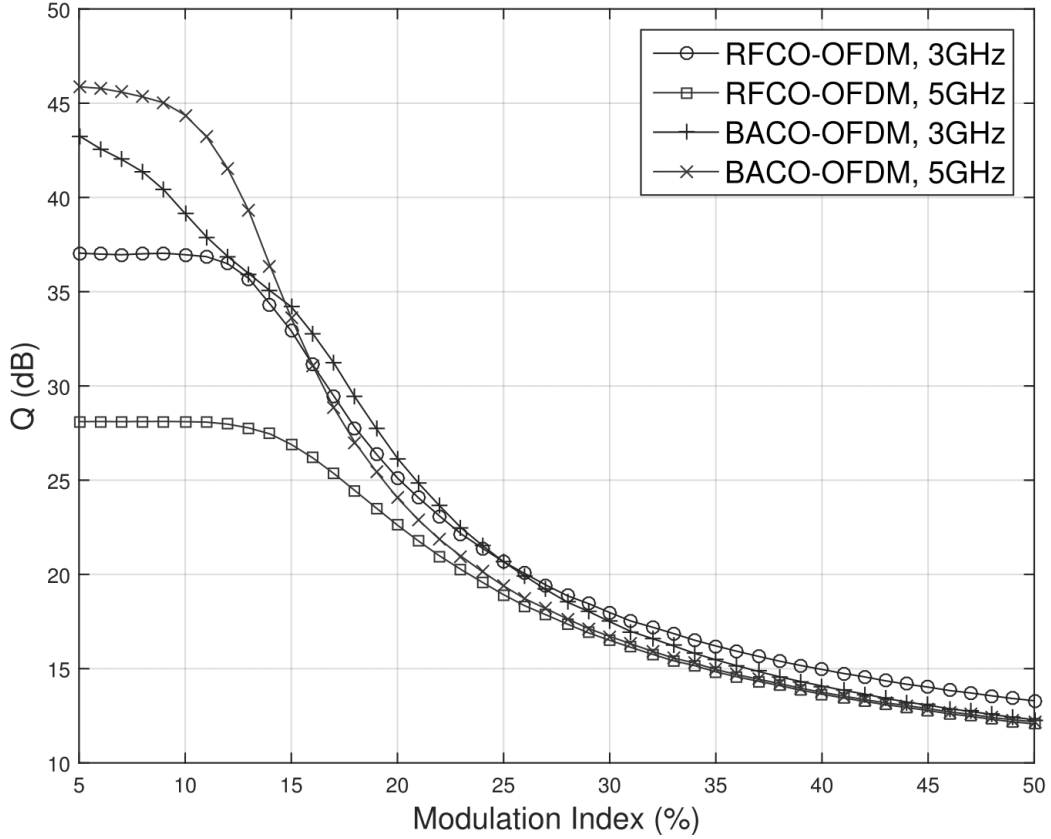


Figure 3.6: Q-factor comparison for two different number of subcarriers corresponding to 5GHz and 3GHz signal bandwidth. It is measured at the output of the modulator where noise power is negligible.

that OSNR for BACO-OFDM is higher than RFCO-OFDM if the same noise level is present at the receiver.

### 3.4.2 With optical amplifier

For applications requiring an optical amplifier after modulating the signal, carrier suppression makes using a low modulation index possible. In such a case, OFDM modulations can benefit from less distortion due to clipping while at the same time carrier to signal ratio can be adjusted to achieve optimum performance. However, carrier suppression is only advantageous in BACO-OFDM where dc bias level and

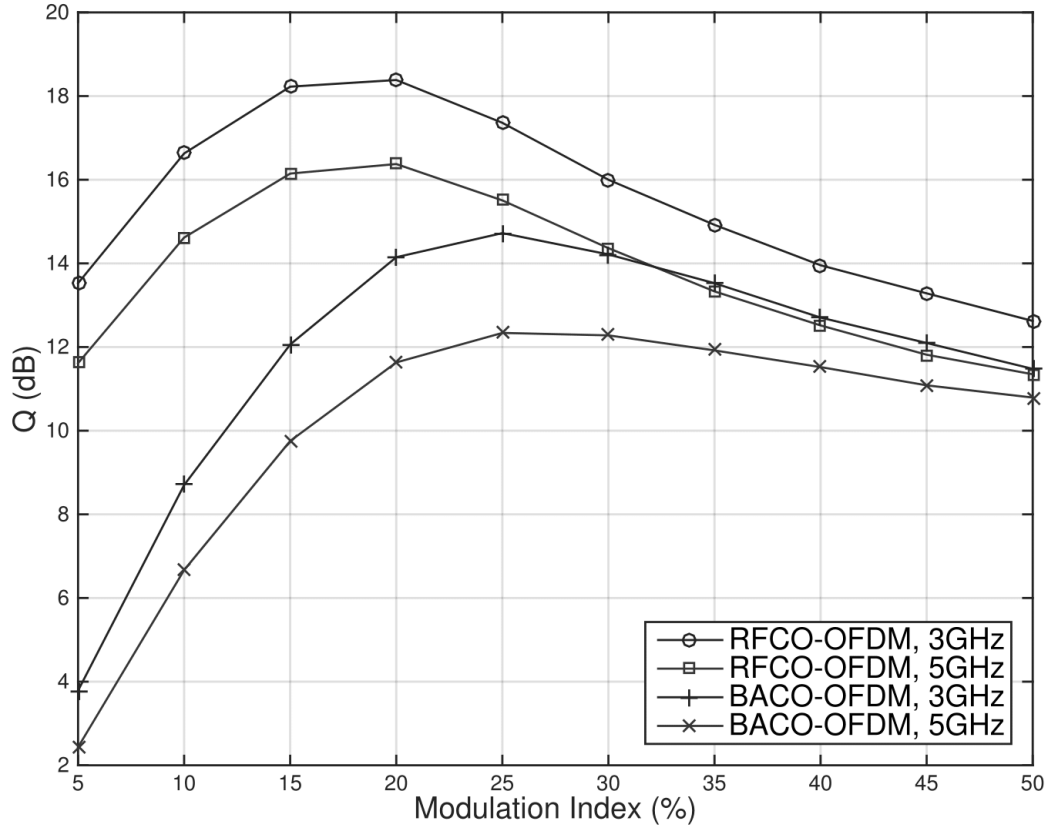


Figure 3.7: Q-factor comparison for two different number of subcarriers corresponding to 5GHz and 3GHz signal bandwidth. Measurements are done at the receiver input considering a 20dB OSNR for BACO-OFDM.

modulation index are independent. In RFCO-OFDM, bias is created by clipping the signal at zero, depending as a result on signal power. For low modulation indexes where clipping is negligible, dc bias for RFCO-OFDM is proportional to modulation index. As a result, suppressing carrier in RFCO-OFDM actually decreases its performance unlike on BACO-OFDM.

Figure 3.8 shows Q-factor for various modulation indexes and carrier suppression ratios in BACO-OFDM. As can be seen here, the higher modulation indexes require less carrier suppression to achieve their respective maximum Q-factors. However, they tend to have lower Q-factors due to clipping noise resulting from increased probability of reaching the clip level.



On the other hand, lower modulation indexes can achieve higher Q-factors because clipping becomes a rare event. In the mean time lower modulation index results in a strong optical carrier component which requires higher carrier suppression and optical amplification to obtain optimum performance. A suppression ratio of 23dB along with an 11% modulation index achieves good performance while the required amplifier gain is still reasonable. Figure 3.5 also shows the difference in optical power between RFCO-OFDM and BACO-OFDM for various modulation indexes and carrier suppression levels. As can be observed, RFCO-OFDM requires less amplifier gain to achieve the same power level as BACO-OFDM for practical carrier suppressions of higher than 20dB and modulation indexes of higher than 6%.

Figure 3.9, shows a comparison between Q-factor from BACO-OFDM with a carrier suppression of 23dB and RFCO-OFDM for various modulation indexes. Consider that both systems are taking advantage of optical amplifiers, thus in RFCO-OFDM lower modulation index is translated into lower clipping probability and does not mean lower output power. In fact, for modulation indexes lower than 15%, Q-factor for RFCO-OFDM is limited by OSNR rather than clipping noise. However for modulation indexes over 15% clipping noise starts to affect the system performance leading to a decrease in the Q-factor. Note that a modulation index of 11% reaches the maximum Q-factor for BACO-OFDM, which is still more than 6dB below the Q-factor achieved by RFCO-OFDM.

To see the improvement in sensitivity, Fig. 3.10 shows Q-factor under various OSNR conditions. Observe that in order to have a Q-factor of 10dB, BACO-OFDM with carrier suppression of 23dB and 11% modulation index requires about 7 dB more OSNR, which translates into higher sensitivity of the proposed RFCO-OFDM system.

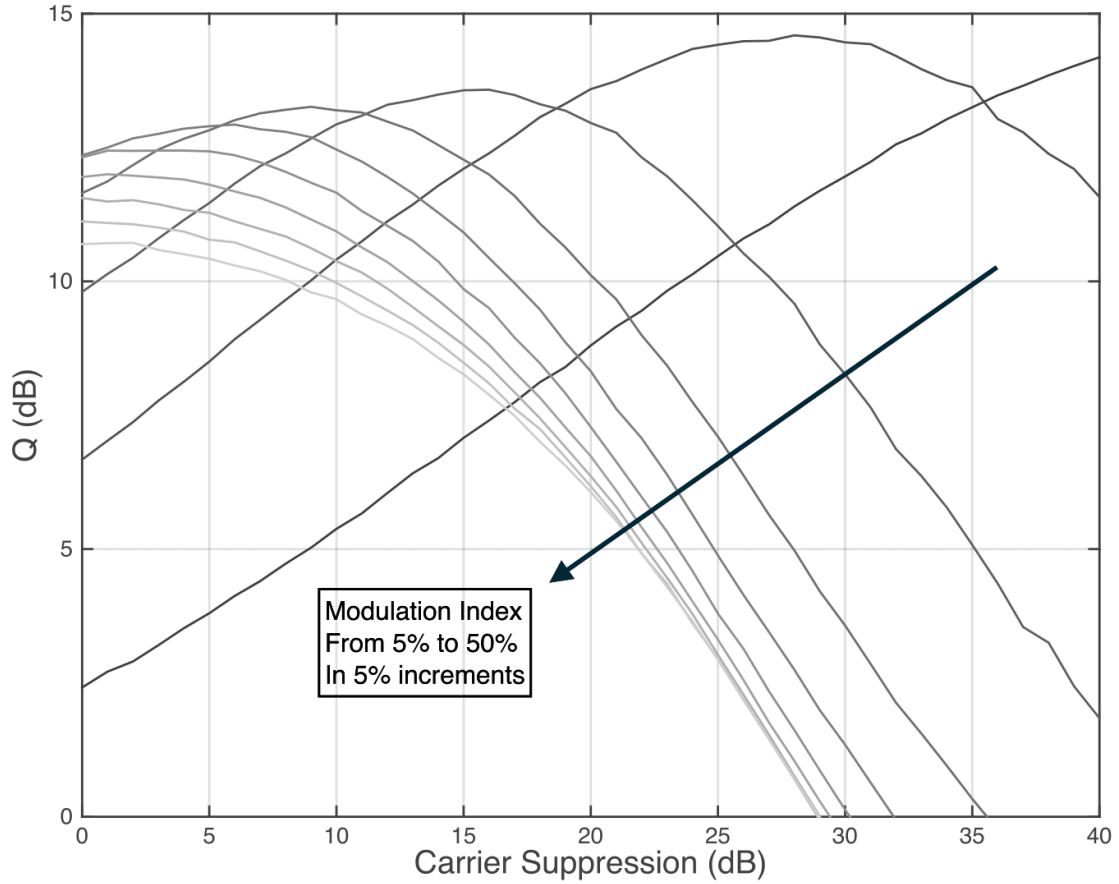


Figure 3.8: Effect of carrier suppression and modulation index on Q-factor for BACO-OFDM.

### 3.5 Conclusion

In this chapter, an optical modulation method was introduced in order to achieve better Q-factors than carrier suppressed biased optical OFDM. The method is especially suited for RoF applications with the RF carrier being high enough as compared to signal bandwidth. In fact, the proposed approach proved analytically that higher carrier to bandwidth ratios result in lower distortion levels due to clipping the signal at zero. The study provides a comparison of system performance for two cases with and without optical amplification. In both cases RFCO-OFDM achieves higher Q-factor as compared to carrier suppressed BACO-OFDM under same OSNR con-

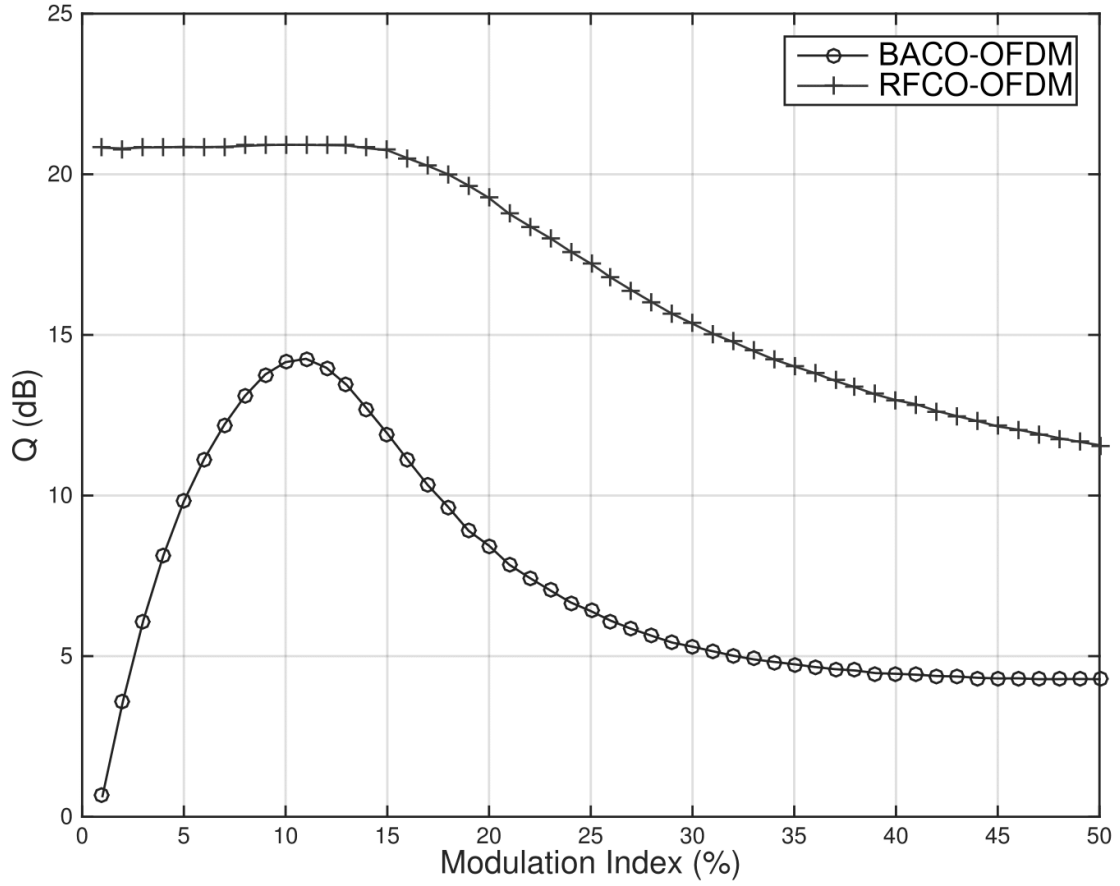


Figure 3.9: BACO-OFDM with 23dB carrier suppression compared to RFCO-OFDM for various modulation indexes.

ditions. Moreover, the study also shows that when effective carrier suppression is applied, output optical power of RFCO-OFDM is higher than carrier suppressed BACO-OFDM.

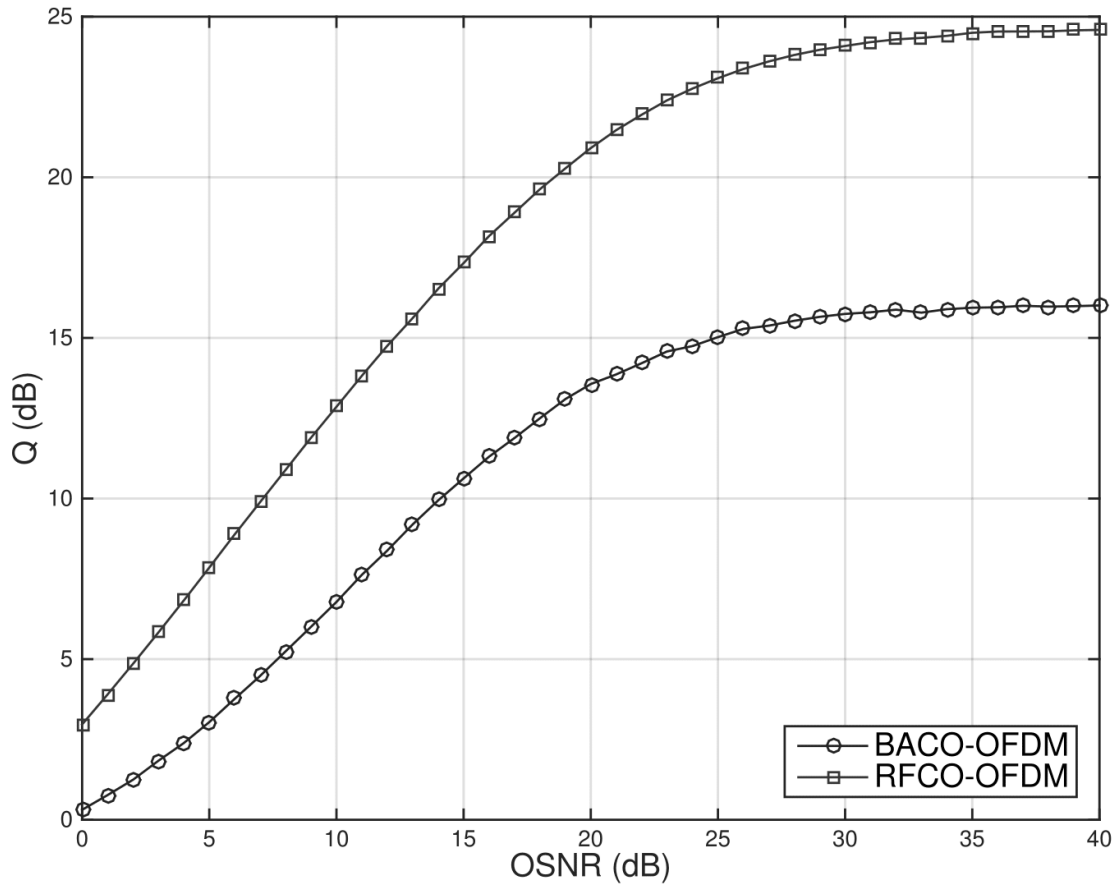


Figure 3.10: Q-factor achievable on different OSNR values at the receiver.

## CHAPTER 4

### INTEGRATED DUAL BEAM OPTICAL MODULATOR

In the previous chapter, It was shown that if a mm-wave RF signal is clipped at zero level, the resulting unipolar signal can be used to modulate the intensity of a laser with a better performance compared to carrier suppressed double side band optical OFDM. However, no matter if the laser is modulated directly or an external modulator is used, generation of the proposed unipolar signal requires high frequency electronics that increase the complexity and cost of the system. In fact, for the system to work, a mm-wave RF signal should be mixed with a baseband OFDM signal and the result should be applied to the modulator with appropriate biasing in order to clip the negative part.

In this chapter a novel method is proposed for implementing RFCO-OFDM. The newly proposed modulator does not depend on high frequency electronic components to create an optical mm-wave signal. Instead, it uses a baseband OFDM signal to modulate consecutive optical pulses of an optical pulse train generated by a mode locked laser (MLL) to create an optical signal similar to RFCO-OFDM. This architecture will also be able to support other optical modulation schemes like Optical Single Side Band (OSSB) as in [SYZ15] and [SF05].

#### 4.1 Generating RoF signals

RoF systems can be classified by the method of generating mm-wave signal. In electrical generation, an RF electrical signal is used to modulate a single mode laser. Thus, basically an optical carrier is modulated by a high frequency electrical signal to result in the desired RoF optical signal. In optical generation, mm-Wave signal is created by beating two different optical wavelengths either from a multi-mode laser

or from two separate lasers. In this case, generally one or both optical wavelengths are modulated by a baseband signal albeit with low modulation indexes. Direct detection at the receiver mixes these two signals together resulting in a mm-wave RF signal and some other distortion components that can either be filtered out or has minimal effect on in-band components.

### 4.1.1 Electrical Generation

There are two methods for electrical generation of mm-wave signals. The first one, uses direct modulation of a single mode laser with a mm-wave electrical signal. To decrease frequency chirp in direct modulation due to changes in refractive index of the active region [SKM05], direct modulation may be applied to an Optical Injection Locked laser [LWW09]. The second Electrical generation method uses external modulators to modulate an RF electrical signal on a single mode laser. External modulation can be performed using MZM or EAM modulators as in [WHS<sup>+</sup>08] and [LLSS04], respectively. Moreover, because of the inherent nonlinearity of external modulators, mm-wave generation is possible by generating harmonics of an IF electrical signal as in [LCS<sup>+</sup>10].

### 4.1.2 Optical Generation

In optical mm-wave generation, the RF signal is created by mixing of two separate optical wavelengths in the receiver. This can be done by externally modulating a dual-mode laser with mode separation equal to mm-wave signal as in [WLD95] or a mode-locked laser as in [OSF<sup>+</sup>00]. It can also be done by heterodyning two separate laser sources in an injection locked [HWH<sup>+</sup>02] or free running [IPS10] configuration.

## 4.2 RFCO-OFDM

In the previous chapter it was shown that if a mm-wave electrical signal is clipped at zero before being applied to an intensity modulator, the resulting optical signal can achieve good performance with higher power efficiency than a carrier suppressed optical OFDM. However, the method still requires up-converting the electrical signal into mm-wave carrier frequency resulting in higher cost and complexity. To develop a more efficient method of modulating RFCO-OFDM signals a closer examination of their structure is necessary. Considering the following expression for the RF modulated signal:

$$x(t) = s(t) \cos(2\pi f_c t) \quad (4.1)$$

Expanding this equation, the carrier signal can be defined as the sum of two sampling impulse trains  $p(t)$  and  $p(t - T_c/2)$  where  $T_c = 1/f_c$  is the period of the RF carrier tone. This impulse train is then convolved in time domain by a half cosine pulse shaping function  $g(t)$  as shown below:

$$x(t) = s(t)(p(t) - p(t - T_c/2)) * g(t) \quad (4.2)$$

where

$$p(t) = \sum_{n=-\infty}^{\infty} \delta(t - nT_c) \quad (4.3)$$

and

$$g(t) = \begin{cases} \cos(2\pi f_c t), & \text{if } -T_c/2 < t < T_c/2 \\ 0, & \text{elsewhere} \end{cases} \quad (4.4)$$

Considering that the pulse shaping function  $g(t) \geq 0$  in  $(-T_c/2, T_c/2)$  and zero elsewhere, clipping  $x(t)$  at zero results in  $x^+(t)$  where:

$$x^+(t) = \begin{cases} s(t)(p(t)) * g(t), & \text{if } s(t) \geq 0 \\ -s(t)(p(t - T_c/2)) * g(t), & \text{if } s(t) < 0 \end{cases} \quad (4.5)$$

Thus  $x^+(t)$  can be generated by adding two signals together. The first one is a pulse train modulated by  $s(t)$  clipped at zero and the other one is a shifted pulse train modulated by  $-s(t)$  clipped at zero, that is:

$$x^+(t) = \frac{1}{2} \left[ (|s(t)| + s(t))p(t) + (|s(t)| - s(t))p(t - T_c/2) \right] * g(t), \quad (4.6)$$

Considering  $g(t)$  as a pulse shaping function, one can interpret the expression for  $x^+(t)$  as a combined intensity modulation of two fast laser pulse trains with repetition rate of  $T_c$  and relative delay  $T_c/2$ . Consequently, if two phase locked optical pulse trains are modulated with  $s(t)$  and  $-s(t)$  using two separate electro-absorption modulators. The modulators must be carefully biased to clip the input at zero. The combined output creates a RFCO-OFDM modulated signal without any electrical RF up-conversion involved.

### 4.3 Double beam optical modulator

Here an integrated optical modulator is introduced based on a Mode Locked Lasers (MLLs), two electro-absorption modulators and an optical coupler. The system can modulate baseband OFDM signals into a mm-wave RF carrier with higher power efficiencies. Figure 4.1 depicts the schematic diagram of a typical proposed system. The basic idea is to get laser pulses from both facet mirrors of a laser cavity instead of just one of them. In an MLL these two pulses are in sync and have a time



difference equal to half of the laser cavity round trip time. Each of these pulse trains is then modulated using preferably an EAM which can be integrated into the laser itself.

Biassing EAMs at the verge of transmission, creates a condition in which EAM1 only modulates positive parts of the baseband signal and absorbs the laser pulses when the baseband signal is negative. On the other hand because EAM2 receives the inverted baseband signal, it modulates optical pulses whenever the input signal is negative and blocks the path when it is positive. When these two pulse trains are combined together in a coupler, the result is an efficient mm-wave signal modulated around MLL pulse repetition frequency.

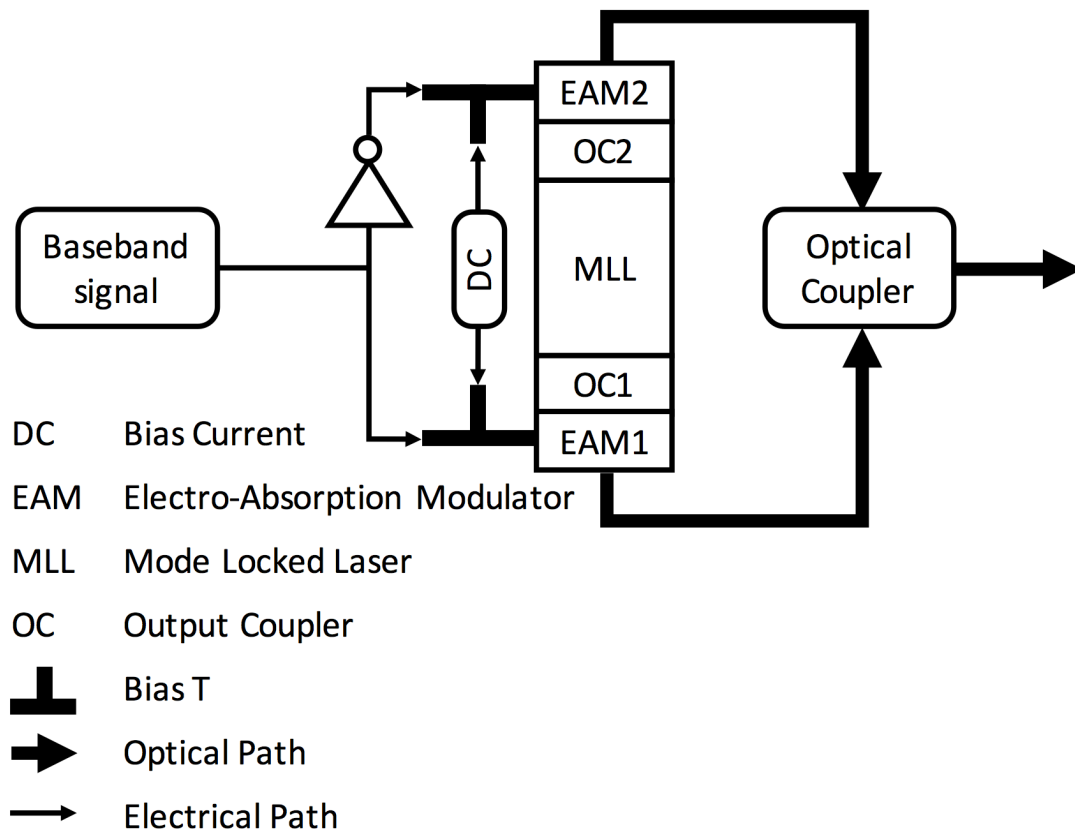


Figure 4.1: Schematic of the proposed modulator

It should be noted that although Fig. 4.1 may imply a Fabry-Perot laser cavity, the proposed method is applicable to most cavity configurations. The proposed method of intensity modulation is like modulating a band limited signal on an RF carrier where RF frequency is much higher than signal bandwidth and then removing the negative part of the result. This process maintains the RF modulated signal but introduces some distortion in the baseband which has negligible effect on the demodulated signal in the receiver.

### 4.3.1 Mode Locked Laser

Mode Locked Lasers provide promising means to implement mm-Wave RF systems as they are readily available in low cost configurations. They can also generate optical and RF carriers simultaneously by tuning the frequency difference between consecutive longitudinal modes of the laser. They can be modulated with an external modulator operating at baseband frequency while requiring very low modulation index as both the optical and RF carriers are being modulated. The low modulation index decreases the sensitivity and efficiency of the system which in turn requires using an optical amplifier afterwards.

In a typical diode laser, theoretically there is an infinite number of possible longitudinal modes that can sustain inside cavity. In fact any wavelength with  $\lambda = 1/n\Delta f$  can resonate inside the cavity where  $\Delta f = C/2L$  is the resonant frequency spacing,  $C$  is the light speed in vacuum and  $L$  is the optical length of the cavity. However, not all of these modes will be present in the output as the gain medium inside the cavity has a limited bandwidth which results in a net gain on a number of wavelengths. For continuous wave laser, these longitudinal modes have random phases which create a random time behavior for the intensity of emitted light.

To have a better insight, Fig. 4.2 illustrates the intensity of a continuous wave (CW) laser oscillating on 5 longitudinal modes. In fact, this intensity is like the output of an OFDM modulator when random data is modulated in it. However, in a mode locked laser, the phases for all longitudinal modes in the cavity are locked together in a linear form. In Fig. 4.2, the same 5 modes are locked together in a way that  $\phi_n - \phi_{n-1} = \Delta\phi$ , where  $\phi_n$  is the phase of the  $n$ th longitudinal mode and all modes have the same amplitude. It can be shown that the pulse width is inversely proportional to the optical bandwidth or the number of modes locked together. As a result, the short pulses required to generate the impulse train for the proposed modulation can be generated by a MLL. There are several methods to achieve mode locking in a laser which are referred to here:

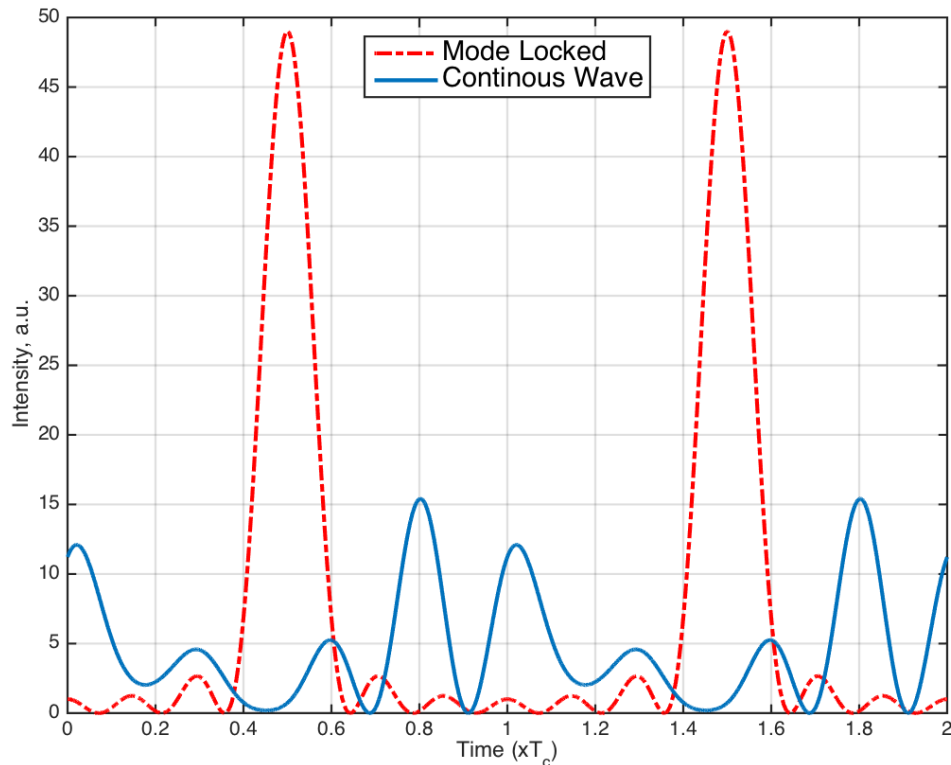


Figure 4.2: Comparison of cw vs mode locked output intensity.

Active mode locking requires modulation of either pump current, amplitude or phase inside the laser cavity by an external oscillator [Sve10]. In these methods an external electrical reference signal is used which should have the same frequency as the fundamental cavity frequency ( $\Delta f$ ) with a high precision. The requirement for high frequency external oscillator shadows the cost effective requirements of the system proposed here and thus Passive mode locking seems to be a more viable solution. However, it is practical to use active mode locked laser as a pulse source for the proposed system.

Passive mode locking takes advantage of a saturable absorber inside cavity to cut off low intensity pulses [Hau00]. A single saturable absorber placed on one end of the cavity results in a single high intensity pulse inside the cavity which is referred to as fundamental mode locking. On the other hand, the saturable absorber can be placed in different places inside cavity to achieve harmonic mode locking that creates multiple simultaneous pulses inside cavity. The only requirement is that for laser pulses to arrive at one cavity facet with half pulse repetition interval ( $T_c/2$ ) delay compared to the other facet. This in turn results in the MLL laser to be mode locked in fundamental frequency or odd harmonics. For even harmonics there is going to be optical pulses simultaneously at both cavity facets.

### **4.3.2 Electro-absorption Modulator**

Electroabsorption modulators are probably the simplest of optical components. In the most basic form this kind of modulator is in fact a piece of optical waveguide that is reverse biased to lower the absorption edge which results in increased absorption of incoming light [CCM12]. The attenuation is not linear on input voltage which is not a problem for general on-off keying operation. However, linear operation is a

requirement for OFDM modulation and as a result most of the times a pre-distortion circuit is adapted to linearize the electro-absorption modulator as in [SHZ<sup>+</sup>10].

## 4.4 Frequency Stabilization

Frequency stabilization has a dramatic effect on the performance of any RoF system. More importantly it is crucial for the system to always maintain the phase difference between two pulse trains. Any deviation from this requirement dramatically decreases the Q-factor at the output. While single sideband modulation systems like [SF05] and [SOS<sup>+</sup>01] use external phase shifters, the method proposed here intrinsically generates phase shifted outputs inside a single cavity. Any mechanical or electrical distortion, while affecting the mode locked frequency, does not disturb the orthogonality of two pulse trains. As a result, closed loop techniques used to stabilize the mode locking frequency, maintain the phase difference as well. After all, there might be slight variations in the pulse trains time difference.

## 4.5 Simulation

To make a comparison between the proposed system and intensity modulation applied on mode locked laser for RoF communications the systems are simulated in MATLAB, Both methods are supposed to modulate a pulsed light source with the same average power. Thus in case of the dual beam modulator, each beam has half the intensity of the single beam mode locked laser.

### 4.5.1 OFDM Modulator

The baseband OFDM modulator is where the input to optical modulators is generated first. To simulate the system, a 250 carrier OFDM modulator is used with 10MHz separation between orthogonal frequencies. Constellation size is 4 and after inverse Fourier transform with 2x oversampling, a 2.5GHz real baseband signal is created. This signal is then fed into an electro-absorption modulator biased at half intensity coupled to a mode locked laser to simulate a single modulator RoF transmitter.

The positive and negative parts of the real OFDM signal are separately fed into two electro-absorption modulators biased at null point. The output of these modulators are combined to simulate dual beam optical modulator proposed in this research. The electro-absorption modulator is simulated by changing the intensity of the optical pulses which are simulated by corresponding electrical field. The result will be in the form of double side band optical OFDM with 5 GHz bandwidth on each sideband.

### 4.5.2 Electrical Field for Pulses

Electrical field for both mode locked pulses in which 9 longitudinal modes are locked together are shown in Fig. 4.3. Mode separation frequency is 60GHz except when modified as a simulation parameter. It is assumed that all modes have the same amplitude. These two pulse trains are used for simulation of the proposed modulation method while only one of them is used for simulation of the single modulator system. Although their power spectral density is the same in frequency domain (as shown in Fig. 4.4), their combination only has the even modes because the odd

ones have opposite phases in each pulse train which tend to cancel each other at the combined output.

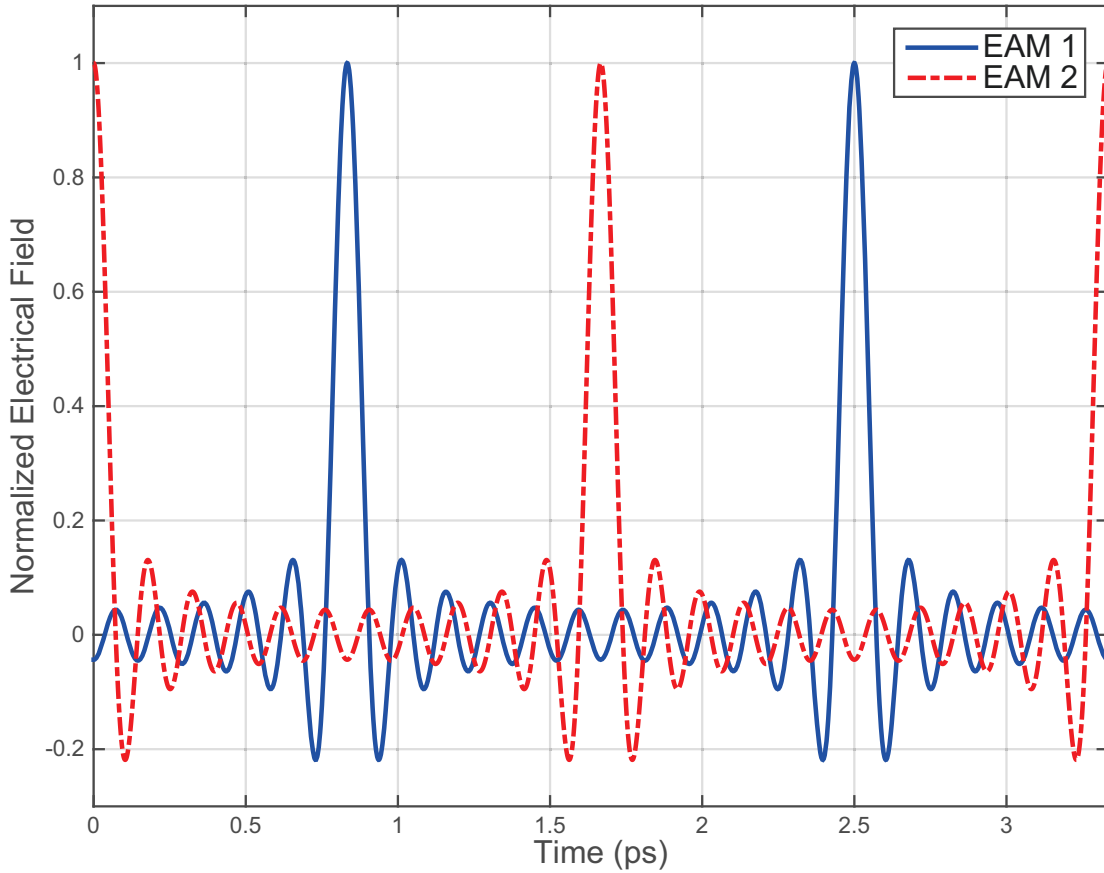


Figure 4.3: Two pulse trains at the outputs of electroabsorption modulators.

In Fig. 4.5, the output spectrum of both modulators are shown in 0-120 GHz range. It can be seen that while the intensity for data carrying frequencies are the same for both systems, optical carrier have less power compared to the single modulator mode locked laser output. Moreover no optical tone is present in the data carrying band which reduces filtering requirements at the receiver. Thus unlike intensity modulation of a single ended mode locked laser which requires RF carrier suppression at the base station to meet power emission requirements, the signal from the proposed system can be easily retransmitted.

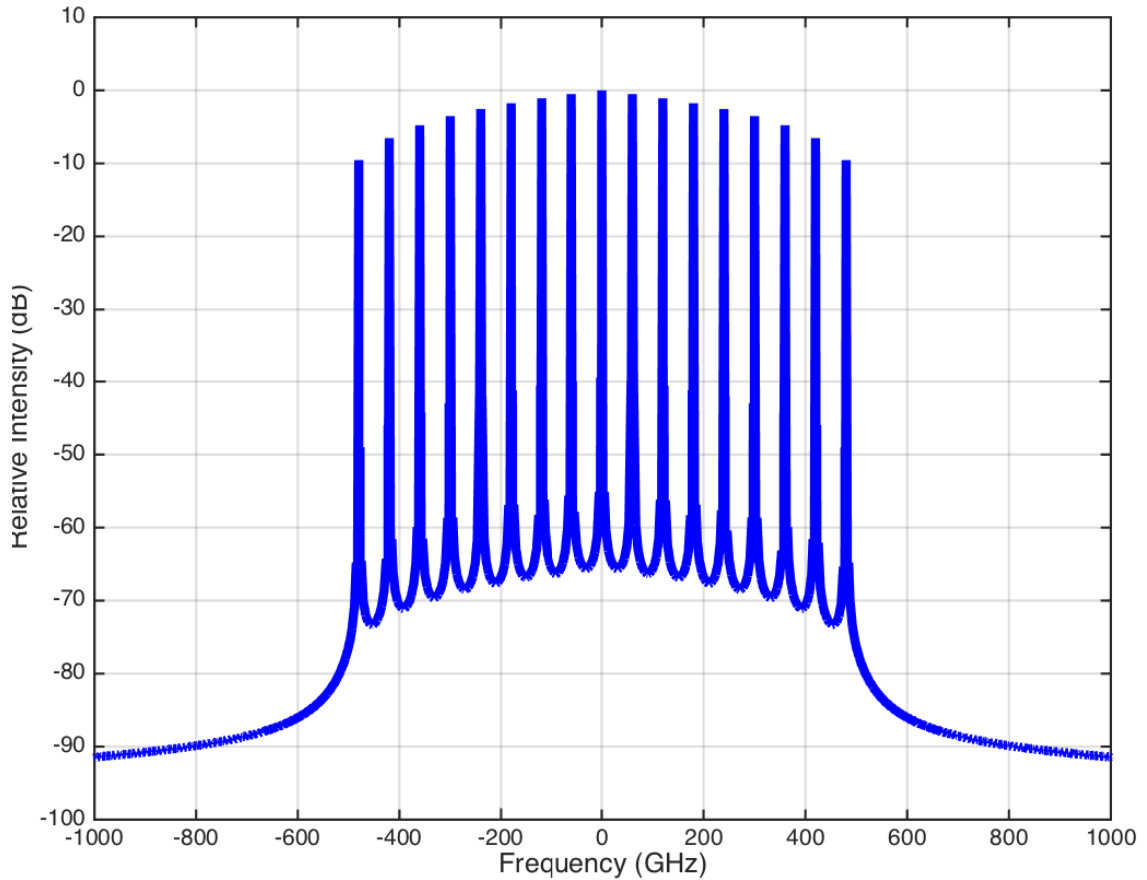


Figure 4.4: Spectrum of a single pulse train for the simulated mode locked laser.

### 4.5.3 Modulation Index

We define modulation index as the standard deviation of the electrical signal as a percentage of the input range for the intensity modulator as in section 3.3.2. While the single modulator is biased at 50% intensity, its average output power will remain unchanged regardless of the modulation index. However, average optical power of the dual modulator varies with modulation index. Figure 4.6 depicts the excess optical power of single modulator vs the proposed dual modulator considering that the detected electrical signal power at the modulated subcarriers is the same for both systems. As a result, the proposed system has a 4dB sensitivity advantage over the single modulator counterpart.



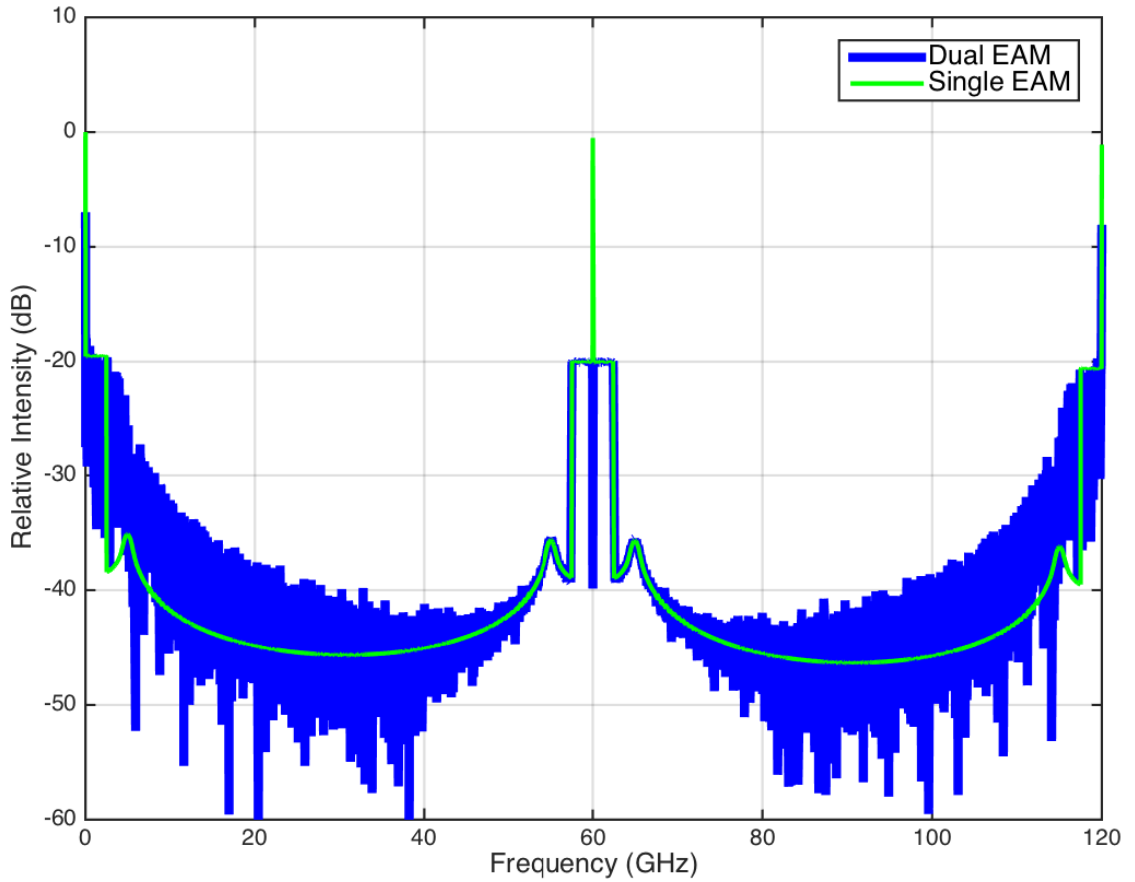


Figure 4.5: Comparison of spectrum for the modulated signals.

Increasing the modulation index lowers the difference in average optical output power of both systems; however, it also increases the distortion due to clipping of the peaks of the OFDM signal. Figure 4.7 shows this decrease in Q-factor by increasing modulation index. It is observed that at around 25% the Q-factor starts to rapidly decrease. It should be noted that for  $f_c$  of 60GHz both systems achieve nearly identical Q-factors; however, lower  $f_c$  forces more distortion on the dual modulator which uses RFCO principle.

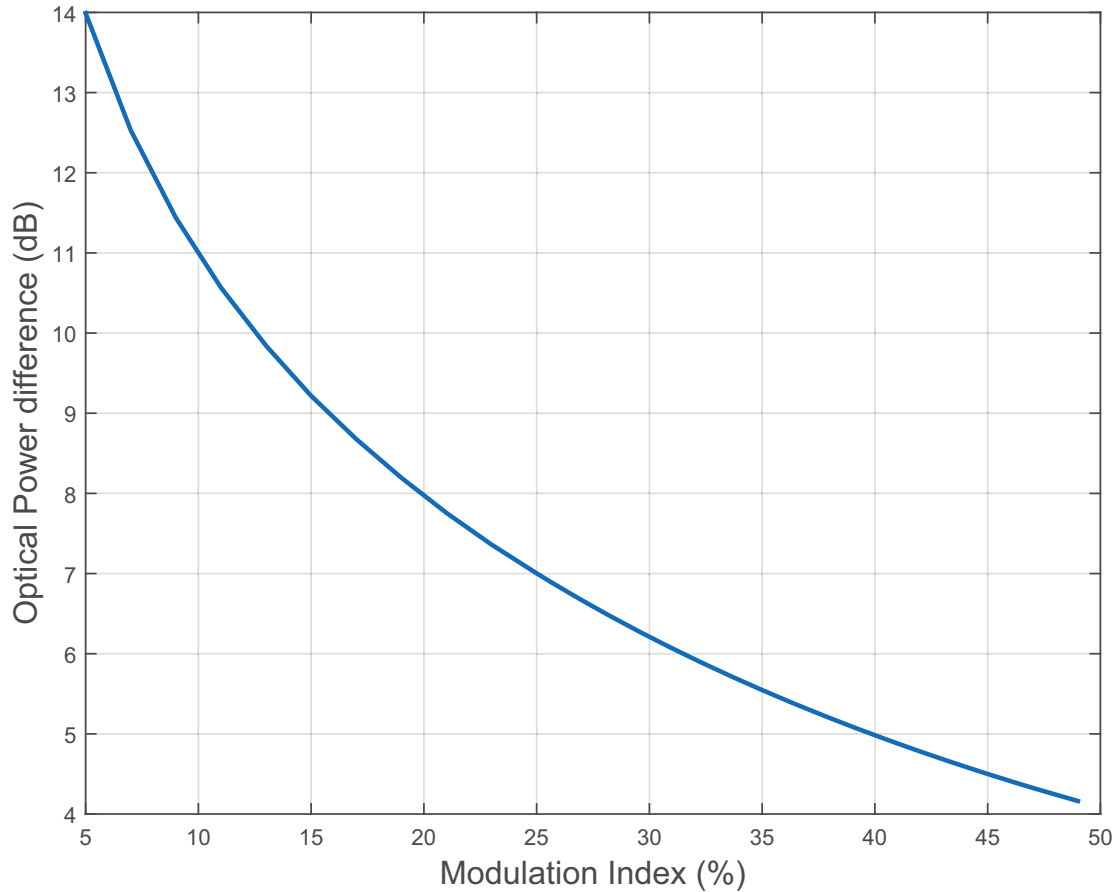


Figure 4.6: Optical power difference between single modulator and the proposed dual modulator. At lower modulation indexes dual modulator achieves the same signal power at the receiver with much less optical power.

#### 4.5.4 Mode Locking Frequency

If both systems are modulated with the same modulation index and clipping levels for OFDM signal, the Q-factor is almost identical unless the carrier frequency is too low compared to signal bandwidth resulting in zero clipping distortions to affect the signal. Figure 4.8 shows the change in Q-factor due to changing the carrier frequency which is in fact the mode locking frequency as no electrical carrier signal is present here. Q-factor for single modulator is not expected to depend on carrier frequency (unless it is less than signal bandwidth which causes the signal modulated

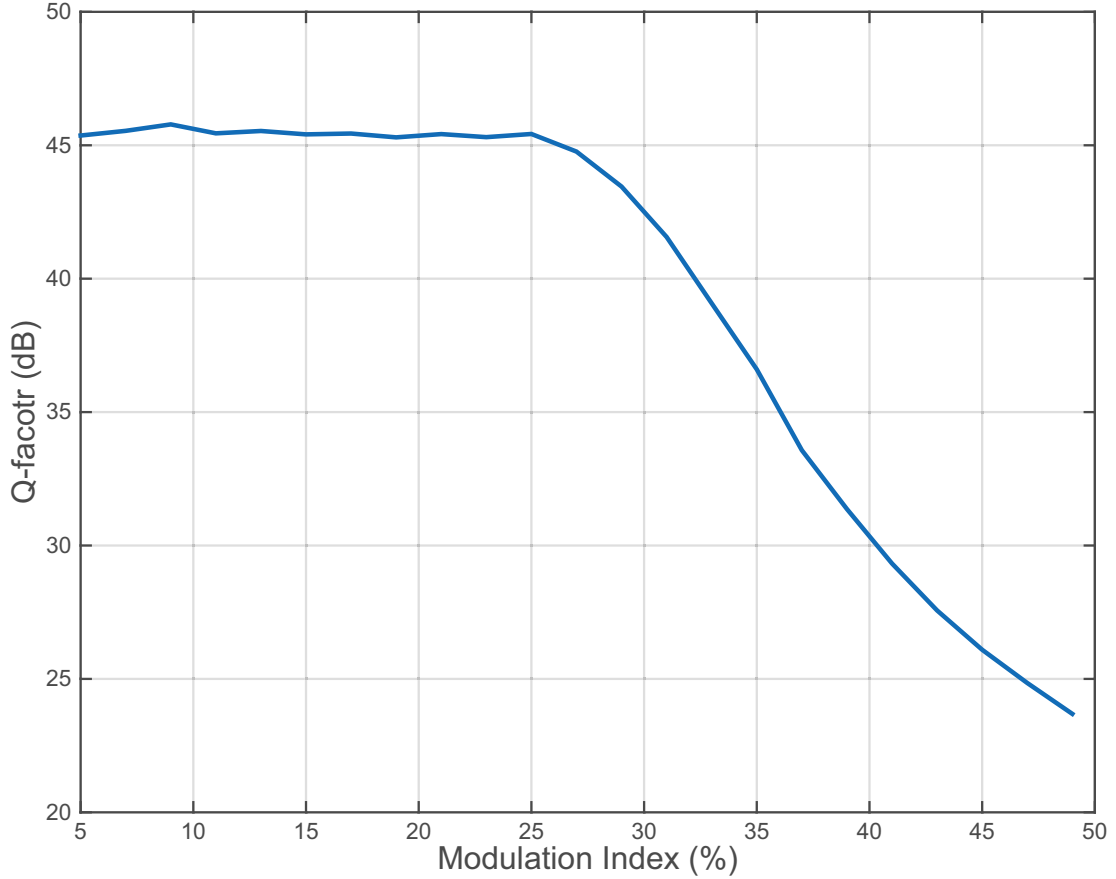


Figure 4.7: Changes in Q-factor due to Modulation index.

on adjacent optical modes to interfere). Thus Q-factor at the output of the transmitter is only a factor of modulation index and clipping levels. For single modulator system it is about 45dB considering a 25% modulation index. Consequently, the high Q-factor of the single modulator is retained even in lower carrier frequencies.

On the other hand, the dual modulator system loses Q-factor by lowering mode locking frequency, which is a direct result of wider distortions on the baseband frequencies as described in chapter 3. Despite this lower Q-factor, It can be seen that the Q-factor curve almost flattens for carrier frequencies higher than 30-40GHz when it reaches the maximum Q-factor achieved by single modulator system. As mm-wave RoF systems generally use the 60GHz band, this dependence of Q-factor

to carrier frequency should not have any practical problems for such a system.

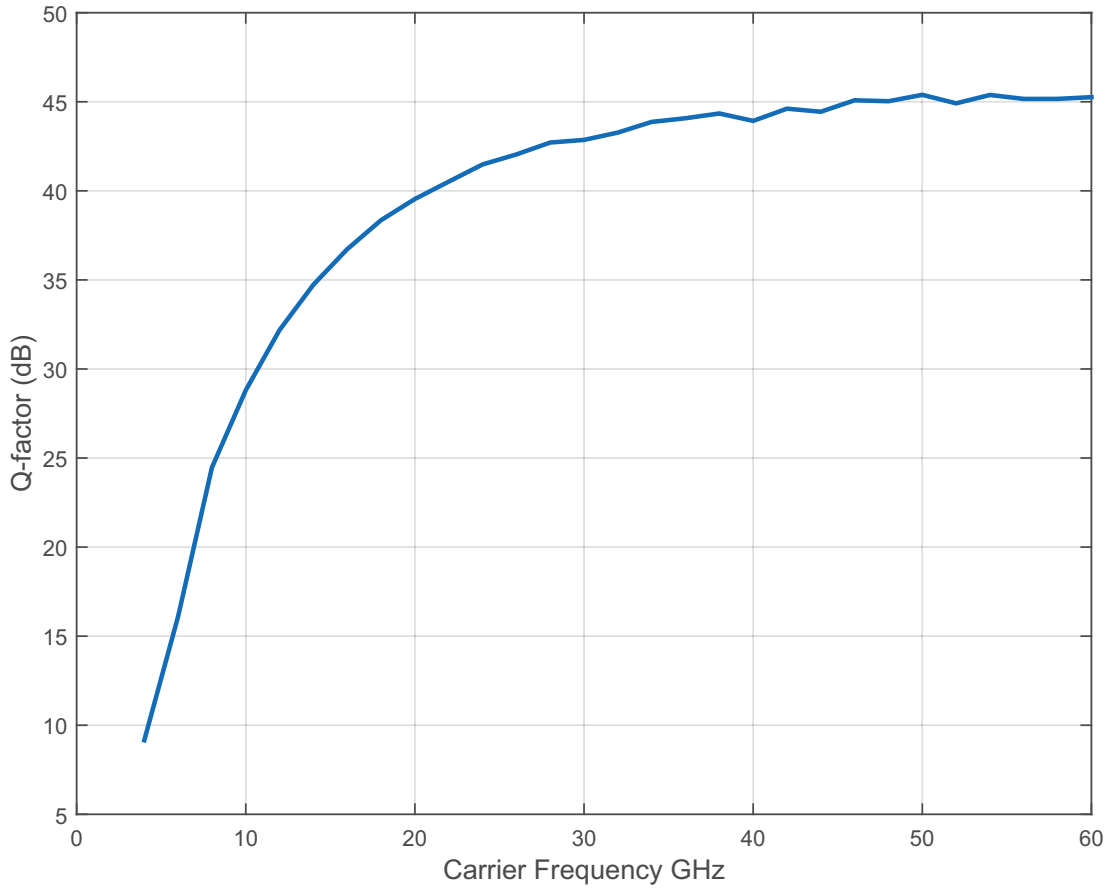


Figure 4.8: Changes in Q-factor due to carrier frequency.

## 4.6 Results

In chapter 3, it was shown that RF clipped optical OFDM as an efficient method for intensity modulation in RoF applications required a high frequency up-conversion circuit to work with current external modulation methods. In this chapter it was shown that the RFCO-OFDM modulation can be implemented using dual electro-absorption modulators connected to both cavity ends of a mode locked laser. The system proved to have better power efficiency compared to a single modulator system

as less power is spent on optical carriers. It was also shown that modulation indexes of 25% and mode locking frequencies above 40GHz both systems could achieve the same Q-factor while the proposed system emitted 7 dB less optical power. Moreover the proposed system can be implemented in a single optical integrated circuit which greatly reduces the adoption cost for next generation radio over fiber infrastructures.

## CHAPTER 5

### CONCLUSIONS AND RETROSPECTIVE

In this dissertation three innovative methods for optical modulation were introduced and examined. At first a new 2D barcode modulation method was developed that can mitigate extensive relative movements of the displayed barcode surface (in this case an LCD) and the receiving camera.

Test results revealed that even slight hand movements during image capture for barcode detection can result in high error probability. Most of the time the movement renders the captured image useless and thus another frame needs to be captured in order to correctly detect a 2D barcode. It was revealed that as the barcode size increases detection probability decreases. For instance while the frames captured from a paper printed V1 QR-Code almost always can be decoded under our particular test conditions, only 6% of the V101 QR-Codes frames were decodable.

It was shown that although using QPSK-OFDM for modulation of 2D barcodes can enhance error rate in case of image blur and slight movements, it is out performed by DPSK-OFDM. As a result, in this dissertation, differential phase shift keying was combined with orthogonal frequency division multiplexing in order to modulate data stream into visual two-dimensional barcodes. It was shown that QPSK-OFDM modulation has serious shortcomings in the mitigation of camera LCD movements where the phase of each element changes continuously. On the other hand, addition of a differential phase modulator before OFDM to modulate the data stream into phase differences of adjacent frequencies (DPSK-OFDM) causes the relative motion to have less effect. This is due to the fact that the phase gradually changes between adjacent frequency bins, contributing to a small deviation from the ideal phase in the received signal. It was observed that under relative LCD-camera motions that

generate error rates in excess of 30% in PAM and QPSK-OFDM, the proposed system of DPSK-OFDM sustains an error rate less than 8% which is practically correctable using error correction coding.

Future inquiries have to address the best choice of differential pattern to optimize performance for various motion scenarios. Moreover, it is possible to increase the bit per symbol for the OFDM signal from the current 4 bits to 8 bits and beyond in order to increase the data transfer rate. However, extensive BER performance evaluation is required to ensure that the error rate does not exceed error correction requirements under normal LCD-camera movements. Nevertheless, a study on the effect of perspective correction errors on the BER performance of this algorithm compared to the other ones could augment our understanding of its applicability to real world scenarios.

Although dc bias of the 2D OFDM signal was used for intensity modulation of the barcode pixels, advantages of using more power efficient ACO-OFDM may be investigated. Because ACO-OFDM sacrifices half of the usable frequency bins, in its primitive form it can only achieve half of the bit rate of the DCO-OFDM system implemented here. The proposed barcode modulation algorithm may be enhanced by combining differential modulation with proper bit loading required for ACO-OFDM to be efficient. While further research may be done to implement this combination, the computational complexity may render any slight improvements in performance useless due to power constraints in handheld devices. Saving some power on LCD using the combined algorithm may ultimately require more power used in the processing units of both transmitter and receiver, which is a main constraint when the systems are battery powered.

The research to find more efficient intensity modulation method for optical communications led us to the RF clipped optical OFDM modulation scheme. Although

more efficient methods are already available for baseband intensity modulation, it was shown that the proposed method has a clear advantage when used in RoF applications. In RoF systems, the signal bandwidth is much less than the carrier frequency. Moreover, base stations in RoF applications only retransmit the amplified optical signal which means that the detected optical signal should be the same as the RF signal that is going to be retransmitted. Thus, any modulation scheme that requires structural alteration of the RF OFDM signal cannot be adopted.

It was shown that RFCO-OFDM has a better power efficiency compared to carrier suppressed double side band optical OFDM. In short range applications where no optical amplifier is required, RFCO-OFDM can achieve the same Q-factor with less total optical power. On the other hand when an optical amplifier was used RFCO-OFDM can achieve higher a Q-factor when optical power at the output of the amplifier is the same for both systems.

The performance of the system when used in a more efficient single side band configuration can be the subject of future research. Although power efficiency resulted from removing one of the side bands may be beneficial in a system that uses optical amplifiers, current short range applications generally do not require dispersion mitigation capabilities of single side band optical modulation.

The proposed intensity modulation method can be used in RoF systems by clipping the RF signal which requires RF up conversion. However, a novel system was introduced which can efficiently generate the RFCO-OFDM signal by using the baseband OFDM and a novel double sided laser modulator. It was analytically shown that the proposed optical integrated system can be used to efficiently implement the RFCO-OFDM. The modulator works by applying positive and negative parts of a baseband OFDM signal to successive pulses of a mode locked laser and combining the results. Pulse separation for this purpose is achieved by getting mode locked



optical pulses out of both facets of the laser cavity which makes them essentially in quadrature phase. As a result, it can be used to implement other RoF systems that require a quadrature optical modulator.

External modulators of the electro-absorption type used in the implementation of the system are fed by baseband signal and not by a high frequency mm-Wave signal. Thus their construction is much easier with less frequency chirp compensation requirements. Moreover, any frequency stabilization method used in the system equally affects both pulse trains and thus the pulses maintain better orthogonality under various thermal or mechanical variations.

Future investigations can focus on the optimum bias point for electro-absorption modulators used in the system. The bias point along with the length of the EAM modulator determines the optical carrier pulses passing through EAM when they are supposed to be stopped which can affect efficiency and performance for the system. Adaptation of the proposed method of generating RFCO-OFDM to other resonator types such as ring resonators or dye lasers can be of future interest as these systems see increased adaption in communications systems. Pre-distortion circuits optimized for the proposed optical integrated modulator and their effect on the performance of the system are also an interesting topic for future research.

Throughout this dissertation, the intent was to investigate various algorithms and methods for optical modulation applications. Some of the proposed methods may find applications in consumer devices in near future owing to their straightforward software-based implementation. However, others may require further adoption of optical communications as a distribution method of RF signals for next generation high bandwidth cellular communications to make them a feasible investment.

## BIBLIOGRAPHY

- [AAI<sup>+</sup>14] Iraj Sadegh Amiri, Sayed Ehsan Alavi, Sevia M. Idrus, Abu Sahmah Mohd Supaat, Jalil Ali, and Preecha P. Yupapin. W-Band OFDM transmission for radio-over-fiber link using solitonic millimeter wave generated by MRR. *IEEE Journal of Quantum Electronics*, 50(8):622–628, 2014.
- [ABC<sup>+</sup>14] Jeffrey G. Andrews, Stefano Buzzi, Wan Choi, Stephen V. Hanly, Angel Lozano, Anthony C K Soong, and Jianzhong Charlie Zhang. What will 5G be? *IEEE Journal on Selected Areas in Communications*, 32(6):1065–1082, 2014.
- [AFH11] Kasra Asadzadeh, Ahmed A Farid, and Steve Hranilovic. Spectrally factorized optical ofdm. In *Information Theory (CWIT), 2011 12th Canadian Workshop on*, pages 102–105. IEEE, 2011.
- [AJG<sup>+</sup>14] A Ashok, S. Jain, M. Gruteser, N. Mandayam, Wenjia Yuan, and K. Dana. Capacity of pervasive camera based communication under perspective distortions. In *Pervasive Computing and Communications (PerCom), 2014 IEEE International Conference on*, pages 112–120, March 2014.
- [AL06] Jean Armstrong and AJ Lowery. Power efficient optical ofdm. *Electronics Letters*, 42(6):370–372, 2006.
- [Ale97] Stephen B Alexander. *Optical communication receiver design*. SPIE Optical engineering press, Bellingham, Washington, USA, 1997.
- [Arm09] Jean Armstrong. Ofdm for optical communications. *Journal of light-wave technology*, 27(3):189–204, 2009.
- [BCA<sup>+</sup>13] Joaquin Beas, Gerardo Castanon, Ivan Aldaya, Alejandro Aragon-Zavala, and Gabriel Campuzano. Millimeter-Wave Frequency Radio over Fiber Systems: A Survey. *IEEE Communications Surveys & Tutorials*, 15(4):1593–1619, 2013.
- [BH13] Luiz F. F. Belussi and Nina S. T. Hirata. Fast Component-Based QR Code Detection in Arbitrarily Acquired Images. *J. Math. Imaging. Vis.*, 45(3, SI):277–292, MAR 2013.

- [BOO98] AM Bruckstein, L O’Gorman, and A Orlitsky. Design of shapes for precise image registration. *IEEE Trans. Inf. Theory*, 44(7):3156–3162, Nov 1998.
- [Boy00] John P Boyd. *Chebyshev and Fourier Spectral Methods: Second Edition*. DOVER Publications, 2 edition, 2000.
- [BSM<sup>+</sup>09] D.M. Boroson, J.J. Scozzafava, D.V. Murphy, B.S. Robinson, and H. Shaw. The lunar laser communications demonstration (llcd). In *Space Mission Challenges for Information Technology, 2009. SMC-IT 2009. Third IEEE International Conference on*, pages 23–28, July 2009.
- [Bur04] Russell W Burns. *Communications: an international history of the formative years*, volume 32. IET, 2004.
- [CCM12] Larry A. Coldren, Scott W. Corzine, and Milan L. Mashanovitch. *Diode Lasers and Photonic Integrated Circuits*. John Wiley & Sons, Inc., 2nd edition, 2012.
- [CEPB02] S. Coleri, M. Ergen, A. Puri, and A. Bahai. Channel estimation techniques based on pilot arrangement in OFDM systems. *IEEE Trans. Broadcast.*, 48(3):223–229, Sep 2002.
- [CKE09] L. Chen, B. Krongold, and J. Evans. Performance Evaluation of Optical OFDM Systems with Nonlinear Clipping Distortion. *2009 IEEE International Conference on Communications*, pages 1–5, 2009.
- [CKE12] Liang Chen, Brian Krongold, and Jamie Evans. Theoretical characterization of nonlinear clipping effects in IM/DD optical OFDM systems. *IEEE Transactions on Communications*, 60(8):2304–2312, 2012.
- [CT06] T.M. Cover and J.A. Thomas. *Elements of Information Theory*. Wiley Interscience, Hoboken, N.J., second edition, 2006.
- [DSH12a] Svilen Dimitrov, Sinan Sinanovic, and Harald Haas. Clipping Noise in OFDM-Based Optical Wireless Communication Systems. *IEEE Trans. Commun.*, 60(4):1072–1081, Apr 2012.
- [DSH12b] Svilen Dimitrov, Sinan Sinanovic, and Harald Haas. Clipping noise in OFDM-based optical wireless communication systems. *IEEE Transactions on Communications*, 60(4):1072–1081, 2012.

- [GM90] J P Gordon and L F Mollenauer. Phase noise in photonic communications systems using linear amplifiers. *Optics Letters*, 15(23):1351–1353, 1990.
- [GW07] R.C. Gonzalez and R.E. Woods. *Digital Image Processing*. Pearson Education, Upper Saddle River, NJ, third edition, 2007.
- [Hau00] Herman a. Haus. Mode-locking of lasers. *IEEE Journal on Selected Topics in Quantum Electronics*, 6(6):1173–1185, 2000.
- [HF05] P. Horvath and I. Frigyes. Effects of the nonlinearity of a Mach-Zehnder modulator on OFDM radio-over-fiber transmission. *IEEE Communications Letters*, 9(10):921–923, 2005.
- [HWH<sup>+</sup>02] Moon-Ki Hong, Yong-Yuk Won, Sang-Kook Han, K M Sauer, H Kojucharow, D Kaluzni, W Sommer, and A Nowak. Gigabit radio-over-fiber link for converged baseband and millimeter-wave band signal transmission using cascaded injection-locked Fabry-Pérot laser diodes. *IEEE Trans. Microw. Theory Tech. RF Photonic Technology in Optical Fiber Links*, 50(3):877–887, 2002.
- [IEE14] Zxing project, 2014.
- [Int06] International Organization for Standardization. Information technology — automatic identification and data capture techniques — qr code 2005 bar code symbology specification. ISO/IEC 18004:2006, 2006.
- [IPS10] Ignacio González Insua, Dirk Plettemeier, and Christian G. Schäffer. Simple remote heterodyne radio-over-fiber system for gigabit per second wireless access. *Journal of Lightwave Technology*, 28(16):2289–2295, 2010.
- [JBS00] Michel C Jeruchim, Philip Balaban, and K Sam Shanmugan. *Simulation of communication systems: modeling, methodology and techniques*. Kluwer Academic/Plenum, New York, NY, second edition, 2000.
- [JLN<sup>+</sup>10] Wen Jr Jiang, Chun Ting Lin, Anthony Ng’oma, Po Tsung Shih, Jason (Jyehong) Chen, Michael Sauer, Frank Annunziata, and Sien Chi. Simple 14-Gb/s Short-Range Radio-Over-Fiber System Employing a Single-Electrode MZM for 60-GHz Wireless Applications. *Journal of Lightwave Technology*, 28(16):2238–2246, 2010.

- [KT07a] H. Kato and K.T. Tan. Pervasive 2d barcodes for camera phone applications. *IEEE Pervasive Comput.*, 6(4):76–85, Oct 2007.
- [KT07b] Hiroko Kato and Keng T Tan. First read rate analysis of 2d-barcodes for camera phone applications as a ubiquitous computing tool. In *TENCON 2007-2007 IEEE Region 10 Conference*, pages 1–4. IEEE, 2007.
- [KWH13] Scott Kuzdeba, Alexander M Wyglinski, and Brandon Hombs. Prototype implementation of a visual communication system employing video imagery. In *Proc. CCNC*, pages 184–189, 2013.
- [KWM<sup>+</sup>05] Robert I. Killey, Philip M. Watts, Vitaly Mikhailov, Madeleine Glick, and Polina Bayvel. Electronic dispersion compensation by signal pre-distortion using digital processing and a dual-drive Mach-Zehnder modulator. *IEEE Photonics Technology Letters*, 17(3):714–716, 2005.
- [LCS<sup>+</sup>10] Chun Ting Lin, Jyehong Chen, Po Tsung Shih, W. J. Jiang, and Sien Chi. Ultra-high data-rate 60 GHz radio-over-fiber systems employing optical frequency multiplication and OFDM formats. *Journal of Lightwave Technology*, 28(16):2296–2306, 2010.
- [LDA07] Arthur James Lowery, Liang Bangyuan Du, and Jean Armstrong. Performance of optical OFDM in ultralong-haul WDM lightwave systems. *Journal of Lightwave Technology*, 25(1):131–138, 2007.
- [LDL08] Xu Liu, David Doermann, and Huiping Li. Vcode-pervasive data transfer using video barcode. *IEEE Trans. Multimedia*, 10(3):361–371, 2008.
- [LF13] Jeng An Lin and Chiou Shann Fuh. 2D Barcode Image Decoding. *Math. Probl. Eng.*, 2013.
- [LLSS04] Hai H. Lu, Ying Cong Lin, Yuan Hong Su, and Heng Sheng Su. A Radio-on-Fiber Intelligence Transport System Based on Electroabsorption Modulator and Semiconductor Optical Amplifier. *IEEE Photonics Technology Letters*, 16(1):251–253, 2004.
- [LRBK09] S. C J Lee, Sebastian Randel, Florian Breyer, and A. M J Koonen. PAM-DMT for intensity-modulated and direct-detection optical communication systems. *IEEE Photonics Technology Letters*, 21(23):1749–1751, 2009.

- [LWW09] Erwin K. Lau, Liang Jie Wong, and Ming C. Wu. Enhanced modulation characteristics of optical injection-locked lasers: A tutorial. *IEEE Journal on Selected Topics in Quantum Electronics*, 15(3):618–633, 2009.
- [LY03] G. L. Li and P. K L Yu. Optical Intensity Modulators for Digital and Analog Applications. *Journal of Lightwave Technology*, 21(9):2010–2030, 2003.
- [LYL08] Yue Liu, Ju Yang, and Mingjun Liu. Recognition of qr code with mobile phones. In *Control and Decision Conference, 2008. CCDC 2008. Chinese*, pages 203–206. IEEE, 2008.
- [MA12] M.R.H. Mondal and J. Armstrong. Impact of linear misalignment on a spatial OFDM based pixelated system. In *Communications (APCC), 2012 18th Asia-Pacific Conference on*, pages 617–622, Oct 2012.
- [MA14] M Rubaiyat H Mondal and Jean Armstrong. Analysis of the effect of vignetting on mimo optical wireless systems using spatial OFDM. *Journal of Lightwave Technology*, 32(5):922–929, 2014.
- [MCW01] R. Morrison, L.J. Cimini, and S.K. Wilson. On the use of a cyclic extension in OFDM. In *Vehicular Technology Conference, 2001. VTC 2001 Fall. IEEE VTS 54th*, volume 2, pages 664–668 vol.2, 2001.
- [MH02] John C Mason and David C Handscomb. *Chebyshev polynomials*. CRC Press, 2002.
- [MM01] M. Morelli and U. Mengali. A comparison of pilot-aided channel estimation methods for OFDM systems. *IEEE Trans. Signal Process.*, 49(12):3065–3073, Dec 2001.
- [MSWS13] Jeton Memeti, Flávio Santos, Martin Waldburger, and Burkhard Stiller. Data transfer using a camera and a three-dimensional code. *Praxis der Informationsverarbeitung und Kommunikation*, 36(1):31–37, 2013.
- [Nak05] Junichi Nakamura. *Image sensors and signal processing for digital still cameras*. CRC press, 2005.
- [NFP+10] Anthony Ng’Oma, Davide Fortusini, Devang Parekh, Weijian Yang, Michael Sauer, Seldon Benjamin, Werner Hofmann, Markus C. Amann,

- and Connie J. Chang-Hasnain. Performance of a multi-Gb/s 60 GHz radio over fiber system employing a directly modulated optically injection-locked VCSEL. *Journal of Lightwave Technology*, 28(16):2436–2444, 2010.
- [NP00] Richard van Nee and Ramjee Prasad. *OFDM for Wireless Multimedia Communications*. Artech House, Inc., Norwood, MA, USA, 2000.
- [NS09] Anthony Ng’oma and Michael Sauer. Radio-over-fiber technologies for high data rate wireless applications. In *2009 IEEE Sarnoff Symposium*, pages 1–6. IEEE, mar 2009.
- [OI02a] H Ochiai and H Imai. Performance analysis of deliberately clipped OFDM signals. *IEEE Trans. Commun.*, 50(1):89–101, Jan 2002.
- [OI02b] Hideki Ochiai and Hideki Imai. Performance analysis of deliberately clipped OFDM signals. *Communications, IEEE Transactions on*, 50(1):89–101, 2002.
- [OSF<sup>+</sup>00] Tetsuichiro Ohno, Kenji Sato, Seiji Fukushima, Yoshiyuki Doi, and Yutaka Matsuoka. Application of DBR mode-locked lasers in millimeter-wave fiber-radio system. *Journal of Lightwave Technology*, 18(1):44–49, 2000.
- [PAK10] Samuel David Perli, Nabeel Ahmed, and Dina Katabi. Pixnet: interference-free wireless links using lcd-camera pairs. In *Proc. MobiCom*, pages 137–148. ACM, 2010.
- [Pra04] Victor V. Prasolov. *Polynomials*, volume 11 of *Algorithms and Computation in Mathematics*. Springer, Berlin, Germany, 2004.
- [PS07] J. Proakis and M. Salehi. *Digital Communications*. McGraw-Hill Education, New York, NY, fifth edition, 2007.
- [PS08] John G Proakis and Masoud Salehi. *Digital Communications*. McGraw-Hill, 5 edition, 2008.
- [PZZ13] Chengcheng Pei, Zaichen Zhang, and Shujian Zhang. Softoc: Real-time projector-wall-camera communication system. In *Proc. ICCE, 2013*, pages 100–101, Jan 2013.

- [RMA12] M. Rubaiyat, H. Mondal, and Jean Armstrong. The effect of defocus blur on a spatial OFDM optical wireless communication system. In *2012 14th International Conference on Transparent Optical Networks (ICTON)*, volume 1, pages 1–4, 2012.
- [RMA<sup>+</sup>13] T. S. Rappaport, R. Mayzus, Y. Azar, K. Wang, G. N. Wong, J. K. Schulz, M. Samimi, and F. Gutierrez. Millimeter Wave Mobile Communications for 5G Cellular: It Will Work! *IEEE Access*, 1:335–349, 2013.
- [RSS10] Rajiv Ramaswami, Kumar N Sivarajan, and Golen H Sasaki. *Optical networks: a practical perspective*. Elsevier Science, Burlington, 3 edition, 2010.
- [SBC<sup>+</sup>10] Andreas Stohr, Sebastian Babel, Paul J. Cannard, Benoît Charbonnier, Frdric Frédéric Van Dijk, Sascha Fedderwitz, Dave Moodie, Leon Pavlovic, Lalitha Ponnampalam, Cyril C. Renaud, Dave Rogers, Vitaly Rymanov, Alwyn Seeds, Andreas Gerhard Steffan, Andreas Umbach, Mario Weis, Andreas Stöhr, Sebastian Babel, Paul J. Cannard, Benoît Charbonnier, Frdric Frédéric Van Dijk, Sascha Fedderwitz, Dave Moodie, Leon Pavlovic, Lalitha Ponnampalam, Cyril C. Renaud, Dave Rogers, Vitaly Rymanov, Alwyn Seeds, Andreas Gerhard Steffan, Andreas Umbach, Mario Weiß, Paul J. Cannard, Dave Moodie, and Dave Rogers. Millimeter-wave photonic components for broadband wireless systems. *IEEE Transactions on Microwave Theory and Techniques*, 58(11 PART 2):3071–3082, 2010.
- [SD09] William Shieh and Ivan Djordjevic. *OFDM for Optical Communications*. Academic Press, Burlington, 2009.
- [SF05] A.B. Sharma and M. Fujise. Optical Single-Sideband Modulation at 60 GHz Using Electro-Absorption Modulators. In *2005 International Topical Meeting on Microwave Photonics*, pages 121–124. IEEE, 2005.
- [SHZ<sup>+</sup>10] Yiming Shen, Bouchaib Hraïmel, Xiupu Zhang, Glenn E. R. Cowan, Ke Wu, and Taijun Liu. A Novel Analog Broadband RF Predistortion Circuit to Linearize Electro-Absorption Modulators in Multiband OFDM Radio-Over-Fiber Systems. *IEEE Transactions on Microwave Theory and Techniques*, 58(11):3327–3335, 2010.



- [SKM05] Kenji Sato, Shoichiro Kuwahara, and Yutaka Miyamoto. Chirp characteristics of 40-Gb/s directly modulated distributed-feedback laser diodes. *Journal of Lightwave Technology*, 23(11):3790–3797, 2005.
- [SMAB15] Tong Shao, Eamonn P. Martin, Prince M. Anandarajah, and Liam P. Barry. 60-GHz Direct Modulation-Direct Detection OFDM-RoF System Using Gain-Switched Laser. *IEEE Photonics Technology Letters*, 27(2):193–196, 2015.
- [SOS<sup>+</sup>01] S. Shimotsu, S. Oikawa, T. Saitou, N. Mitsugi, K. Kubodera, T. Kawanishi, and M. Izutsu. Single side-band modulation performance of a LiNbO<sub>3</sub> integrated modulator consisting of four-phase modulator waveguides. *IEEE Photonics Technology Letters*, 13(4):364–366, 2001.
- [SS77] A.B. Sripad and D. Snyder. A necessary and sufficient condition for quantization errors to be uniform and white. *IEEE Trans. Acoust., Speech, Signal Process.*, 25(5):442–448, Oct 1977.
- [ST01] Kanagaratnam Sathananthan and Chinthananda Tellambura. Probability of error calculation of OFDM systems with frequency offset. *Communications, IEEE Transactions on*, 49(11):1884–1888, 2001.
- [Sve10] Orazio Svelto. *Principles of lasers*. Springer US, Boston, MA, 2010.
- [SYZ15] Jingling Sun, Lan Yu, and Yanping Zhong. A single sideband radio-over-fiber system with improved dynamic range incorporating a dual-electrode dual-parallel MachZehnder modulator. *Optics Communications*, 336:315–318, 2015.
- [TSH13] Dobroslav Tsonev, Sinan Sinanovic, and Harald Haas. Complete Modeling of Nonlinear Distortion in OFDM-Based Optical Wireless Communication. *J. Lightwave Technol.*, 31(18):3064–3076, Sep 15 2013.
- [WHS<sup>+</sup>08] Mario Weiß, Mathieu Huchard, Andreas Stohr, Benoît Charbonnier, Sascha Fedderwitz, and Dieter Stefan Jager. 60-GHz Photonic Millimeter-Wave Link for Short- to Medium-Range Wireless Transmission Up to 12.5 Gb/s. *Journal of Lightwave Technology*, 26(15):2424–2429, 2008.
- [WLD95] David Wake, Claudio R. Liana, and Phillip A. Davies. Optical generation of millimeter-wave signals for fiber-radio systems using a dual-mode

DFB semiconductor laser. *IEEE Transactions on Microwave Theory and Techniques*, 43(9 /2):2270–2276, 1995.

- [WNG10] David Wake, Anthony Nkansah, and Nathan J. Gomes. Radio over fiber link design for next generation wireless systems. *Journal of Lightwave Technology*, 28(16):2456–2464, 2010.
- [WS52] Norman J. Woodland and Bernard Silver. Classifying apparatus and method, October 1952.
- [ZZ14] Mingxuan Zhang and Zaichen Zhang. An Optimum DC-Biasing for DCO-OFDM System. *IEEE Communications Letters*, 18(8):1351–1354, 2014.

## VITA

### AMIN MOTAHARI

Born, Rasht, Iran

- |           |   |
|-----------|---|
| 2003      | B.S., Electrical Engineering<br>Sharif University of Technology<br>Tehran, Iran           |
| 2008      | M.S., Electrical Engineering<br>Isfahan University of Technology<br>Isfahan, Iran         |
| 2015      | Dissertation Year Fellowship<br>Florida International University<br>Miami, FL             |
| 2015-2016 | Manuel and Mercedes Mosteiro Scholarship<br>Florida International University<br>Miami, FL |
| 2013-2016 | Doctoral Candidate<br>Florida International University<br>Miami, FL                       |

### PUBLICATIONS AND PRESENTATIONS

Motahari, Amin, and Malek Adjouadi. "Barcode Modulation Method for Data Transmission in Mobile Devices." *Multimedia, IEEE Transactions on* 17, no. 1 pp. 118-127, 2015.

Vedala, Krishnatej, S. M. Motahari, Mohammed Goryawala, Mercedes Cabrerizo, Ilker Yaylali, and Malek Adjouadi. "Quasi-Stationarity of EEG for Intraoperative Monitoring during Spinal Surgeries." *The Scientific World Journal* 2014.

Motahari, S. M., Krishnatej Vedala, Mohammed Goryawala, Mercedes Cabrerizo, Ilker Yaylali, and Malek Adjouadi. "A somatosensory evoked potential monitoring algorithm using time frequency filtering." In *Neural Engineering (NER), 2013 6th International IEEE/EMBS Conference on*, pp. 351-354. IEEE, 2013.

Vedala, Krishnatej, S. M. Motahari, Mohammed Goryawala, Mercedes Cabrerizo, Ilker Yaylali, and Malek Adjouadi. "Novel time-frequency-eigen filter for intraoperative neurophysiologic monitoring in spinal surgeries." In *Neural Engineering (NER), 2013 6th International IEEE/EMBS Conference on*, pp. 1578-1581. IEEE, 2013.

Motahari, S. M. A., and Hai Deng. "Clutter rejection processing for airborne radar in rotated space-time domain." In *Antennas and Propagation Society International Symposium (APSURSI), 2012 IEEE*, pp. 1-2. IEEE, 2012.

Motahari, SM Amin, and Hai Deng. "Ground clutter rejection for airborne radar using doppler compensation." In *Proceedings of the 2012 IEEE International Symposium on Antennas and Propagation*. 2012.

Faghani, Mohammad Reza, and SM Amin Motahari. "Sectorized Location Dependent Key Management." In *Wireless and Mobile Computing, Networking and Communications, 2009. WIMOB . IEEE International Conference on*, pp. 388-393. IEEE, 2009.